Archive

Stainless Steel Clad for Light Water Reactor Fuels

by

J. E. Rivera and J. E. Meyer

Energy Laboratory Report No. MIT-EL 80-021
July 1980

Stainless Steel Clad for Light Water Reactor Fuels

by

J. E. Rivera and J. E. Meyer

Energy Laboratory
and
Department of Nuclear Engineering

Massachusetts Institute of Technology
Cambridge, Massachusetts 02139

Final Report for Research Project

sponsored by

Northeast Utilities Service Co.
Southern California Edison Co.

under the

MIT Energy Laboratory Electric Utility Program

Energy Laboratory Report No. MIT-EL 80-021

July 1980

TABLE OF CONTENTS

LIST OF FIGURES

SUMMARY

The long and short term behavior of light water reactor stainless steel clad fuel has been investigated in order to establish more adequate or applicable operation/design criteria. The performance record of stainless steel clad fuel used in both the Connecticut Yankee and San Onofre 1 power stations has remained essentially unmarred until the recent past. While the San Onofre 1 plant has maintained this record, the Connecticut Yankee station has experienced a number of fuel element failures since 1977. Consequently, emphasis has been placed on cladding behavior for anomalous operation experienced by the Connecticut Yankee reactor prior to its first observed coolant activity increase.

In order to predict cladding behavior, a fuel performance code (STRESS) has been developed with the capabilities of analyzing long term cladding creepdown behavior, cladding conditioning, and behavior during up-power ramping and power maneuvers. The effects of varied fill gas pressure and cladding creep rate on the stress/deformation behavior of stainless steel cladding for these performance areas have been investigated. Similar calculations are also performed for Zircaloy clad fuel so that a comparison can be made between these materials. Code limitations are discussed and some methods which compensate for insufficient modeling are reviewed.

Fuel element design and reactor operation recommendations are made for Connecticut Yankee (and San Onofre 1) stainless steel clad fuel. These include fill gas pressurization level, up-power ramp rate limitations, and possible cladding material preference. These

recommendations are based on the results of the STRESS code and the trends which may be inferred from them.

1. INTRODUCTION

1.1 Objective

Proper reactor operation and design guidelines are necessary to assure fuel integrity. The occurrence of fuel rod failures for operation in compliance with existing guidelines suggests the need for more adequate or applicable operation/design criteria. The intent of this study is to develop such criteria for light water reactor fuel rods with stainless steel clad and to indicate the nature of uncertainties in its development. The performance areas investigated herein are:

- long term creepdown and fuel swelling effects on clad dimensional changes and on proximity to clad failure; and
- short term clad failure possibilities during up-power ramps.

1.2 Observed Behavior

The performance record of stainless steel clad fuel used in both Connecticut Yankee and San Onofre 1 reactors has remained essentially unmarred until the recent past. While the San Onofre 1 plant has maintained this record, Connecticut Yankee has experienced a number of fuel element failures since 1977. The only notable difference between element designs for these reactors is the fill gas pressurization level (recent San Onofre 1 rods have been pressurized).

An overview of operational history and observed coolant activity for Connecticut Yankee suggests a correlation between operating events (less than full power) and increased activity. Sipping results and visual examinations (Ref. 1) indicate that most failures are unique to one batch (batch 8: 36 out of 48 assemblies were identified as leakers). It has been estimated that approximately 1% of the fuel elements in this batch had failed (Ref. 2).

Similar non-full power operation has occurred since the removal of batch 8.* However, return to full power was t a reduced rate as recommended by BNFL (Ref. 2). It is not known if any fuel element failures** resulted from this maneuver.

1.3 Approach

In order to develop design/operation criteria, a somewhat comprehensive picture of the behavior of stainless steel clad fuel elements under operation characteristic of Connecticut Yankee must be established. This entails the development of computational methods which attempt to simulate rod behavior. It should be mentioned that even the most detailed (also benchmarked and calibrated) state of the art fuel performance modeling codes often lack the deterministic capabilities intended in their design. It is in this light that the approach also includes a comparative study.

The following outlines the steps used to classify the behavior of stainless steel. They are

- to perform rough calculations (and subsequent detailed calculations) which determine the approximate burnup for initial Pellet-Cladding Mechanical Interaction (PCMI) due to long term cladding creepdown;
- to investigate the concept of cladding conditioning and deconditioning;
- to model various short term up power ramps and operating events coincident with increased coolant activity levels; and
- to compare results with similar calculations done for rods of different design/material.

---

* This operation occurred in 1979. At that time, about 160 rods with identical fabrication as batch 8 were still in the core.

** There is a present estimate of 2-6 failed rods; correlation with this maneuver has not been established.

The above procedure is also repeated for variations in cladding creep rate, necessitated by the lack of benchmarking data and more detailed modeling of PCMI.

2. BACKGROUND

2.1 Observed Fuel Performance

Information on performance of the Connecticut Yankee fuel (all with stainless steel - type 304 cladding) has been obtained from discussions with Northeast Utilities personnel and from detailed records (Ref. 3). Coolant activity levels have remained at low values (indicative of few, if any, fuel element failures) until 1977.

The average specific degassed activity values for Connecticut Yankee from 1975 to mid-1978 are shown in Fig. 2-1. Cycle refueling periods between cycles V through VIII are also indicated. Significant activity increases (above an earlier level averaging about 0.4 μc/mℓ) are observed in:

- the latter part of cycle VII, September 1977 (average degassed activity value = 0.75 μc/mℓ);
- cycle VIII, December 1977 (1.75 μc/mℓ); and
- cycle VIII, April 1978 (2.23 μc/mℓ).

Operational events and conditions just prior to these increases are given special scrutiny and initially serve as a base for the selection of specific fuel assemblies for detailed analysis.

2.2 Representative Fuel Power Histories

The largest increase in coolant activity occurred in April 1978, as noted in Section 2.1. A representative fuel assembly was selected from each batch of fuel in the Connecticut Yankee core at that time. Selection was based on the fuel assemblies having the highest nuclear heat flux hot channel factor (F_Q^N) in March 1978.*

*More detailed information and preliminary calculations suggested the inclusion of the batch 8 assembly having the highest F_Q^N value just prior to the first observed activity increase. This assembly (denoted 8-H22) has been selected for further analysis rather than assembly 8-H16 which has a higher F_Q^N value in March 1978.

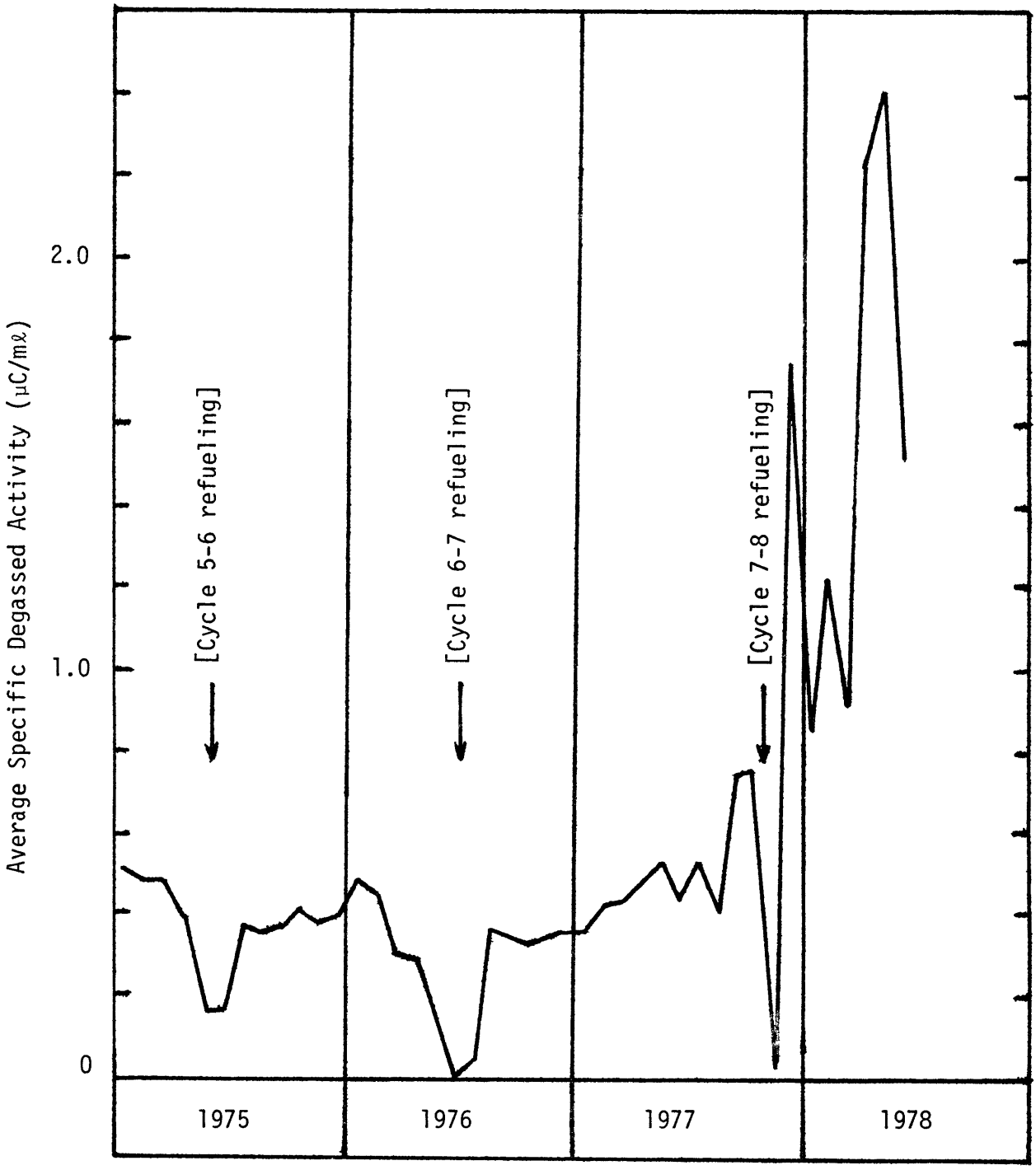

Figure 2-1 Connecticut Yankee Coolant Activity Behavior

The channel factors and relative assembly power values were supplied (Ref. 4) from the results of 100% full power core flux maps analyzed with the INCORE code and are plotted in Fig. 2-2 as a function of core equivalent full power days. For example, consider the set of curves labeled 8-H22. These apply to assembly H22 in fuel batch 8. This assembly is shown to be present in the core during cycles VI, VII, and VIII. The assembly average depletion (MWD/kgU) is given as 6.5, 21.4, and 30.9 at the end* of each of the three cycles. The peak values of F_Q^N are 1.37, 1.74, and 1.36 at the beginning of cycles VI, VII, and VIII, respectively.

2.3 Operational Information

Unusual operation, particularly at times just prior to activity increases, may be related to the observed fuel rod failures.** Review of the daily average reactor thermal output data from July 1974 to November 1978 indicates several possibly significant periods of non-full power operation (Ref. 3). Special attention has been given to events just prior to the above mentioned coolant activity increases. The following list, which also includes refueling dates, summarizes these events. In chronological order they are for 1975:

- Cycle V-VI refueling, mid-May to July 1;

for 1976:

- Cycle VI-VII refueling, mid-May to Mid-July;

---

* Cycle VIII data is only complete through November 1978.

** An alternate explanation is that the fuel has failed earlier and that power changes cause increased release.

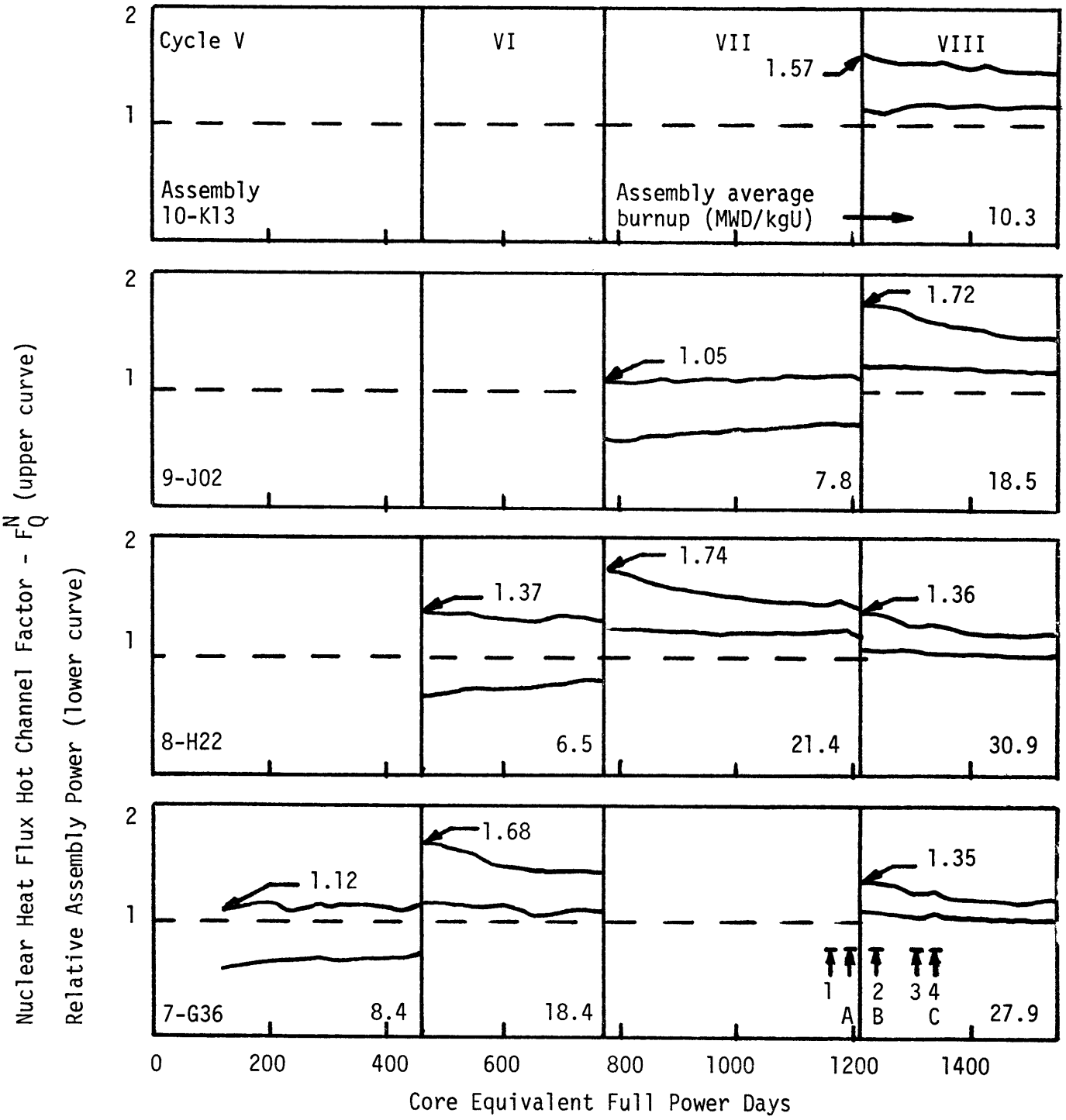

Figure 2-2 Connecticut Yankee Representative Fuel Assembly Power Historie

A-Activity increase (∿400-425 EFPD, Cycle 7) Sept. 1977
B-Activity increase (∿0-25 EFPD, Cycle 8) Dec. 1977
C-Activity increase (∿100-125 EFPD, Cycle 8) Apr. 1978
1-Non-full power operation (∿375-390 EFPD, Cycle 7) Aug. 9-20, 1977.
2-Multiple power changes (∿5-25 EFPD, Cycle 8) Dec. 10-30, 1977
3-Three loop operation (∿90-100 EFPD, Cycle 8) Mar. 23-30, 1978
4-Multiple power changes (∿120-130 EFPD, Cycle 8) Apr. 29-May 4, 1978

for 1977:

- Cycle VII, operation at approximately 1170 MW(th) from August 9 to 15 followed by operation at approximately 1285 MW(th) to August 20 (note that full power operation is 1825 MW(th);

- Cycle VII-VIII refueling, October 15 to December 1; and

- Cycle VIII, numerous power changes in the period December 10 to 30;

for 1978:

- Cycle VIII, operation at approximately 1200 MW(th) from March 23 to 30 for replacement of reactor coolant pump seals (3 loop operation); and

- Cycle VIII, 5 subsequent power changes ranging from 760 to 1825 MW(th) during the period April 29 to May 4.

Many full to zero power changes have been omitted from this list. Detailed power ramp information on these (and the above listed) occurrences may indicate some that should be included. The four non-refueling events are indicated by numerals in Fig. 2-2.

2.4 Interpretation

In order to establish a plausible cause for fuel element failure, careful consideration of both operational information and coolant activity levels must be made. As stated in Section 2.3, the near coincidence of operation events/activity increase* does not confirm a cause/effect relation between a given maneuver and fuel element failure. Fuel which has previously failed could exhibit increased release during power changes. A key therefore to the cause/effect relation is the judgment of whether previous failure (during steady operation) had occurred.

*Power changes followed by coolant activity increases.

If batch 8 satisfies an "all things equal" batch fabrication assumption, then steady state failure is not expected (few or no failures occurred with seven previous batches and roughly equivalent steady state operating conditions). If batch 8 is not sufficiently similar to previous batches, then no conclusion regarding causes from steady operation versus low power/ramp operation can be made. In the remainder of this study, the work is directed toward occurrences during power ramps after low power operation. The possibility of alternate explanations as indicated in this section should be noted, however.

3. METHODS FOR STRESS/DEFORMATION CALCULATIONS

This chapter is specifically dedicated to the computational procedures used in the STRESS code (a listing is provided in Appendix D). Its development was based on an axisymmetric fuel/cladding model in which the fuel remains intact (uncracked). Local effects of pellet-cladding mechanical interaction (PCMI), such as stress concentrations due to fuel pellet hourglassing, have not been considered. An outline and discussion of the more detailed models and computational methods used in the STRESS code are now presented.

3.1 Outline of Computer Code

The STRESS code capabilities are both versatile and two-fold. Its structure may be viewed as two separate main routines utilizing identical subroutines. Depending on the choice of input variables, the STRESS code predicts

- long term cladding creepdown/fuel swelling from BOL to fuel/cladding contact; or
- fuel/cladding behavior for rod conditioning at a prescribed burnup and subsequent power maneuvers.

The analysis is performed for a particular assembly, the historical data for which is provided internally as block data. Either stainless steel or Zircaloy may be investigated for a given (semi-tunable) creep acceleration factor. Variations in rod prepressurization level or any other mechanical design data change must be edited.* A simplified flow diagram is provided in Fig. 3-1.

*This is not input data but is a part of the code as is block data.

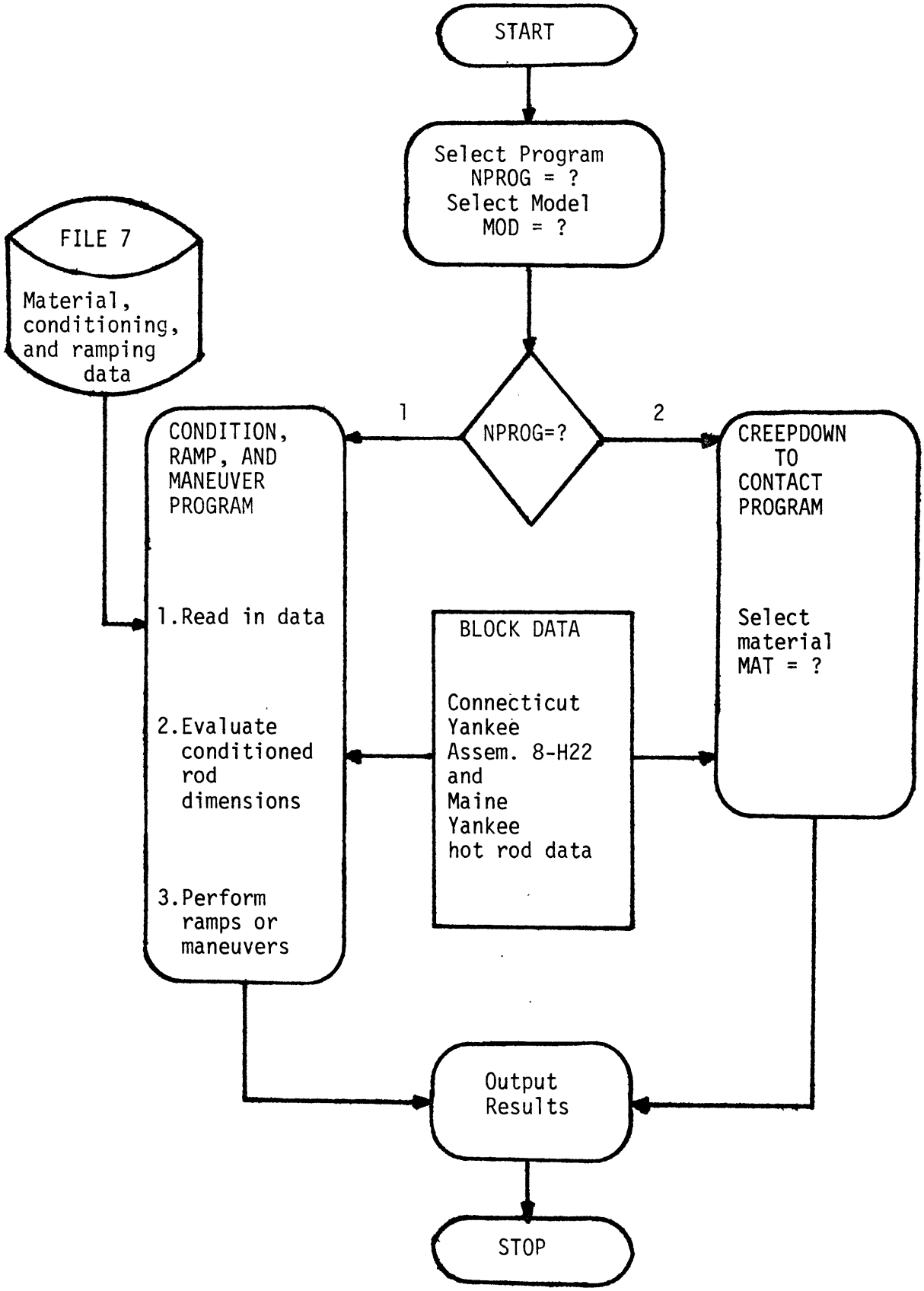

Figure 3-1 Simplified Flowchart for STRESS

The output is designed to extract a wealth of pertinent thermal and mechanical data characterizing the state of the fuel element at various time intervals. Its structure and interpretation is discussed in Appendix D. The input format and procedure is also presented therein.

3.2 Element Power Characteristics

3.2.1 Linear Heat Generation Rate Calculations

The linear heat generation rate (LHGR) at a particular location along a rod may be simply calculated as

$$q' = \bar{q}' \, F_Q^N(B) \quad ;$$

where

q' = local LHGR (kW/m);

$\bar{q}'$ = core average LHGR (kW/m); and

$F_Q^N(B)$ = nuclear heat flux hot channel factor at a given core burnup, B.

In the Connecticut Yankee case, the monthly F_Q^N values predicted for a given assembly by the INCORE code correspond to different rods and locations within that assembly. The STRESS code LHGR calculation assumes that these values are for a single rod and location, typifying "worst" conditions.

In order to avoid voluminous data entry, only beginning of cycle (BOC), end of cycle (EOC), and two in-cycle F_Q^N values are used (a set of 4 for each of 3 cycles experienced by a given assembly). These values are entered as block data with their corresponding core burnup values. The F_Q^N value at any core burnup value may now be approximated by linear interpolation.

A similar representation using 4 in-cycle points (6 total per cycle) is employed for Zircaloy. The hot rod data for this case was obtained from Maine Yankee (Ref. 5).

Figure 3-2 shows the linear representation used in F_Q^N (and also relative assembly power) calculations for Connecticut Yankee. Thus,

$$F_Q^N(B) = \left[\frac{\left(F_Q^N\right)_{i,j+1} - \left(F_Q^N\right)_{i,j}}{B_{i,j+1} - B_{i,j}}\right](B - B_{i,j}) + (F_Q^N)_{i,j}$$

where

B = some cumulative core burnup between $B_{i,j}$ and $B_{i,j+1}$ (MWD/kgU);

i = assembly cycle value (1, 2, or 3); and

$$j = \begin{cases} 1 - 3 \text{ for Connecticut Yankee} \\ 1 - 5 \text{ for Maine Yankee.} \end{cases}$$

It should be noted that all burnup values used in this code are cumulative (see the following section).

3.2.2 Local and Average Assembly Burnup Calculations

Local (or maximum) and average rod burnup calculations are performed using the representations for F_Q^N and relative assemble power* as shown in Fig. 3-2. Integration of these linear approximations yields

*Indicative of relative rod power.

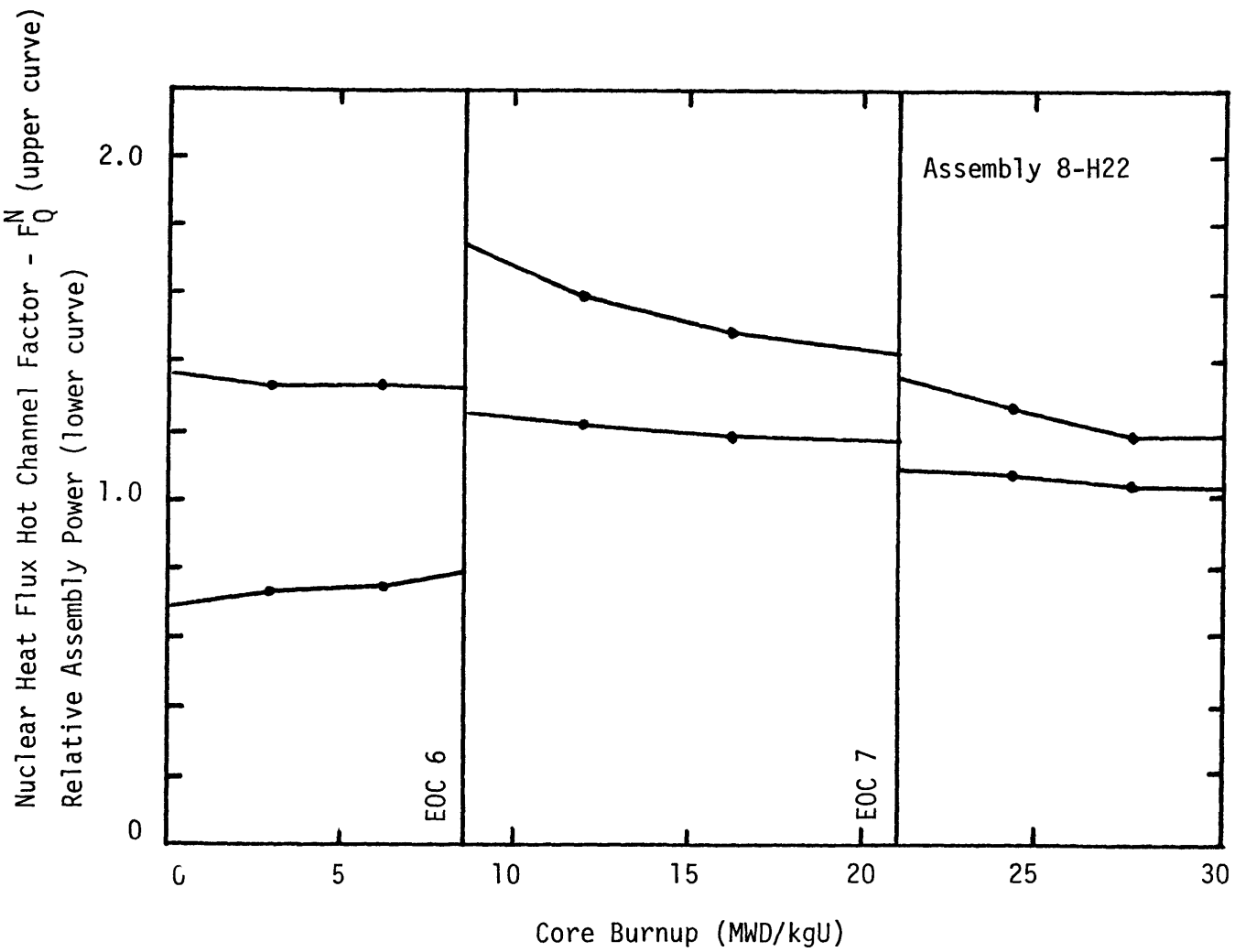

Figure 3-2 Linear Representation Used for LHGR and Burnup Calculations

$$B^{L,R} = \sum_{m=1}^{i} \sum_{n=2}^{k} \left(\frac{Y_{m,n} + Y_{m,n-1}}{2} \right) [B_{m,n} - B_{m,n-1}]$$

$$+ \frac{1}{2} \left(\frac{Y_{i,j+1} - Y_{i,j}}{B_{i,j+1} - B_{i,j}} \right) [B - B_{i,j}]^2$$

$$+ Y_{i,j} [B - B_{i,j}]$$

where

$B^{L,R}$ = local or average rod cumulative burnup (MWD/kgU);

Y = { nuclear heat flux hot channel factor, F_Q^N, for B^L; relative assembly power for B^R;

B = some cumulative core burnup between $B_{i,j}$ and $B_{i,j+1}$ (MWD/kgU);

i = assembly cycle value (1, 2, or 3);

j = { 1 - 3 for Connecticut Yankee; 1 - 5 for Maine Yankee; and

k = { 4 for $m < i$. j for $m = i$.

It should be noted that the phrase "cumulative burnup" means the burnup experienced in the present cycle (either core, local, or average for cycle i) plus any previous cycle burnup values. For instance, the cumulative core burnup for an assembly in its second cycle is the core burnup at that time for that cycle plus the core burnup at the end of its first cycle.

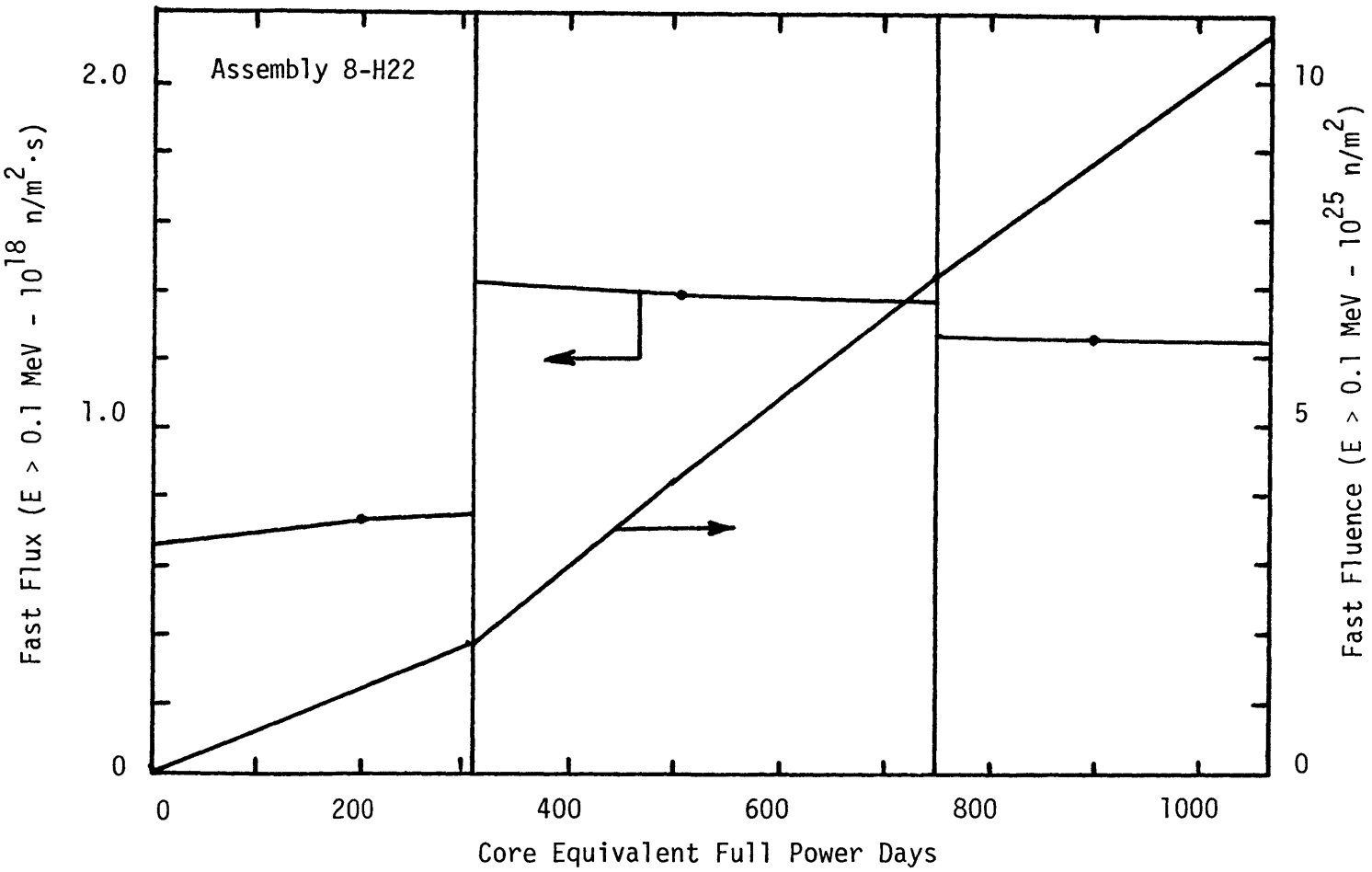

Figure 3-3 Fast Flux Representation and Calculated Fluence Values

3.2.3 Fast Flux and Fluence Calculations

The fast flux model consists of a piece-wise linear approximation to data supplied by Northeast Utility Service Company (Ref. 6). These values were converted from neutron flux energies greater than 1.85 eV to 0.1 MeV using a 0.543 conversion factor. Fast fluence calculations are performed in a similar fashion to burnup calculations presented in the previous section. The only major differences are that flux values are entered along with core EFPD rather than burnup and cycles are divided into 2 rather than 3 sections.

Figure 3-3 shows the fast flux representation and calculated fluence values* for typical converted flux data. It should be mentioned that these converted values are used directly in the creep equations for both materials (Section A.6) regardless of the flux energy restrictions placed therein. This would tend to enhance creep rates.

3.3 Cladding Representation

Both stainless steel (type 304) and Zircaloy cladding are modeled using a single element representation. Stress, strain, and deflection calculations are based on original cold beginning of life (BOL) dimensions and any Zircaloy anisotropy effects have been neglected. The model does not compensate for the interactive pellet/clad axial force (i.e., no pellet/clad friction). Details of the representation follow.

3.3.1 Single Element Model for Cladding

Advancement of computer technology has permitted the development of finite element or finite difference methods which

*This representation is for Connecticut Yankee assembly 8-H22. Unavailable flux data for cycle 6 (the first cycle shown) was taken from cycle 8 data. This same representation is used in the Zircaloy case.

very much simplify an otherwise complex analytic thick shell problem. In this study, it has been decided to represent the cladding as a single element or ring (Ref. 7). This approach provides a more realistic analysis than a thin shell model and is considered sufficiently accurate such that multiple elements are not necessary.

The single element component strains are related to the cladding inside and outside deflections by*

$$\begin{bmatrix} \varepsilon_r \\ \varepsilon_\theta \end{bmatrix} = \begin{bmatrix} \frac{1}{b-a} & \frac{-1}{b-a} \\ \frac{1}{b+a} & \frac{1}{b+a} \end{bmatrix} \begin{bmatrix} u_b \\ u_a \end{bmatrix}$$

where

ε_r = total radial strain component $(\frac{mm}{mm})$;

ε_θ = total tangential strain component $(\frac{mm}{mm})$;

u_a = cladding inside surface deflection (mm);

u_b = cladding outside surface deflection (mm);

a = BOL cladding inside radius (mm); and

b = BOL cladding outside radius (mm).

Alternatively, the element deflections may be expressed in terms of element strain components as

*Since the axial strain component does not enter calculations, it is not included.

$$\begin{bmatrix} u_a \\ u_b \end{bmatrix} = \begin{bmatrix} \frac{(b+a)}{2} & -\frac{(b-a)}{2} \\ \frac{(b+a)}{2} & \frac{(b-a)}{2} \end{bmatrix} \begin{bmatrix} \varepsilon_\theta \\ \varepsilon_r \end{bmatrix}$$

The force/stress connection is derived using the principle of virtual work so that on an energy basis the forces will be consistent with deflections. The work per unit axial length due to the product of forces acting on the element and virtual displacements is balanced by the element strain energy. This requirement yields

$$\begin{bmatrix} F_a \\ F_b \\ F_z \end{bmatrix} = \pi(b^2-a^2) \begin{bmatrix} \frac{-1}{(b-a)} & \frac{1}{(b+a)} & 0 \\ \frac{1}{(b-a)} & \frac{1}{(b+a)} & 0 \\ 0 & 0 & 1 \end{bmatrix} \begin{bmatrix} \sigma_r \\ \sigma_\theta \\ \sigma_z \end{bmatrix}$$

where

F_a = inside cladding force per unit length;

F_b = outside cladding force per unit length;

F_z = axial force acting on the element cross section;

σ_r = radial stress component (MPa);

σ_θ = tangential stress component (MPa); and

σ_z = axial stress component (MPa).

The element forces can be expressed in terms of the internal and external rod pressures. Internal rod pressure is due to the combination of gas and contact pressures. Thus,

$$\begin{bmatrix} F_a \\ F_b \\ F_z \end{bmatrix} = \pi \begin{bmatrix} 2a & 2a & 0 \\ 0 & 0 & -2b \\ a^2 & 0 & -b^2 \end{bmatrix} \begin{bmatrix} P_g \\ P_c \\ P_B \end{bmatrix}$$

where

P_g = hot internal rod gas pressure (MPa);

P_c = fuel/cladding contact pressure (MPa); and

P_B = bulk coolant pressure (MPa).

The final step is to relate the component stresses to the pressures by equating the above expressions for element forces. The result is

$$\begin{bmatrix} \sigma_r \\ \sigma_\theta \\ \sigma_z \end{bmatrix} = \begin{bmatrix} \frac{-a}{(b+a)} & \frac{-a}{(b+a)} & \frac{-b}{(b+a)} \\ \frac{a}{(b-a)} & \frac{a}{(b-a)} & \frac{-b}{(b-a)} \\ \frac{a^2}{(b^2-a^2)} & 0 & \frac{-b^2}{(b^2-a^2)} \end{bmatrix} \begin{bmatrix} P_g \\ P_c \\ P_B \end{bmatrix}$$

It should be noted that the above forms for axial force and stress do not consider pellet-clad interaction. As mentioned previously, the model assumes that a pellet in contact with the cladding will "slide" in the event of differential axial fuel/cladding thermal expansion or deformation. Also, the hot internal rod pressure is held constant over life at an estimated value of twice the BOL fill gas pressure.

3.3.2 Cladding Creep Flow Rules

Uniaxial creep strain results are generalized to multiaxial stress states using flow rules developed by Levy and von Mises (Ref. 8). The model assumes that creep deformation occurs under constant volume and that strain rate is not affected by hydrostatic stress components. The relations presented below are, in a strict sense, only applicable to axisymmetric materials. However, since anisotropic effects are ignored, they are adequate for both stainless steel and Zircaloy. The component creep strains, expressed in incremental form, are

$$\begin{bmatrix} \Delta\varepsilon_r^c \\ \Delta\varepsilon_\theta^c \end{bmatrix} = \frac{\Delta\varepsilon_g}{2\sigma_g} \begin{bmatrix} 2 & -1 & -1 \\ -1 & 2 & -1 \end{bmatrix} \begin{bmatrix} \sigma_r \\ \sigma_\theta \\ \sigma_z \end{bmatrix}$$

and

$$\sigma_g = \frac{1}{\sqrt{2}} \left[(\sigma_r-\sigma_\theta)^2 + (\sigma_\theta-\sigma_z)^2 + (\sigma_z-\sigma_r)^2\right]^{1/2}$$

where

ε_r^c = radial creep strain ($\frac{mm}{mm}$);

ε_θ^c = tangential creep strain ($\frac{mm}{mm}$);

ε_g = generalized creep strain ($\frac{mm}{mm}$);

σ_g = generalized stress (MPa); and

σ_r, σ_θ, σ_z = radial, tangential, and axial stresses (MPa).

The increment of generalized strain is calculated during the solution for total component creep strains using

$$\Delta\varepsilon_g = \dot{\varepsilon}_g \Delta t$$

where

$\dot{\varepsilon}_g$ = generalized creep strain rate (given in Section A.6); and

t = time (in consistent units).

The numerical techniques used to solve the differential creep strain rates are presented in Section 3.6.2.

3.3.3 Cladding Elastic Strain Calculations

The cladding elastic strain calculations are based on Hooke's Law for linear elastic materials. The model does not compensate for any directional dependence of elastic modulus or Poisson ratio. The familiar relations for component elastic strain are

$$\begin{bmatrix} \varepsilon_r^{e\ell} \\ \varepsilon_\theta^{e\ell} \end{bmatrix} = \frac{1}{E} \begin{bmatrix} 1 & -\nu & -\nu \\ -\nu & 1 & -\nu \end{bmatrix} \begin{bmatrix} \sigma_r \\ \sigma_\theta \\ \sigma_z \end{bmatrix}$$

where

$\varepsilon_{r,\theta}^{e\ell}$ = radial and tangential strain components ($\frac{mm}{mm}$);

$\sigma_{r,\theta}$ = radial and tangential stress (MPa);

E = cladding modulus of elasticity (MPa); and

ν = cladding Poisson ratio.

The temperature dependence of elastic modulus and Poisson ratio for both stainless steel and Zircaloy are given in Sections A.3 and A.4, respectively. Since the cladding temperature varies across the element, the elastic modulus corresponds to a volume averaged quantity and Poisson's ratio is evaluated at the cladding average temperature. The averaging process is analogous to that performed for thermal strain which is presented in the following section.

Repetitious calculations may be avoided by relating the elastic strains to the pressures acting on the element. Since the bulk coolant and internal gas pressures are constant, the elastic response due to them does not have to be re-evaluated every time the pellet/clad contact pressure varies. Thus,

$$\begin{bmatrix} \varepsilon_r^{e\ell} \\ \varepsilon_\theta^{e\ell} \end{bmatrix} = \frac{1}{(b^2-a^2)E} \begin{bmatrix} a^2(1-2\nu)-ab(1+\nu) & a^2(1-\nu)-ab(1+\nu) & -b^2(1-2\nu)+ab(1+\nu) \\ a^2(1-2\nu)+ab(1+\nu) & a^2(1-\nu)+ab(1+\nu) & -b^2(1-2\nu)-ab(1+\nu) \end{bmatrix} \begin{bmatrix} P_g \\ P_c \\ P_B \end{bmatrix}$$

where all symbols are previously defined.

3.3.4 Temperature Profile and Thermal Strain Calculations

The cladding temperature profile solution begins with the one-dimensional heat flow equation which may be written in cylindrical coordinates as

$$q' = -2\pi r k_c \frac{dT}{dr}$$

where

q' = linear heat generation rate;

k_c = cladding thermal conductivity; and

T = cladding temperature;

all in consistent units. Any internal heat deposition is neglected.

Rearranging and integrating yields

$$\int_{T_o}^{T} k_c \, dT = \frac{q'}{2\pi} \ln \frac{b}{r}$$

where

T_o = outside cladding temperature;

T = cladding temperature at radius r; and

b = BOL outside cladding radius.

Since the form of cladding thermal conductivity for stainless steel and Zircaloy differ (see Appendix A.1), two separate solution procedures are used.

The thermal conductivity for SS304 has the form

$$k_c = C_o + C_1 T + C_2 T^2 + C_3 T^3 \quad ;$$

where the constants are defined in Section A.1. Integrating over temperature yields a quartic equation which can be iteratively solved. By making the substitution

$$T = T_o + \Delta T \quad ,$$

the amount of calculations performed in the iterative loop may be reduced. The final form is

$$a_1\Delta T + a_2(\Delta T)^2 + a_3(\Delta T)^3 + a_4(\Delta T)^4 = \frac{q'}{2\pi} \ln \frac{b}{r} \quad ;$$

where

$$a_1 = C_o + C_1T_o + C_2T_o^2 + C_3T_o^3 \quad ;$$

$$a_2 = \frac{C_1}{2} + C_2T_o + \frac{3}{2} C_3T_o^2 \quad ;$$

$$a_3 = \frac{C_2}{3} + C_3T_o \quad ; \text{ and}$$

$$a_4 = \frac{C_3}{4} \quad .$$

The iterative solution uses the bi-section convergence method discussed in Section 3.6.1 and the calculated temperature is accurate to ± 0.001°C.

The temperature profile solution for the Zircaloy case was taken from Ref. 9, using the same form for thermal conductivity as given in Section A.1. In this case, the temperature is solved explicitly as

$$T = -1.015\text{x}10^5 \{1.3959\text{x}10^{-2} - [1.9485\text{x}10^{-4} + 1.9704\text{x}10^{-5} (1.3959\text{x}10^{-2}T_o + 4.9261\text{x}10^{-6}T_o^2 + \frac{q'}{2\pi} \ln(\frac{b}{r}))]^{1/2}\}$$

where

T = cladding temperature at radius r (°C);

T_o = outside cladding temperature (°C); and

q' = LHGR (kW/m).

Having a method of calculating cladding temperatures allows the computation of various volume averaged, temperature dependent (therefore radius dependent) quantities. The following outlines the method of solution for averaging cladding thermal strain, however, the technique is directly applicable for averaging cladding temperature and elastic modulus by replacing the argument. This calculation, as all previous ones, uses beginning of life (BOL) cold cladding dimensions. The form is

$$\overline{\varepsilon_c^T} = \frac{2}{b^2-a^2} \int_a^b \varepsilon_c^T \, r \, dr$$

where

$\overline{\varepsilon_c^T}$ = average cladding thermal strain;

ε_c^T = cladding thermal strain at radius r;

and a,b are the cold BOL inner and outer radii. The thermal strain expressions for either material are found in Section A.2. Integration is performed using Simpson's one-third rule over 30 equispaced radial intervals.

3.4 Pellet Representation

The fuel pellet is represented as a solid cylinder with the densification and swelling characteristics discussed in Section A.11.

It is assumed that pellet-cladding mechanical interaction (PCMI) has no effect on pellet swelling (i.e., ignores restrained swelling or creep deformation effects) and, as stated in Section 3.3, does not impose an axial friction force condition at the pellet/clad interface. The only forces acting on the pellet are due to the hydrostatic gas pressure and the normal contact pressure force at the pellet surface (if PCMI exists). The pellet stress state may be represented as

$$\begin{bmatrix} \sigma_r \\ \sigma_\theta \\ \sigma_z \end{bmatrix} = \begin{bmatrix} -1 & -1 \\ -1 & -1 \\ -1 & 0 \end{bmatrix} \begin{bmatrix} P_g \\ P_c \end{bmatrix}$$

where

$\sigma_{r,\theta,z}$ = radial, tangential, and axial stresses (MPa);

P_g = hot internal rod gas pressure (MPa); and

P_c = fuel/cladding contact pressure (MPa).

Unlike the cladding calculations, the fuel does not use cold beginning of life (BOL) dimensions. Depending on the burnup, the densified or swelled cold radius at the beginning of a ramp or set of maneuvers is used. This radius may be calculated using

$$R_F = R_{F_o} \left(\frac{d_o}{d} \right)^{1/3}$$

where

R_F = densified or swelled cold fuel radius (mm);

R_{F_o} = BOL cold fuel radius (mm);

d_o = BOL cold fuel density (%TD); and

d = fuel density at a prescribed burnup (%TD).

The representation used for fuel density at a given local burnup is given in Section A.11. With this definition of fuel radius, the radial deflection of the fuel surface is calculated as

$$u_F = R_F \left(\varepsilon_\theta^{e\ell} + \overline{\varepsilon_F^T} + \varepsilon_v\right)$$

where

u_F = deflection of the fuel surface (mm);

$\varepsilon_\theta^{e\ell}$ = fuel tangential elastic strain component ($\frac{mm}{mm}$);

$\overline{\varepsilon_F^T}$ = fuel average thermal strain ($\frac{mm}{mm}$); and

ε_v = fuel volume strain with respect to a reference volume strain at the burnup used to obtain R_F ($\frac{mm}{mm}$).

A more in-depth discussion of volume strain is given in Section A.12. Fuel elastic and thermal strain calculations are presented in the following sections.

3.4.1 Fuel Elastic Strain

Like the cladding, the fuel pellet elastic strain calculations are based on Hooke's Law for a linear elastic material. Also, it is assumed that the elastic modulus and Poisson ratio are independent of direction. Since the fuel elastic strain relations are based on the same assumptions used for the cladding elastic strains, the stress/strain relations (of Section 3.3.3) are directly applicable.

The modulus of elasticity and Poisson ratio for the fuel are averaged quantities. These temperature dependent relations are given in Sections A.9 and A.10. The averaging process is analogous to that done for fuel average thermal strain (Section 3.4.2).

The fuel pellet elastic strain components may be expressed in terms of the gas and contact pressures as

$$\begin{bmatrix} \varepsilon_r^{e\ell} \\ \varepsilon_\theta^{e\ell} \end{bmatrix} = -\frac{1}{E} \begin{bmatrix} (1-2\nu) & (1-\nu) \\ (1-2\nu) & (1-\nu) \end{bmatrix} \begin{bmatrix} P_g \\ P_c \end{bmatrix}$$

Note that the relations for these components are identical. Also, if P_c is set to zero, the relations reduce to hydrostatic form.

3.4.2 Fuel Temperature Profile and Thermal Strain

The first step in the solution for fuel temperature profile begins with Poisson's steady state heat conduction equation of the form

$$-\nabla(K_f \nabla T) = q'''$$

where

q''' = volumetric heat deposition rate;

K_f = fuel thermal conductivity; and

T = fuel temperature.

Solution of this equation in cylindrical coordinates yields the following conductivity integral equation (Ref. 9)

$$\int_0^T k_F \, dT = \frac{q'}{4\pi} \left[1 - \left(\frac{r}{R_F}\right)^2\right] + \int_0^{T_2} k_F \, dT$$

where

$\int_0^T k_F \, dT$ = UO_2 conductivity integral $(\frac{kW}{m})$;

q' = linear heat generation rate $(\frac{kW}{m})$;

R_F = densified or swelled fuel outside radius cold (mm);

T_2 = fuel pellet outside surface temperature (°C); and

T = fuel pellet temperature at some position $r < R_F$ (°C).

The temperature and porosity dependent relations for fuel thermal conductivity and conductivity integral are given in Section A.7.

Assuming the fuel pellet surface temperature is known, the temperature at a given radius may be determined. This is achieved by relating temperature to the conductivity integral using a cubic spline curve fit. The general form is

$$T = A(x-\alpha)^3 + B(x-\alpha)^2 + C(x-\alpha) + D$$

where

$$x = \frac{1}{PF} \int_0^T k_F \, dT;$$

PF = porosity factor (see Section A.7); and

A, B, C, D, α = constants.

Table 3.1 Constants for Cubic Spline Fit

Temperature Range (°C)	A	B	C	D	α
$0 \leq T < 276.3$ $(0 \leq x < 2)$	1.641	12.962	105.627	0	0
$276.3 < T < 478.3$ $(2 \leq x < 3)$	2.056	22.808	177.177	276.250	2
$478.3 < T < 738.2$ $(3 \leq x < 4)$	1.977	28.974	228.959	478.290	3
$738.2 < T < 1066.3$ $(4 \leq x < 5)$	0.347	34.905	292.838	738.200	4
$1066.3 < T < 1461.3$ $(5 \leq x < 6)$	-4.646	35.946	363.689	1066.290	5
$1461.3 < T < 1895.1$ $(6 \leq x < 7)$	-9.795	22.010	421.645	1461.280	6
$1895.1 < T \leq 2698.0$ $(7 \leq x \leq 9)$	-5.025	-7.3749	436.280	1895.140	7

These constants have been determined for the temperature range $0 \leq T \leq 2698$ °C ($0 \leq x \leq 9$) and are presented in Table 3.1. Temperature values generated by this method are accurate to ± 0.01 °C.

If the fuel temperature distribution is known, average values for temperature dependent fuel properties can be calculated. The average fuel thermal strain may be determined using

$$\overline{\varepsilon_F^T} = \frac{2}{R_F^2} \int_0^{R_F} \varepsilon_F^T \, r \, dr$$

where

$\overline{\varepsilon_F^T}$ = average fuel thermal strain; and

ε_F^T = fuel thermal strain at radius r.

The expression for fuel thermal strain is given in Section A.8. Integration is performed using Simpson's one-third rule over 40 equispaced radial intervals.

3.5 Gap and Interaction Characteristics

3.5.1 Fill and Fission Gas Mole Fraction Calculations

The initial moles of helium fill gas are calculated using the ideal gas law of the form,

$$n = \frac{PV}{RT}$$

where

n = number of helium moles;
P = fill pressure;
V = fill volume
T = absolute temperature; and
R = universal gas constant.

The fill volume may be more specifically defined as the summation of the cold beginning of life (BOL) gap and plenum volumes, neglecting any contributions due to dished and chamfered pellets. The plenum volume for Connecticut Yankee was estimated from Maine Yankee data by assuming equivalent fuel-plenum volume ratios (Maine Yankee fuel-plenum volume ratio = 11.89). The resulting helium mole expression for Connecticut Yankee is

$$n = 8.4325 \times 10^{-6} P$$

where

P = Helium fill gas pressure (kPa)

at an assumed fill temperature of 298° K.

Only two dominant fission product gases, Xenon and Krypton, are considered in the mole fraction and gas conductivity calculations. Their U-235 thermal fission yield fractions* were estimated from data supplied in Ref. 16 and are

$$\beta_{Xe} = 0.2183$$
$$\beta_{Kr} = 0.0386.$$

In order to calculate the mole production of these rare gases, the total amount of rod fissions must be estimated. Thus,

*Possible differences due to U-238 and Pu-239 fissions are neglected.

$$F = \frac{P_o \, C_B \, C_E}{N \, C_F} \; B^R$$

$$= 4.346 \times 10^{18} \; B^R$$

where

F = total fissions per rod;

B^R = cumulative average assembly (or rod) burnup as calculated in Section 3.2.2 ($\frac{MWD}{kgU}$);

P_o = Connecticut Yankee full power thermal output (MW_{th});

N = number of core fuel rods;

$C_B = 2.825 \times 10^{-2}$ $EFPD_{core}/(MWD/kgU)$;

$C_E = 5.4 \times 10^{23}$ MeV/MWD; and

C_F = 200 MeV/fission.

The fraction of fission gas released is determined using Connecticut Yankee graphical data supplied by Northeast Utility Service Company. Figure 3-4 illustrates the piece-wise linear model used to approximate this data. The linear representation may be summarized as

$$f_r = \begin{cases} 1\times10^{-4}T & \text{for} \quad T \leq 190 \\ 7.899\times10^{-4}T - 0.13108 & \text{for} \quad 190 < T \leq 309 \\ 2.6241\times10^{-4}T + 0.03192 & \text{for} \quad 309 < T \leq 450 \\ 8.3893\times10^{-5}T + 0.11225 & \text{for} \quad 450 < T \leq 748 \\ -4.529\times10^{-5}T + 0.2089 & \text{for} \quad 748 < T \leq 1300 \\ 0.15 & \quad T > 1300 \end{cases}$$

where

f_r = fission gas release fraction; and

$T = C_B \, B^R$ = rod average burnup expressed in EFPD.

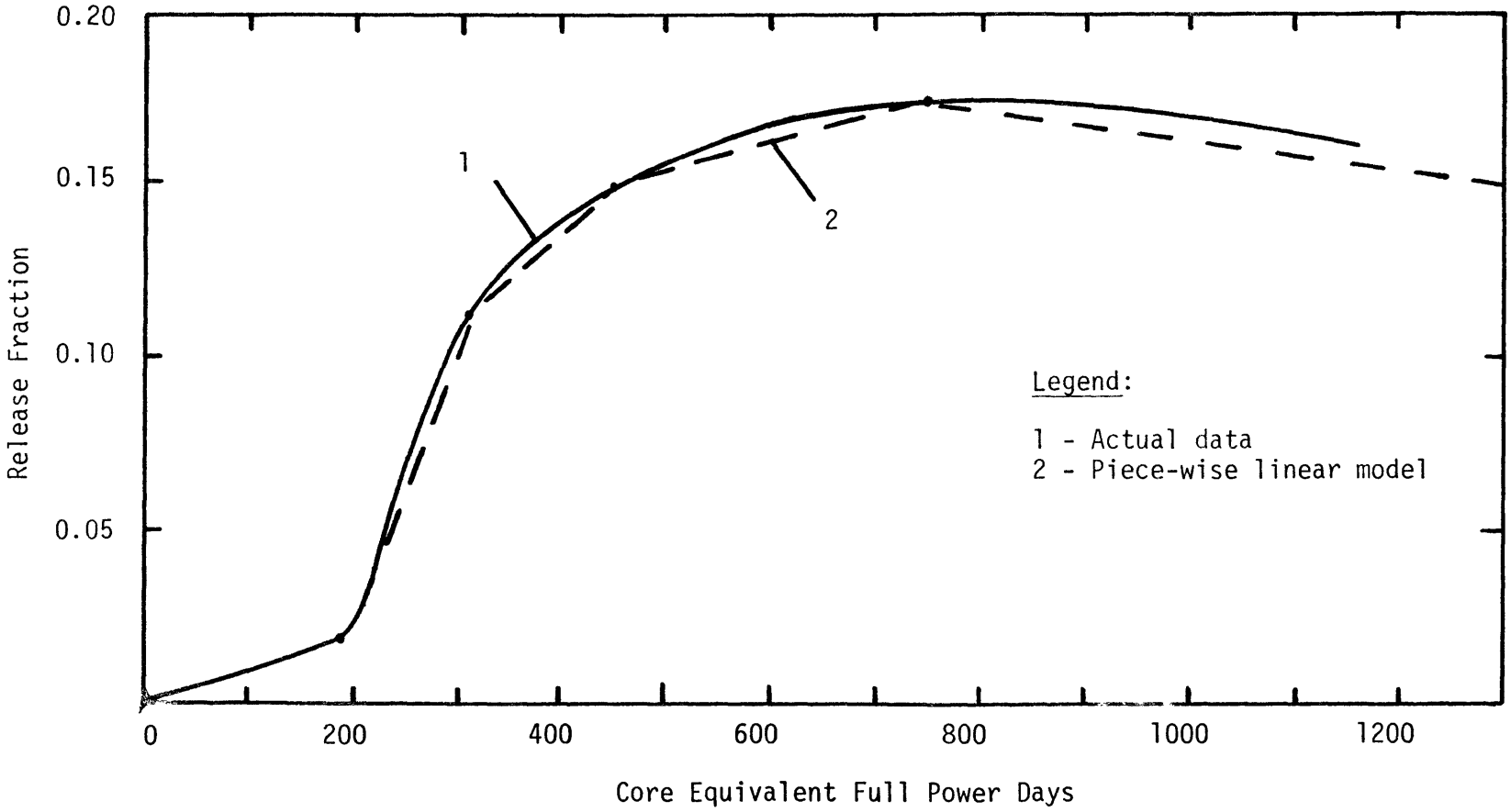

Figure 3-4 Connecticut Yankee Average Fission Gas Release Fraction

Table 3.2 MaineYankee Mole Fraction Data (from Ref. 5)

Local Burnup (MWD/kgU)	Mole Fraction		
	He	Xe	Kr
0	1	0	0
.2	1	0	0
0	.997	.002	.001
10	.987	.011	.002
20	.967	.029	.004
30	.932	.060	.008
40	.890	.097	.013

The moles of Xenon and Krypton which are released and contribute to gap conductivity degradation may now be directly computed from,

$$n_{Xe} = F\ \beta_{Xe}\ f_r \quad ;$$

and

$$n_{Kr} = F\ \beta_{Kr}\ f_r \quad ;$$

thus supplying all the necessary values for Connecticut Yankee mole fraction calculations.

The Zircaloy case mole fraction values are obtained by linear interpolation of Maine Yankee data. This information corresponds to the core hot rod and is given in Table 3.2. Note that local burnup values are given rather than rod average.

3.5.2 Pellet Surface Temperature and Gap Conductance

The fuel surface temperature is obtained using a variation of the covective heat transfer relation of the form

$$T_F = T_a + \frac{q'}{2\pi R_F(h_g+h_c)}$$

where

T_F = pellet surface temperature;

T_a = inside cladding temperature;

q' = linear heat generation rate;

R_F = cold densified or swelled fuel radius from Section 3.4;

h_g = gap gas conductance; and

h_c = fuel-cladding contact pressure conductance from Section A.14.

The gap conductance is related to the gas mixture thermal conductivity by

$$h_g = \frac{k_{mix}}{(\delta+\delta_c'+\delta_F')}$$

where

k_{mix} = thermal conductivity of gas mixture from Section A.13 evaluated at the gap average temperature;

δ = hot gap width;

δ_c' = root mean square cladding surface roughness; and

δ_F' = root mean square fuel surface roughness.

3.6 Solution Techniques

3.6.1 Bi-section Convergence Method

The bi-section convergence method is an iterative procedure which guarantees convergence on a variable to a predetermined accuracy. The method only requires that the dependent function be monotonically increasing or decreasing with respect to this independent variable. The method is now detailed for the case of a monotonically increasing function.

Using a temperature argument for convenience, a non-analytic functional relation of the form

$$f(T) = g(T)$$

may be rearranged to

$$y(T) = f(T) - g(T)$$

where

$y(T)$ = a ficticious, monotonically increasing function of temperature;

and has the unique solution

$$y(T^*) = 0 \quad .$$

An initial guess of $T_g < T^*$ would yield a negative value for $y(T_g)$ and conversely, positive for $T_g > T^*$.

Assuming that $y(T_g)$ is negative, a prescribed quantity, ΔT, is added n times to T_g until the sign of this function is reversed. At this point, the temperatures which encompass the root, T^*, may be defined as

$$T_- = T_g + (n-1)\ \Delta T; \text{ and}$$

$$T_+ = T_g + n\ \Delta T;$$

which satisfy

$y(T_-)$ = negative quantity; and

$y(T_+)$ = positive quantity.

The next temperature guess is the midpoint

$$T_{mid} = \frac{T_+ + T_-}{2}$$

and if

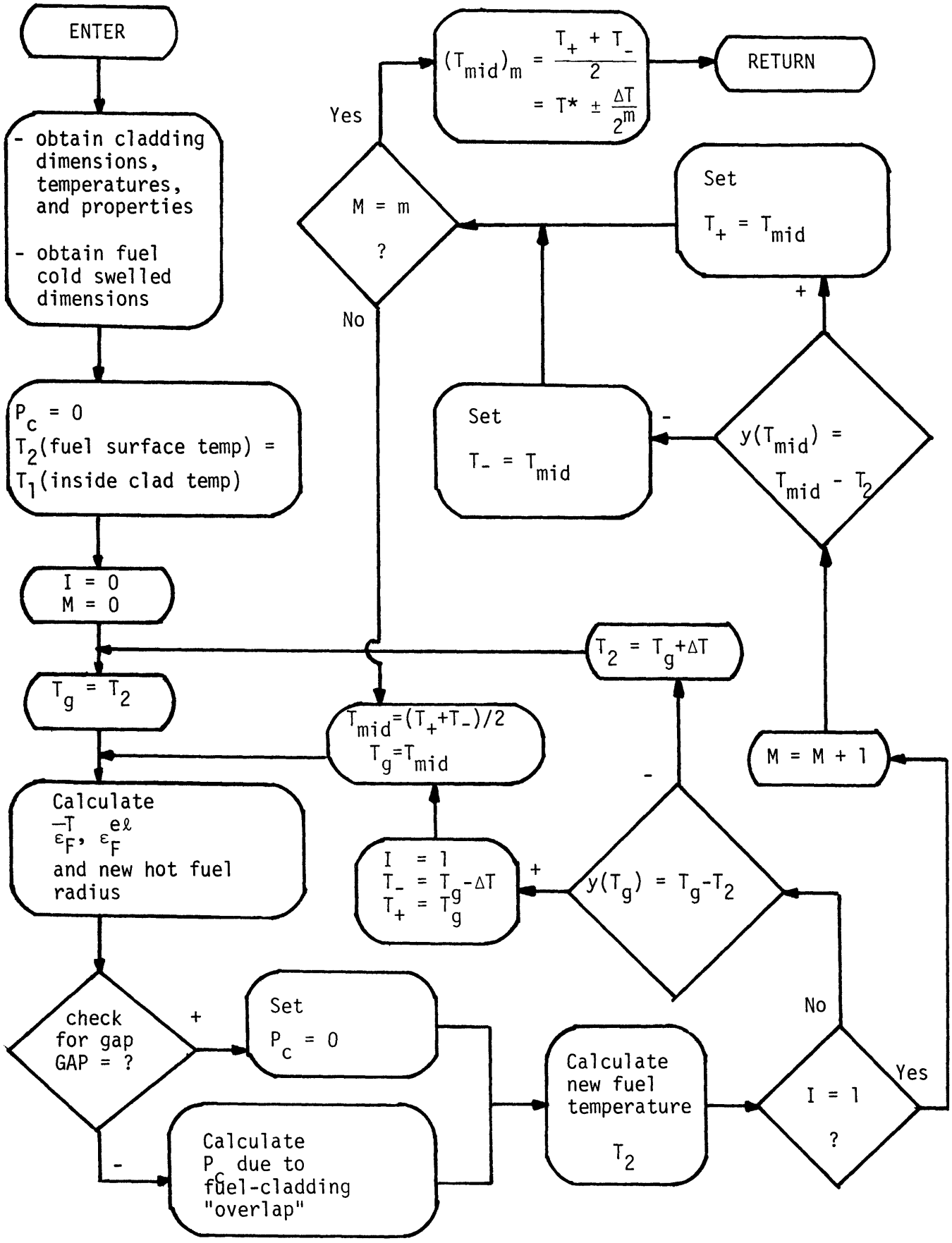

Figure 3-5 Pellet Surface Temperature Solution Strategy Using the Bi-Section Convergence Method.

$y(T_{mid}) < 0$, replace T_- by T_{mid};

$y(T_{mid}) > 0$, replace T_+ by T_{mid}.

This replacement procedure is repeated m times to achieve a final temperature of the accuracy

$$(T_{mid})_m = T^* \pm \Delta T/2^m$$

Although the above solution procedure is specialized for a monotonically increasing function whose initial value, $y(T_g)$, is negative, it establishes a format which may be easily altered to accomodate other cases.

The bi-section method is used to solve for cladding temperature profile and fuel pellet surface temperature. Figure 3-5 illustrates the pellet surface temperature solution strategy. Once this temperature is known, all other variables which characterize the state of the fuel element are known.

3.6.2 Numerical Solution of Creep Rate Equations

The radial and tangential creep strain rate components are solved using a combination of numerical techniques (Ref. 10). The primary solution method is that of Adams-Moulton, but initiation of this method requires the knowledge of four starting values for each strain rate component. These values are generated using a fourth order Runge-Kutta starting method. The component creep strains are solved for simultaneously using the following rate relations inferred from the creep flow rules of Section 3.3.2,

$$\begin{bmatrix} \dot{\varepsilon}^c_r \\ \dot{\varepsilon}^c_\theta \end{bmatrix} = \frac{\dot{\varepsilon}_g}{2\sigma_g} \begin{bmatrix} 2 & -1 & -1 \\ -1 & 2 & -1 \end{bmatrix} \begin{bmatrix} \sigma_r \\ \sigma_\theta \\ \sigma_z \end{bmatrix}$$

where

$\dot{\varepsilon}^c_r$ = radial component of creep strain rate; and

$\dot{\varepsilon}^c_\theta$ = tangential component of creep strain rate.

All other symbols are defined therein.

The fourth order Runge-Kutta method utilizes the following algorithms

$$\varepsilon^c_{r,n+1} = \varepsilon^c_{r,n} + \frac{\Delta t}{6}(\alpha_1 + 2\alpha_2 + 2\alpha_3 + \alpha_4)$$

$$\varepsilon^c_{\theta,n+1} = \varepsilon^c_{\theta,n} + \frac{\Delta t}{6}(\beta_1 + 2\beta_2 + 2\beta_3 + \beta_4)$$

where

$$\alpha_1 = \dot{\varepsilon}^c_{r,n} = \dot{\varepsilon}^c_r(\varepsilon^c_{r,n}, \varepsilon^c_{\theta,n}, t_n) \quad ;$$

$$\alpha_2 = \dot{\varepsilon}^c_r\left((\varepsilon^c_{r,n} + \frac{\alpha_1}{2}), (\varepsilon^c_{\theta,n} + \frac{\beta_1}{2}), (t_n + \frac{\Delta t}{2})\right);$$

$$\alpha_3 = \dot{\varepsilon}^c_r\left((\varepsilon^c_{r,n} + \frac{\alpha_2}{2}), (\varepsilon^c_{\theta,n} + \frac{\beta_2}{2}), (t_n + \frac{\Delta t}{2})\right);$$

$$\alpha_4 = \dot{\varepsilon}^c_r\left((\varepsilon^c_{r,n} + \alpha_3), (\varepsilon^c_{\theta,n} + \beta_3), (t_n + \Delta t)\right);$$

and similarly,

$$\beta_1 = \dot{\varepsilon}^c_{\theta,n}$$

$$= \dot{\varepsilon}_\theta(\varepsilon^c_{r,n},\ \varepsilon^c_{\theta,n},\ t_n);$$

$$\beta_2 = \dot{\varepsilon}^c_\theta((\varepsilon^c_{r,n} + \frac{\alpha_1}{2}),\ (\varepsilon^c_{\theta,n} + \frac{\beta_1}{2}),\ (t_n + \frac{\Delta t}{2}));$$

$$\beta_3 = \dot{\varepsilon}^c_\theta((\varepsilon^c_{r,n} + \frac{\alpha_2}{2}),\ (\varepsilon^c_{\theta,n} + \frac{\beta_2}{2}),\ (t_n + \frac{\Delta t}{2}));\ \text{and}$$

$$\beta_4 = \dot{\varepsilon}^c_\theta((\varepsilon^c_{r,n} + \alpha_3),\ (\varepsilon^c_{\theta,n} + \beta_3),\ (t_n + \Delta t)).$$

Other symbol definitions are,

n = 0, 1, 2, 3 = step sequence from beginning of solution;

t_n = time to the nth step in consistent core equivalent full power time units;

Δt = selected time increment in consistent core equivalent full power time units;

and the quantities at the beginning of the solution, $\varepsilon^c_{r,o}$, $\varepsilon^c_{\theta,o}$, and t_o are known. Time interval selection and estimated accuracy are discussed at the end of this section.

Once the first four creep strain and strain rate values for each component have been obtained, the remainder of the solution may be performed using Adams-Moulton method. This procedure involves a predictor-corrector concept, which for the radial component is,

Predictor:

$$\varepsilon^c_{r,n+1} = \varepsilon^c_{r,n} + \frac{\Delta t}{24}\,(55\ \dot{\varepsilon}^c_{r,n} - 59\ \dot{\varepsilon}^c_{r,n-1} + 37\ \dot{\varepsilon}^c_{r,n-2} - 9\ \dot{\varepsilon}^c_{r,n-3});$$

Corrector:

$$\varepsilon^{c}_{r,n+1} = \varepsilon^{c}_{r,n} + \frac{\Delta t}{24}\left(9\,\dot{\varepsilon}^{c}_{r,n+1} + 19\,\dot{\varepsilon}^{c}_{r,n} - 5\,\dot{\varepsilon}^{c}_{r,n-1} + \dot{\varepsilon}^{c}_{r,n-2}\right);$$

and a similar set of relations for the tangential component.

Two convergence restrictions are placed on the time interval selection for the Adams-Moulton method. They are,

$$\Delta t < \frac{8/3}{|\dot{\varepsilon}^{c}_{r \text{ or } \theta,n}|} \quad ;$$

and

$$\left[\left(\varepsilon^{c}_{r \text{ or } \theta,n+1}\right)_{\text{corrector}} - \left(\varepsilon^{c}_{r \text{ or } \theta,n+1}\right)_{\text{predictor}}\right] \cdot 10^{N} < \frac{8/3}{\Delta t|\dot{\varepsilon}^{c}_{r \text{ or } \theta,n}|}$$

with the accuracy criterion

$$\left[\left(\varepsilon^{c}_{r \text{ or } \theta,n+1}\right)_{\text{corrector}} - \left(\varepsilon^{c}_{r \text{ or } \theta,n+1}\right)_{\text{predictor}}\right] \cdot 10^{N} < 14$$

where N is an indication of decimal place accuracy. Typical strain rate values are in the range of 10^{-6} - $10^{-8}(\text{hr})^{-1}$ for stainless steel and 10^{-4} - 10^{-7} $(\text{hr})^{-1}$ for Zircaloy. The upper end values correspond to maximum creep acceleration factors (on the order of 100) and generalized stress values ($\sim$200 MPa), indicative of extreme conditions. Using these values, a conservative estimate of predictor-corrector differences is,

10^{-6} Δt for stainless steel; and

10^{-4} Δt for Zircaloy;

where $\Delta t < 10$ (hr) for the majority of computer calculations. Substitution into the above convergence and accuracy relations shows that the convergence criteria is easily satisfied and the limiting decimal place accuracy is

$N = 6$ for stainless steel; and

$N = 4$ for Zircaloy.

For the cases investigated in this study, 7th and 5th place accuracies (for stainless steel and Zircaloy, respectively) are more realistic estimates. Since the local errors associated with both solution methods are of the same order, the Runge-Kutta starting method is assumed to have similar accuracies.

4. ILLUSTRATIVE EXAMPLES

This chapter highlights the results of calculations made using the STRESS code. In most cases, the Zircaloy clad fuel results are presented so that a comparison may be made between this material and stainless steel. The effects of different fill gas prepressurization and cladding creep rate are also investigated for certain cases.

As mentioned in Section 3.1, the stainless steel and Zircaloy case historical data used in these calculations is provided as block data. Some of this information is displayed in Figs. 3-2 and 3-3 while the remainder may be found in the code listing (Appendix D). Other characterizing data may also be found therein. It should be noted that the following stainless steel results pertain to assembly 8-H22.

4.1 Creep-down Predictions

Pellet cladding mechanical interaction (and its associated deleterious effects) is probably the major contributor to fuel element failure. Therefore, it is important to know when hard pellet-clad contact takes place. For instance, if a utility experiences what they feel is PCMI related failures, it is important to know which batches are the most likely candidates.

Figures 4-1a and b show the creepdown to contact predictions of the STRESS code for stainless steel using a creep acceleration factor of 11 (Ref. 11). Both pressurized and unpressurized cases are presented as indicated. The upper line represents the inside cladding radius and the lower, the fuel outside radius. The cladding is forced to creep inward since the bulk coolant pressure is much greater than the internal rod pressure. The creep rate appears constant within a

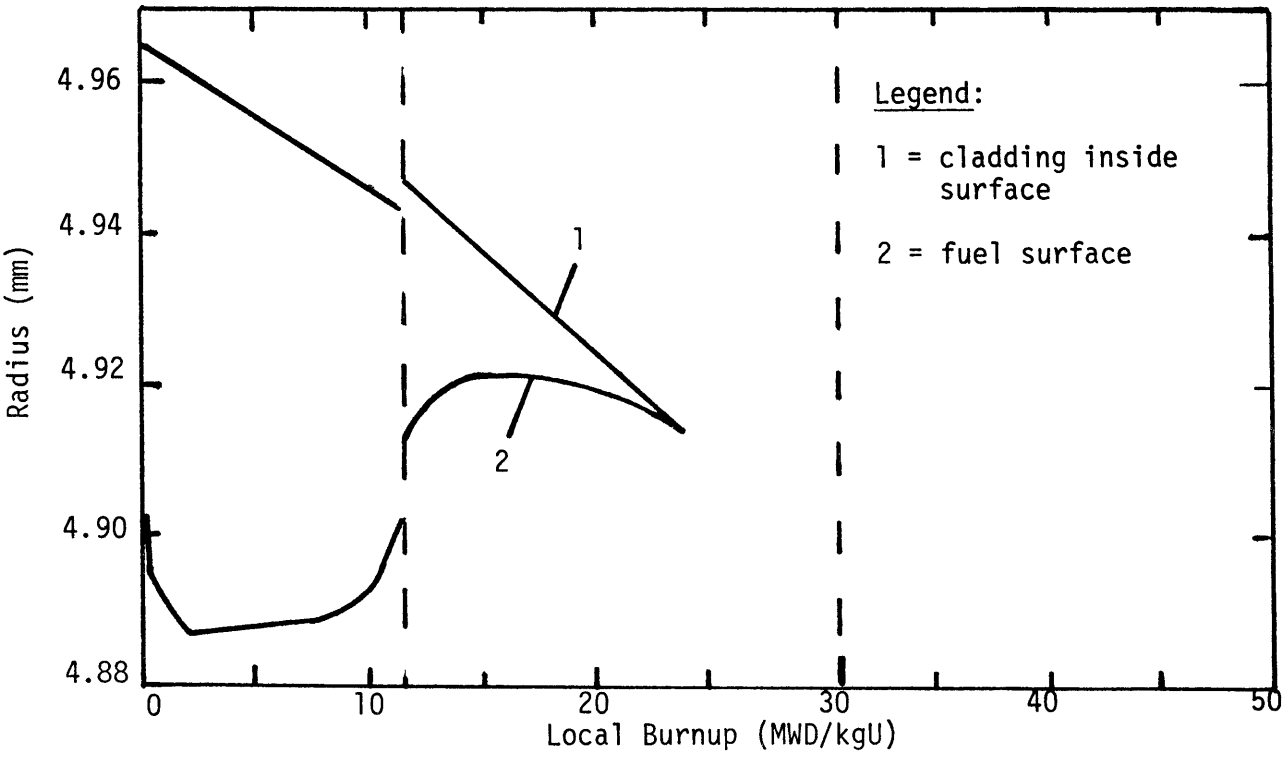

Figure 4-1a Unpressurized SS304 cladding creepdown behavior for a creep acceleration factor of 11 (fill gas pressure = 101 kPa)

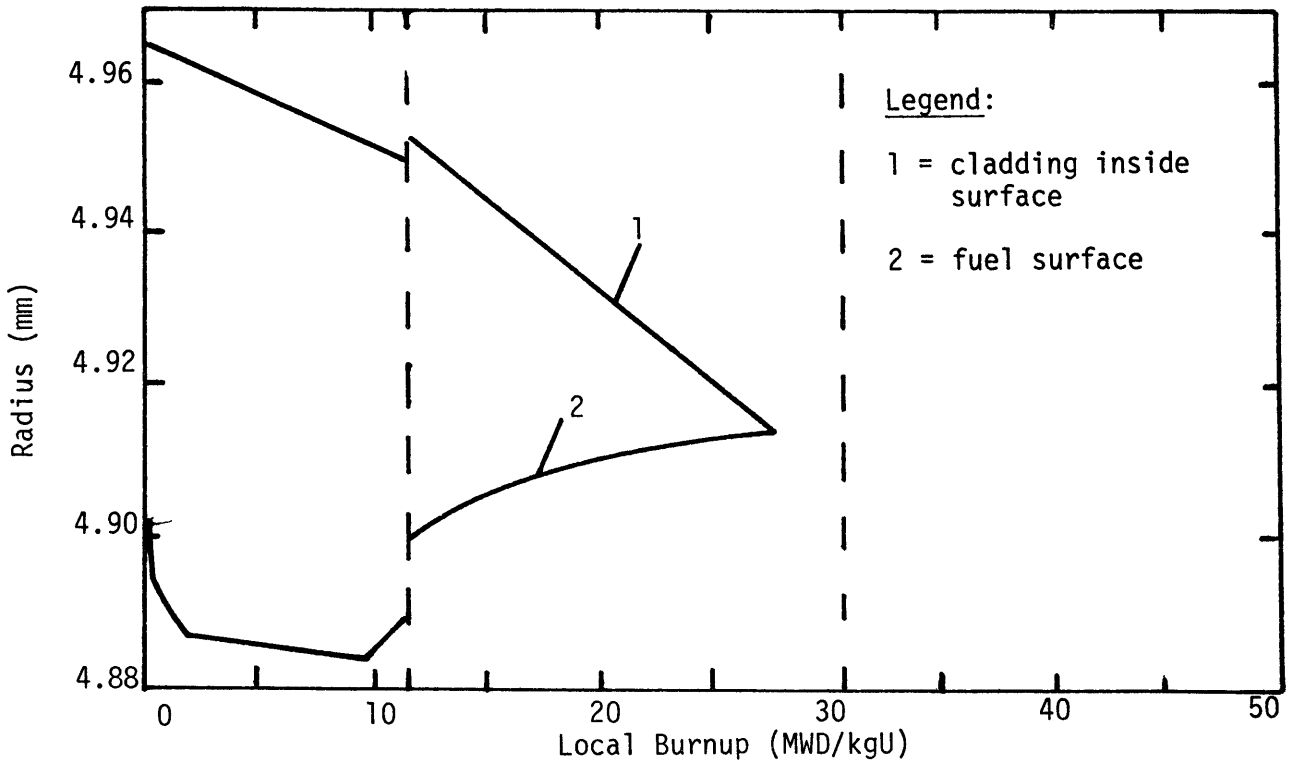

Figure 4-1b Pressurized SS304 cladding creepdown behavior for a creep acceleration factor of 11 (fill gas pressure = 2068 kPa)

cycle, but differs from cycle to cycle due to a variation in fast flux. The discontinuity between the first and second cycle curves is due to fuel and cladding thermal expansion (increased LHGR).

The fuel initially densifies and after 10 MWD/kgU begins to swell. Contact occurs in the region of fuel swelling although the fuel appears to be densifying. The fuel is actually thermally contracting due to gap closure and increased gap conductivity. Comparing the results of both pressurizations shows that the prepressurized rod has an extended contact burnup of about 4 MWD/kgU (local).

Figures 4-2a and b show the creepdown to contact predictions for stainless steel in the absence of accelerated creep. Pellet clad contact does not occur until well into the third cycle. It should be mentioned that the results do not show this cycle in its entirety.* This is the reason for the extrapolated curves in the prepressurized case. A review of these figures and those for accelerated creep (Figs. 4-1a and b) predict that hard contact is expected to occur in the latter second to third cycles.** Preliminary cladding outside diameter measurements (selected batch 8 fuel rods) favor the accelerated creep results.

Maine Yankee (Ref. 5) has predicted contact for Zircaloy at about 25 MWD/kgU. A similar conclusion was reached using the Zircaloy creep relation of Section A.6 with no creep acceleration. Details of this calculation are not included in this report.

---

* This information was not available for the remainder of cycle 8 (denoted "third cycle").

** Regions near pellet interfaces are expected to contact earlier if local effects (i.e., pellet hourglassing) are considered (see Section 4.3.1).

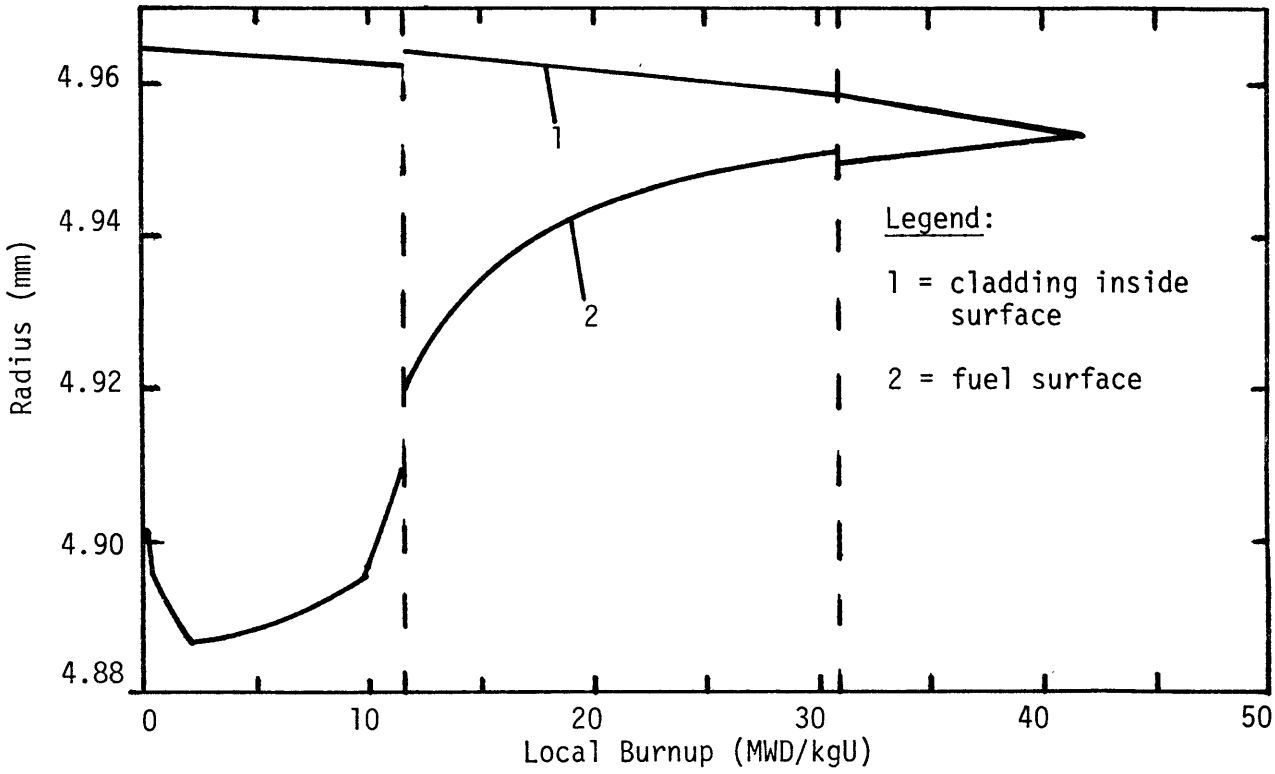

Figure 4-2a Unpressured SS304 cladding creepdown behavior without accelerated creep (fill gas pressure = 101 kPa)

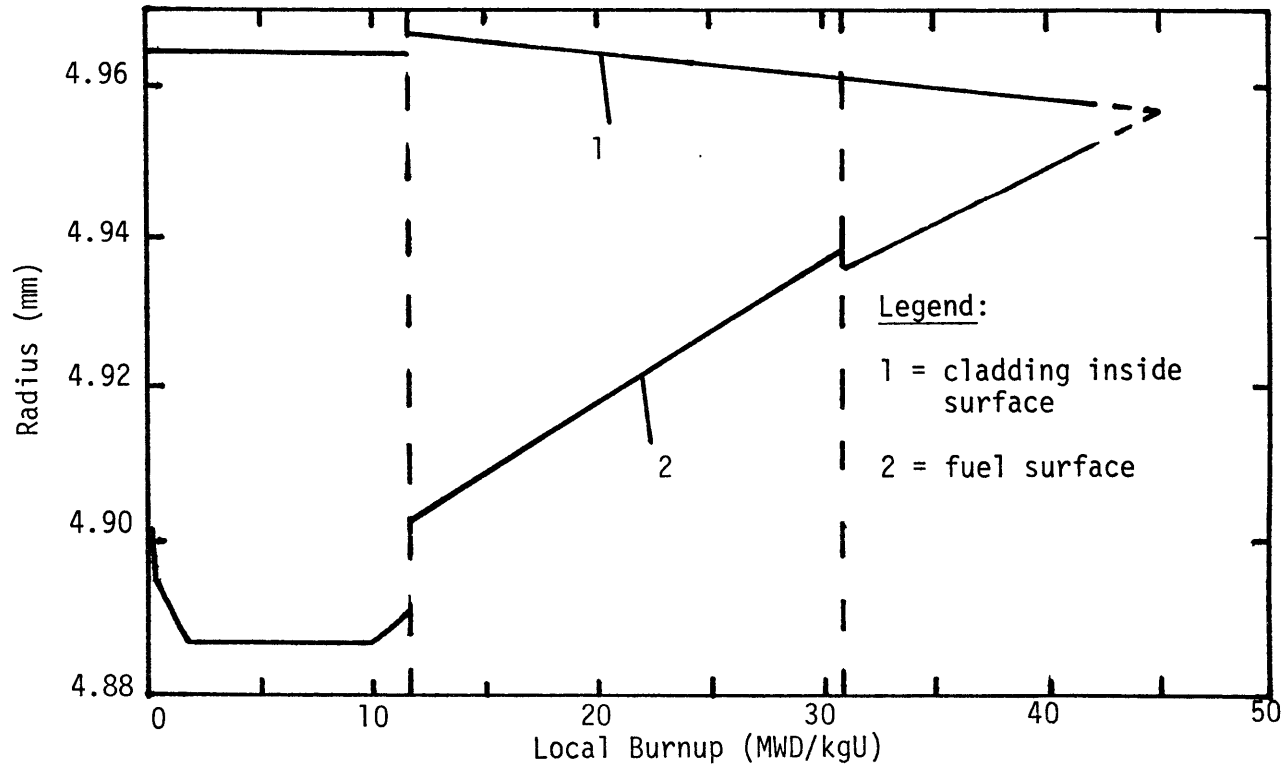

Figure 4-2b Pressurized SS304 cladding creepdown behavior without accelerated creep (fill gas pressure = 2068 kPa)

4.1.1 Temperature Predictions

Some of the benefits of prepressurization may be realized by examining the behavior of fuel surface and centerline temperatures for both fill pressurization cases during cladding creepdown to contact. Figure 4-3 illustrates the differences in temperature behavior as predicted by the STRESS code for a creep acceleration factor of 11. Initially, both pressurization levels exhibit similar behavior since the fission gas inventory is minimal.* In each case, the fuel temperature increases rapidly at BOL due to increasing gap size from fuel densification. As burnup continues, the increasing amounts of fission gas have a greater impact on the gap conductivity of the unpressurized rod since the initial amount of helium fill moles is less. The result is higher fuel temperatures regardless of the increased gap closure as indicated in the previous section.

If the temperature range for equiaxed grain growth is 1300-1650°C and 1700-2150°C for columnar growth (Ref. 12), the centerline temperatures of the unpressurized case extend well into the fuel restructuring regimes over substantial periods of time (burnup). The non-accelerated creep case (Figs. 4-2a and b) would yield higher temperatures over longer periods of burnup. The benefits of prepressurization are significant regardless of the creep acceleration.

*Degradation of gap gas conductivity is primarily due to increasing relative amounts of Xenon and Krypton fission gas in the gap gas mixture. It is interesting to note that different pressurization levels of a single component gas has little or no effect on its conductivity (the conductivity relations of Section A.13 show temperature dependence only). Such is the case at or near BOL when helium is the only or primary gas component.

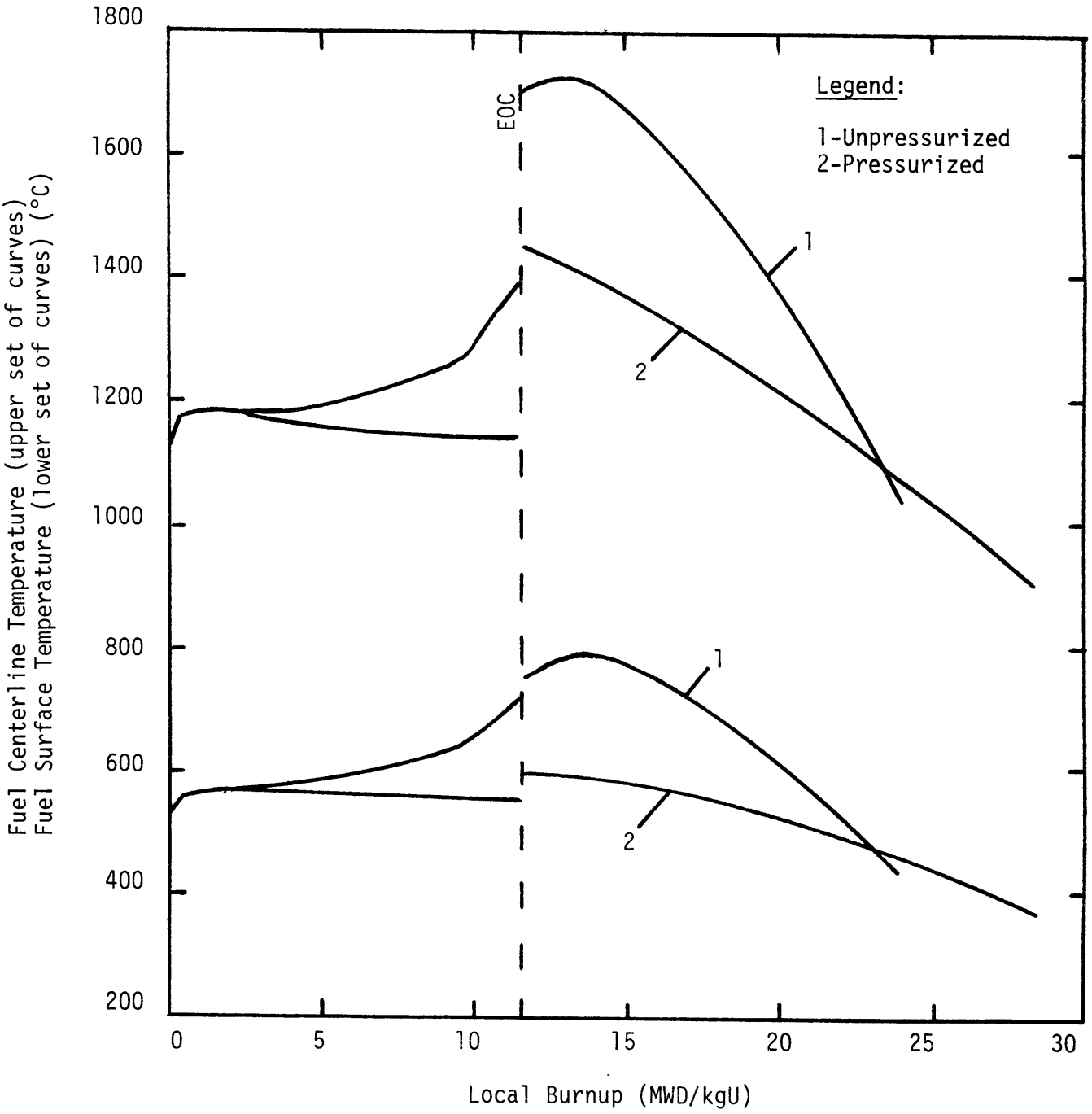

Figure 4-3 Comparison of Fuel Centerline and Surface Temperatures for Pressurized and Unpressurized SS304 Rods

4.2 Cladding Conditioning

The conditioned cladding definition adopted in this study is one in which the cladding inside surface and fuel surface deflection rates are equivalent and constant. If this requirement is met, a steady state constant stress situation exists (and therefore a constant pellet-cladding contact force). The time to achieve this state may be termed "conditioning time" and is unique, as are the stresses, for different fuel swelling and cladding creep rates. In the STRESS code calculations, a 30 EFPD time limit is placed on conditioning. In other words, if the above steady state stress condition is not achieved within 30 EFPD after just contact, the remaining calculations for that creep model are not based on fully conditioned cladding.

Figure 4-4 shows the hoop stress variation experienced after just contact (in a region of fuel swelling, constant power) for unpressurized stainless steel cladding. The plateau region after just contact for the lower acceleration cases is only evident for unpressurized rods. This is due to marked fuel thermal contraction since the contact conductance plays a major role in overall gap conductivity. The effect of this for the faster creep models appears less significant since this stage occurs rapidly.

The results for higher creep acceleration factors (i.e., 55 and 110) are included as compensation for the effects of fuel restrained swelling, creep deformation, and cracked pellet relocation which has been ignored in the fuel pellet model. In a previous study of Zircaloy conditioning and power ramping (Ref. 13) a creep acceleration factor of about 100 was employed for adequate compensation. Additional results for the pressurized stainless steel and Zircaloy cases are illustrated in Figs. 4-5 and 4-6.

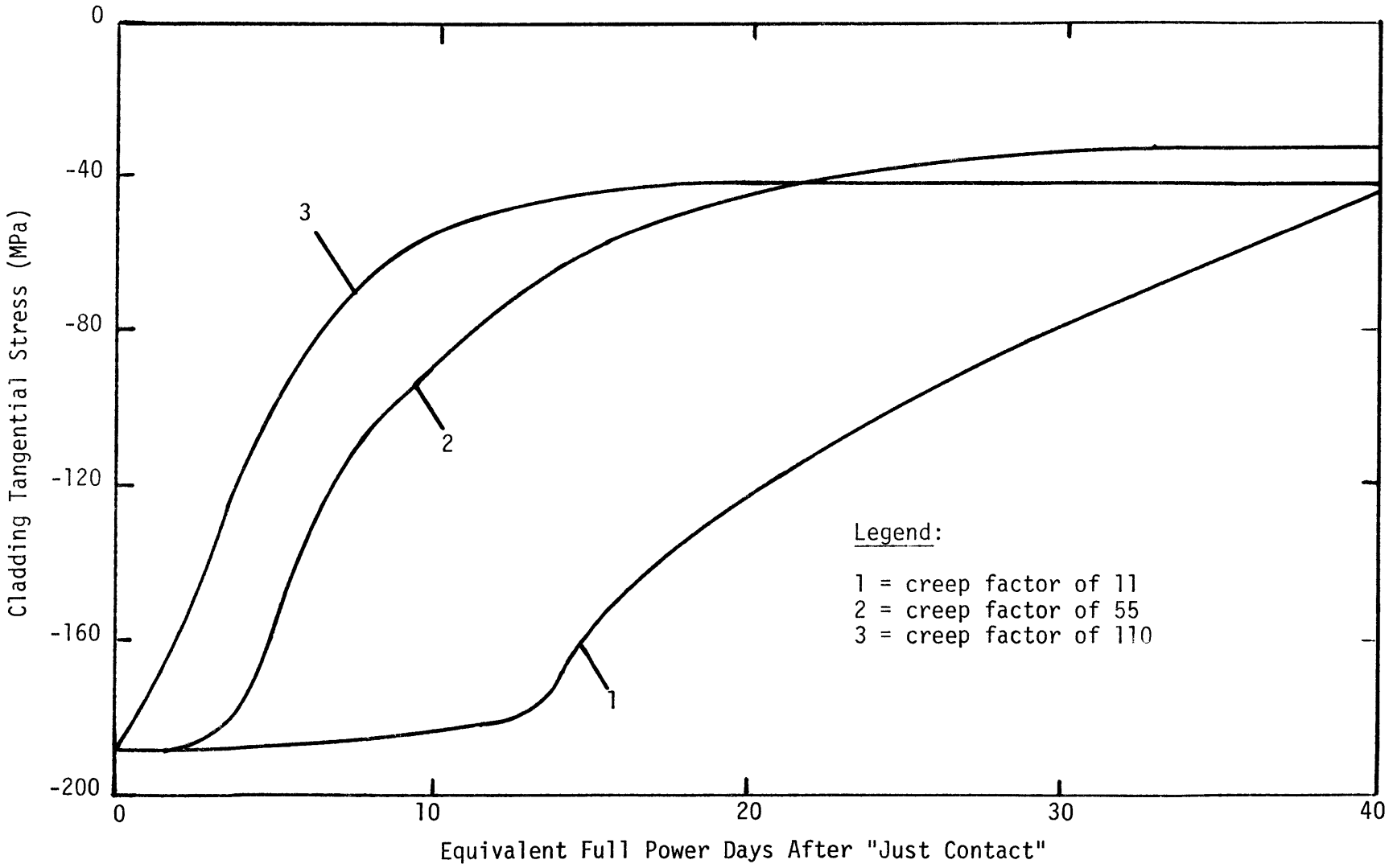

Figure 4-4 Hoop stress variation for unpressurized SS304

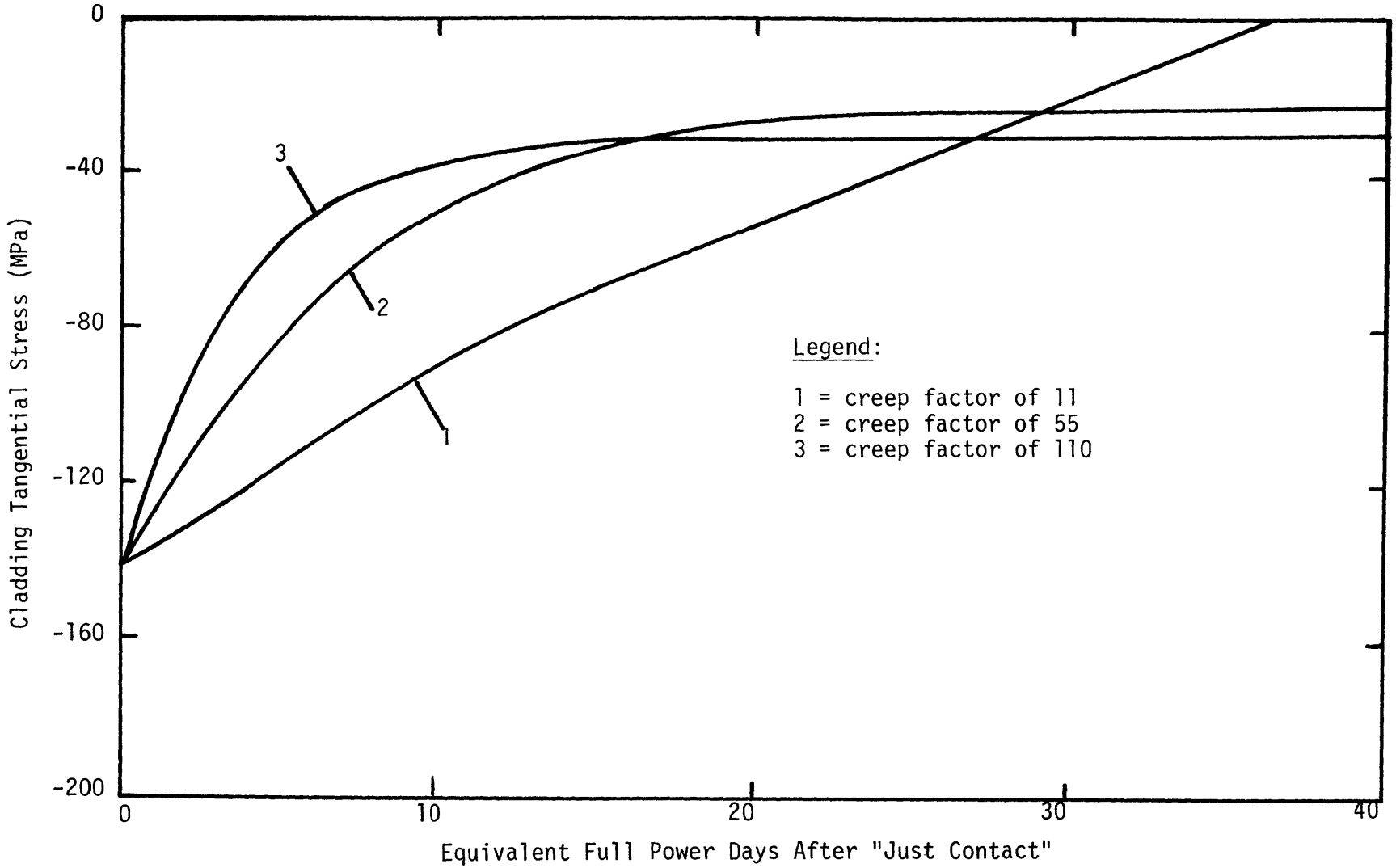

Figure 4-5 Hoop stress variation for pressurized SS304

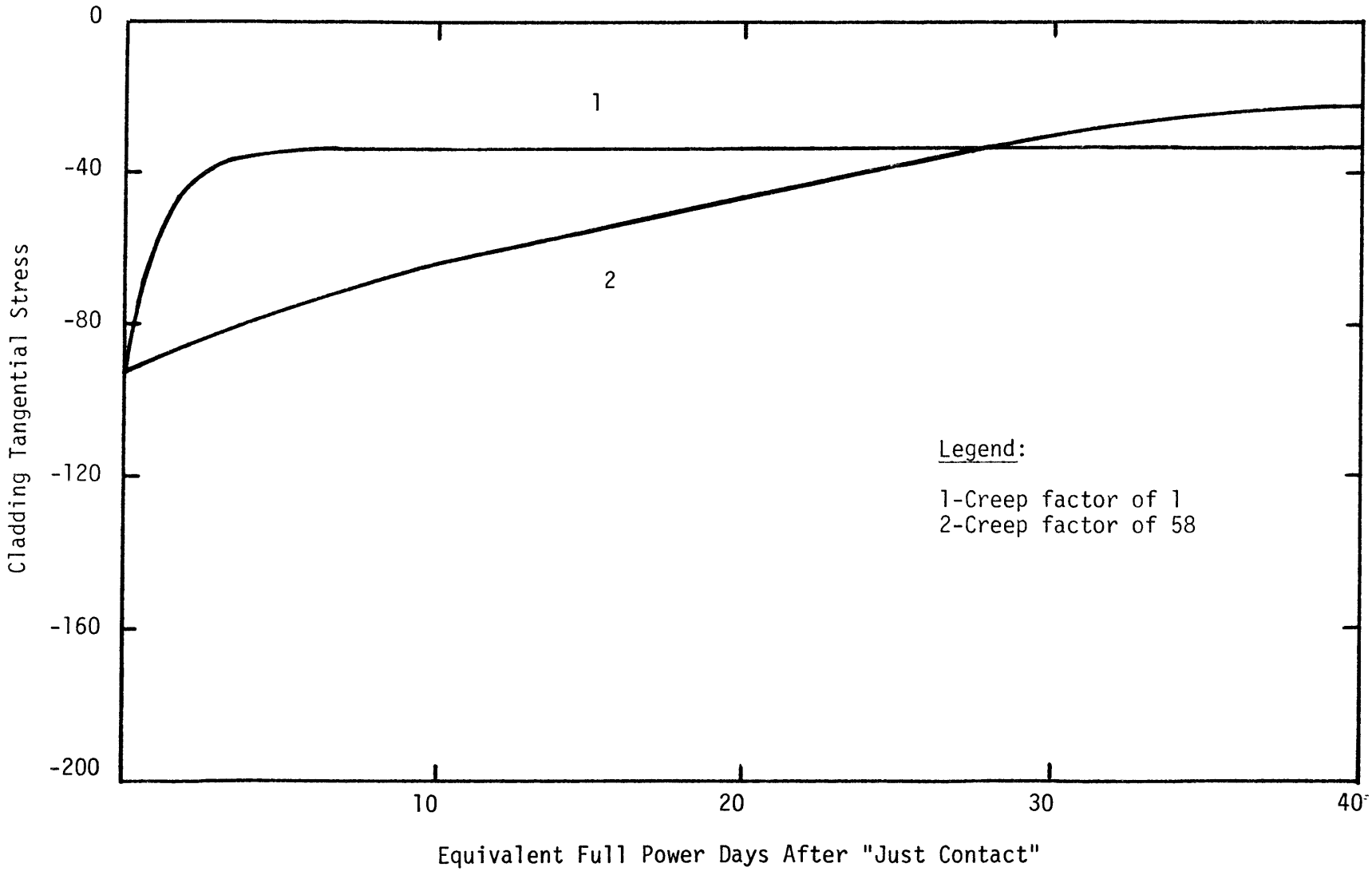

Figure 4-6 Hoop Stress Variation for Pressurized Zircaloy

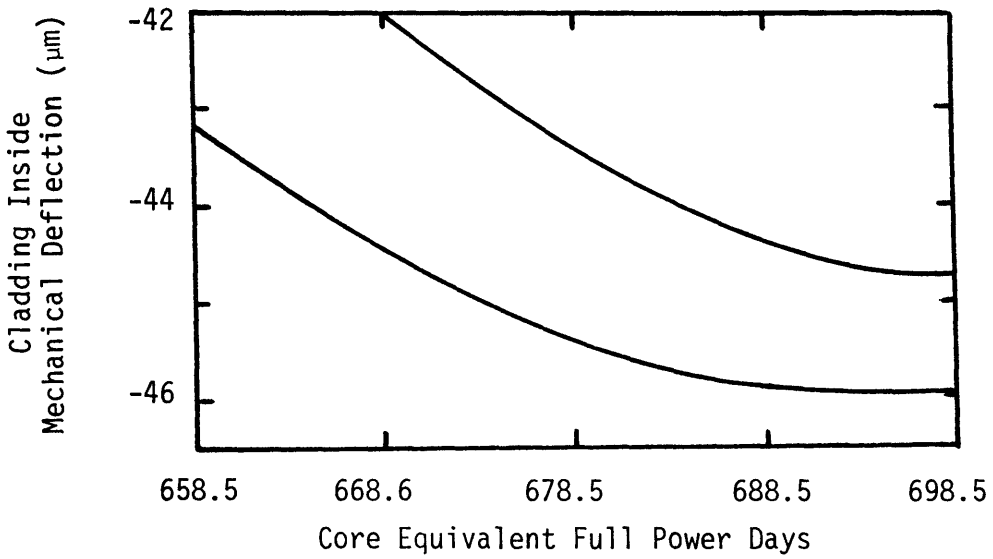

Figure 4-7a Conditioning Deflection Behavior for a Creep factor of 11

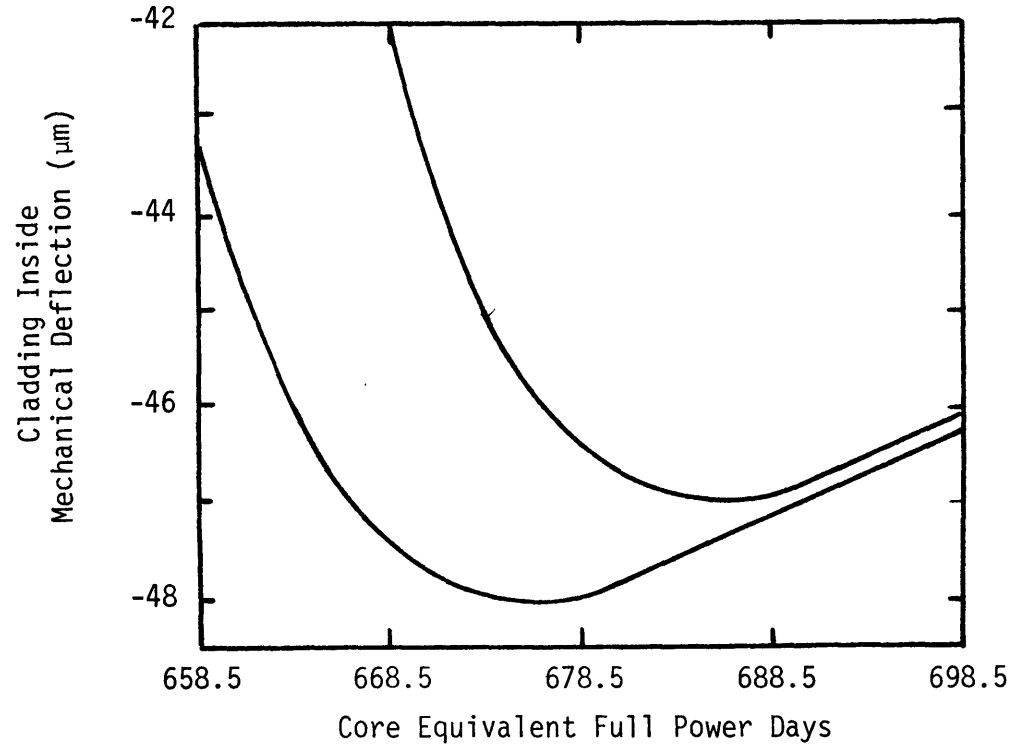

Figure 4-7b Conditioning Deflection Behavior for a Creep Factor of 55

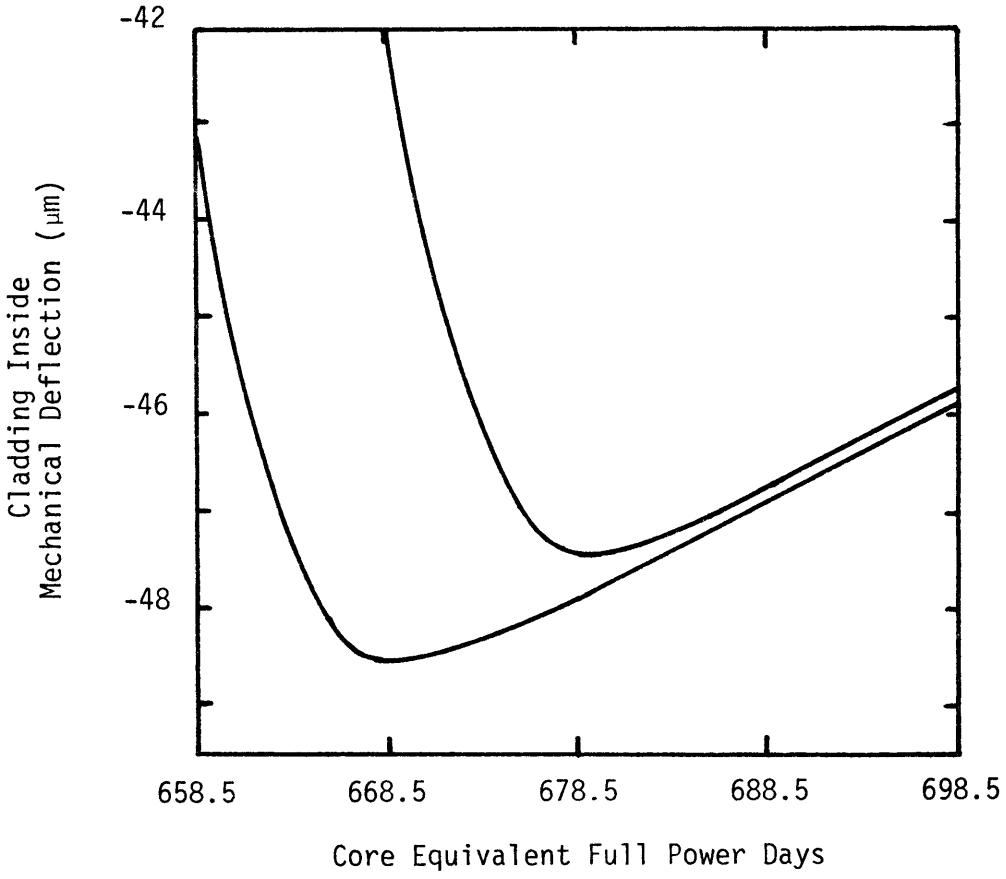

Figure 4-7c Conditioning Deflection Behavior for a Creep Factor of 110

An alternate perspective on the 30 EFPD conditioning phenomenon may be gained by examining Figs. 4-7a,b, and c. The lower curve shows cladding inside mechanical deflection for 40 EFPD after "just contact". The upper curve shows the same but first contact occurs 10 core EFPD later. Complete conditioning for 30 core EFPD should yield insignificant differences between curves at or before 698.5 EFPD.* Figure 4-7a, which corresponds to a creep factor of 11, is the only case where conditioning is not achieved in 30 EFPD. Deflection curves for lower powers yield similar results. It is interesting to note that the steady state hoop stresses are in compression but the cladding is actually mechanically deflecting outward.

4.3 Up Power Ramping

Having a method of conditioning, up power ramps from various lower power conditioned states may be performed and cladding hoop stress variation with different ramp rates may be investigated.** Intuitively, it is expected that low ramp rates or large creep acceleration factors would allow more cladding stress relaxation. In the other extreme, a very rapid power increase would just result in a cladding elastic response with little or no creep deformation/stress relaxation.

Figure 4-8a shows the hoop stresses developed in a 60% preconditioned unpressurized rod ramped to 100% FP at rates ranging from 1%/hr to 50%/hr. The corresponding LHGR values are typical of stainless steel clad fuel recently in the Connecticut Yankee core. These

---

* Note that 688.5 core EFPD (19.45 core MWD/kgU) roughly corresponds to the core average cumulative burnup for batch 8 at the time of the Connecticut Yankee-August 1977 maneuver.

** Cladding hoop stresses are caused by differential pellet-cladding thermal expansion.

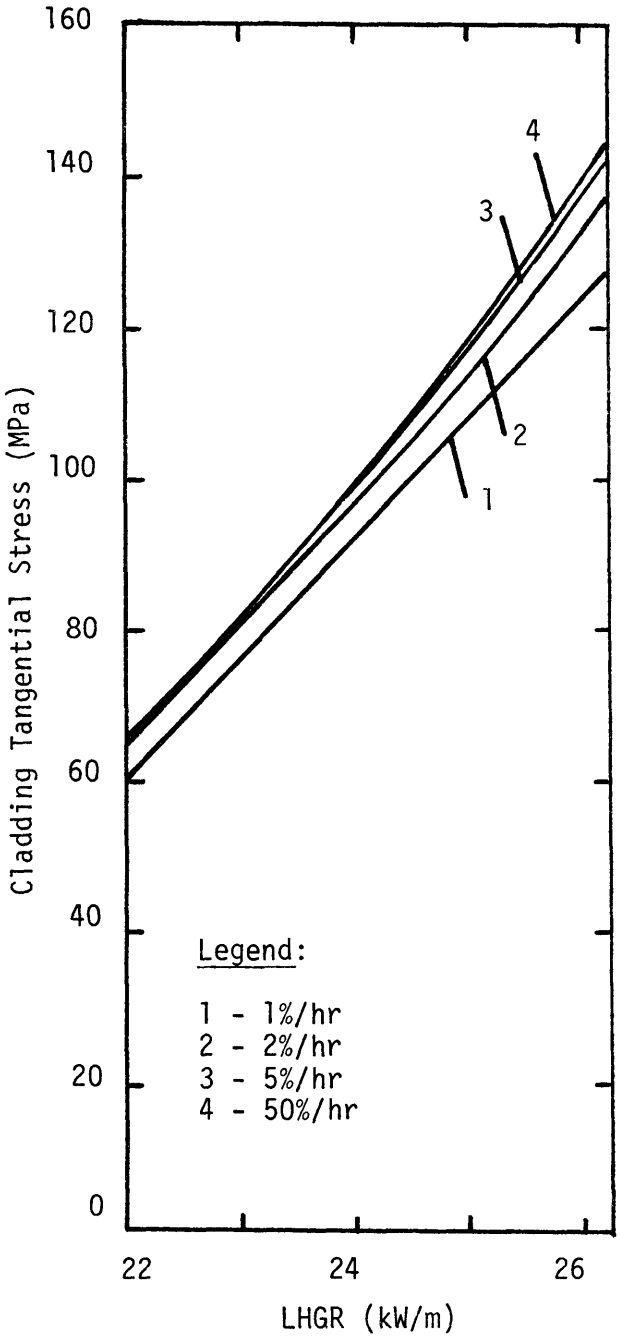

Figure 4-8a Unpressurized SS304 cladding hoop stress behavior for a creep factor of 55 ramping from a 60% conditioned state.

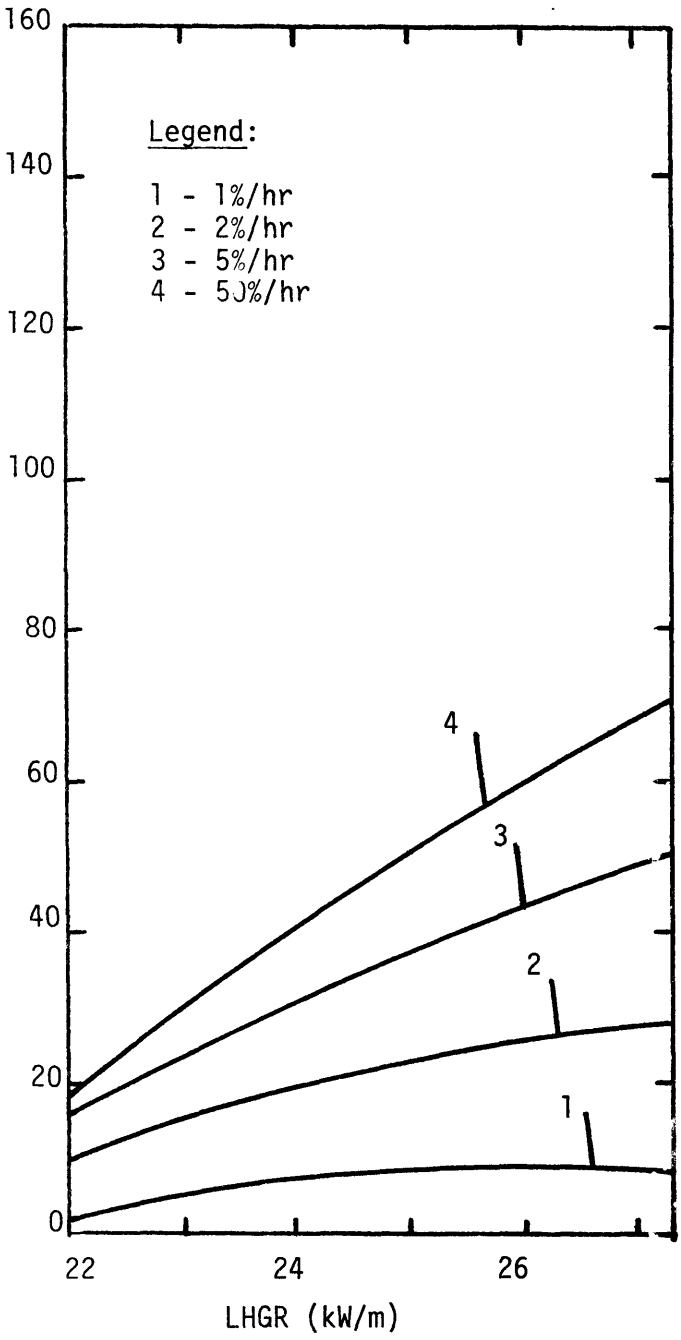

Figure 4-8b Pressurized Zircaloy cladding hoop stress behavior for a creep factor of 58 ramping from a 60% conditioned state.

curves are for a creep acceleration factor of 55 which is about half of the 100 value suggested and used by daSilva for Zircaloy (see Section 4.2). Benefits due to reduced ramp rates are insignificant until 5%/hr or less. The Zircaloy case results are shown in Fig. 4-8b for a 60% pre-conditioned rod using a creep acceleration factor of 58. Notable differences exist between these curves and the stainless steel results. By comparison, Zircaloy cladding exhibits far more stress relaxation. Consequently, stainless steel may be classified as a much more creep resistant material than Zircaloy.

Figures 4-9a and b show the results of unpressurized stainless steel for creep acceleration factors of 11 and 110, respectively. Using the lower creep factor of 11 shows little or no benefit of stress relaxation during these same ramp maneuvers. On the other hand, using a higher creep factor of 110 indicates a good deal of stress relaxation as expected. Once again, however, no significant benefits are realized until 5%/hr or less. Figure 4-10 illustrates the results of a 60% pre-conditioned pressurized stainless steel rod. Comparing the hoop stresses developed in this case with those of the unpressurized case (Fig. 4-8a) show that no major differences exist.

Additional results for 80% pre-conditioned unpressurized stainless steel using creep acceleration factors of 55 and 110 are provided in Figs. 4-11a and b. The hoop stresses developed in these cases are much lower (than the 60% pre-conditioned stress values) since ramping is from a higher conditioned power level. Conversely, ramping from a lower conditioned power level would yield higher hoop stresses.

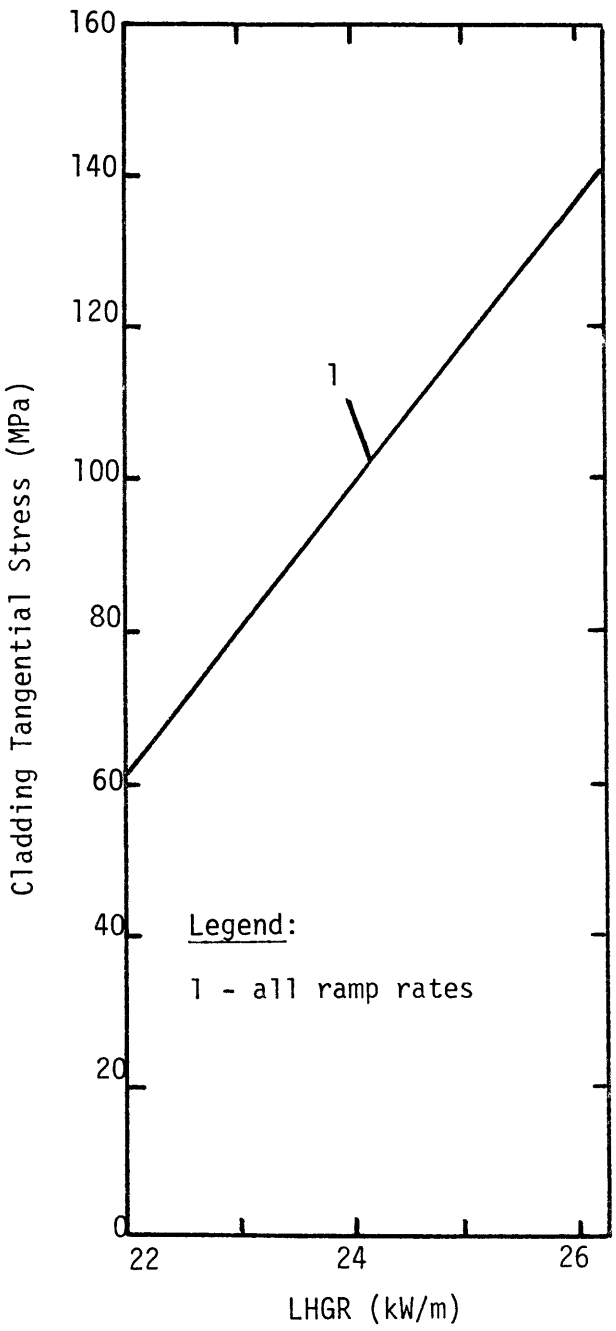

Figure 4-9a Unpressurized SS304 cladding hoop stress behavior for a creep factor of 11 ramping from a 60% conditioned state.

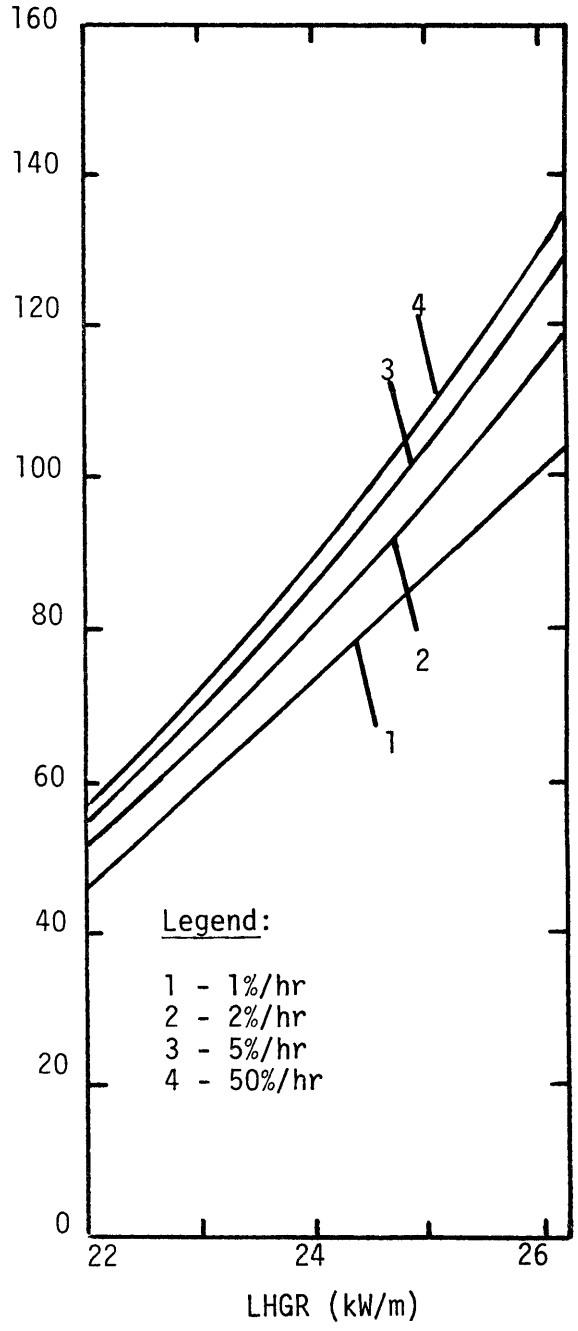

Figure 4-9b Unpressurized SS304 cladding hoop stress behavior for a creep factor of 110 ramping from a 60% conditioned state.

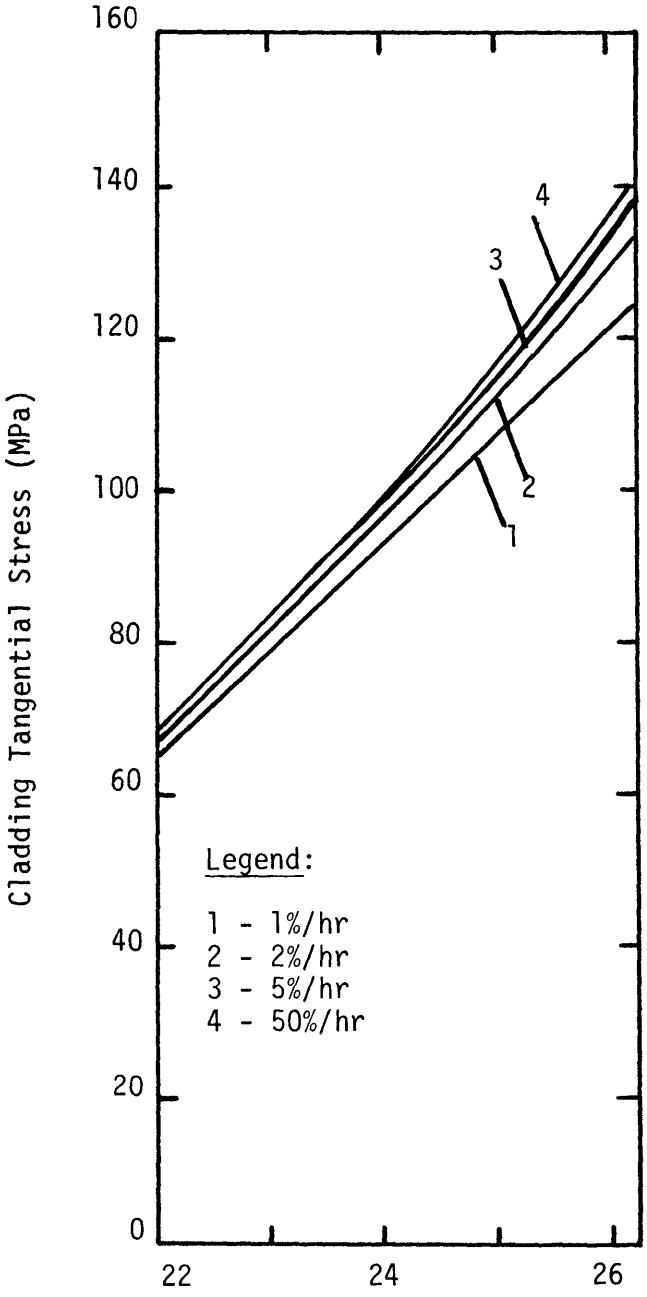

Figure 4-10 Pressurized SS304 cladding hoop stress behavior for a creep factor of 55 ramping from a 60% conditioned state.

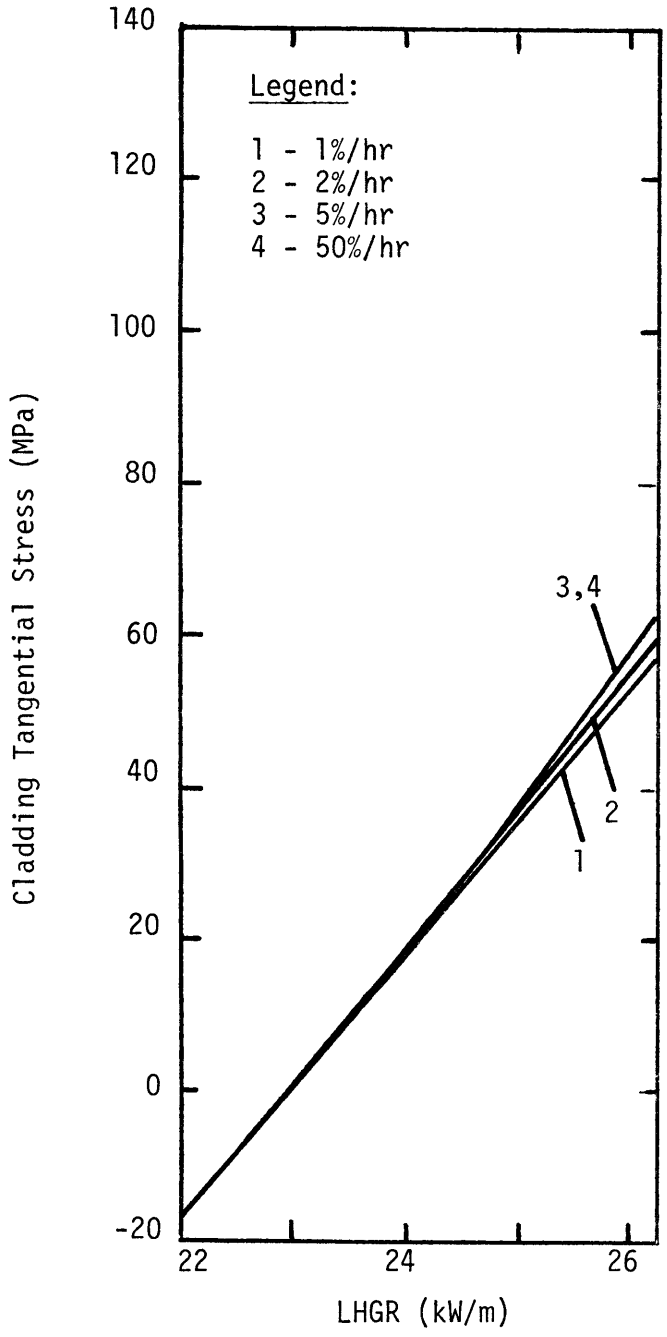

Figure 4-11a Unpressurized SS304 cladding hoop stress behavior for a creep factor of 55 ramping from an 80% conditioned state.

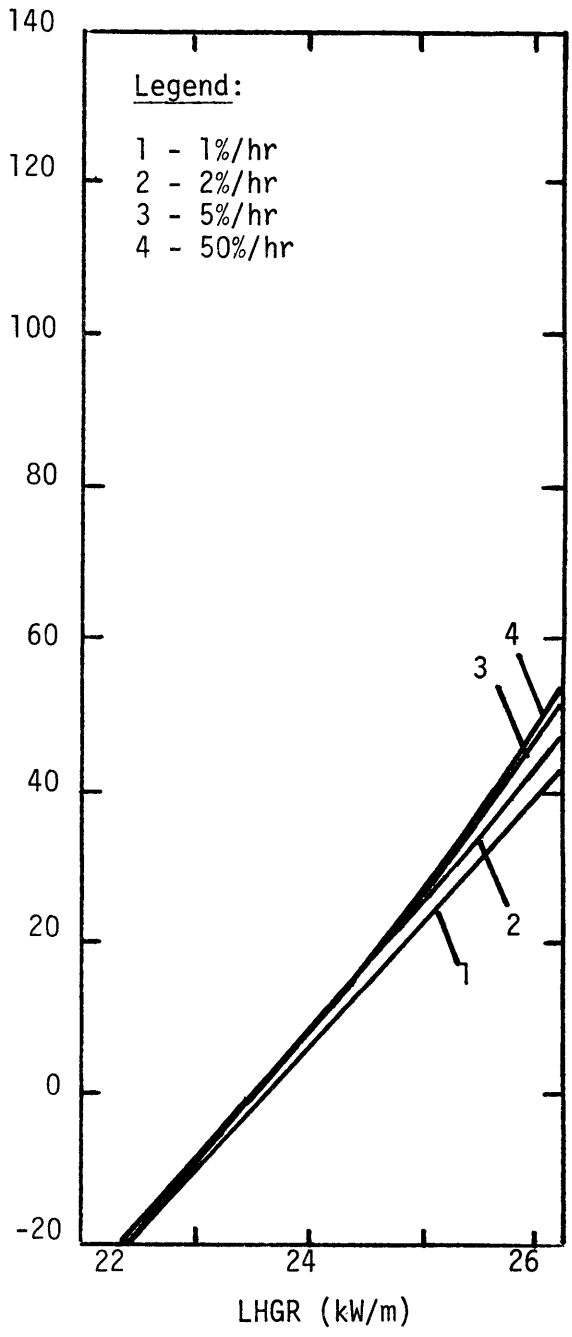

Figure 4-11b Unpressurized SS304 cladding hoop stress behavior for a creep factor of 110 ramping from an 80% conditioned state.

4.4 Connecticut Yankee Maneuver

The Connecticut Yankee - August 1977 power maneuver discussed in Section 2.3 is shown in more detail in Fig. 4-12. This operating event is analyzed by the STRESS code using the modified representation shown in Fig. 4-13. Downtime periods are not included in this model since no fuel-cladding dimensional changes are expected during these times. Small fluctuations in less than full power constant operation are ignored and the only power ramp considered is on return to full power (about a 9% full power per hour ramp rate).

Hoop stress variation during this maneuver for the unpressurized stainless steel case is shown in Fig. 4-14. Differences due to creep acceleration factors of 11, 55, and 110 are also shown. The factor of 11 creep model is the only case in which the cladding is not fully conditioned at the start of the maneuver (hoop stresses are increasing - see the conditioning definition of Section 4.2). For all three cases, an initial reduction in power to 64% opens the gap (hoop stress = -188.5 MPa). The factor of 11 creep model exhibits very little creepdown and maintains an open gap throughout lower power operation until just prior to return to full power. In this case, the increase in hoop stress as a result of this maneuver is not significant and it remains in compression.

The other two creep models recontact within the first couple of days of reduced power operation and begin conditioning at this level. An increase in power to the 70.5% level is accompanied by an increase in stress as expected. Return to full power shows that the hoop stresses for these models change from compression to tension, increasing over 100 MPa from their steady state full power conditioned values. The

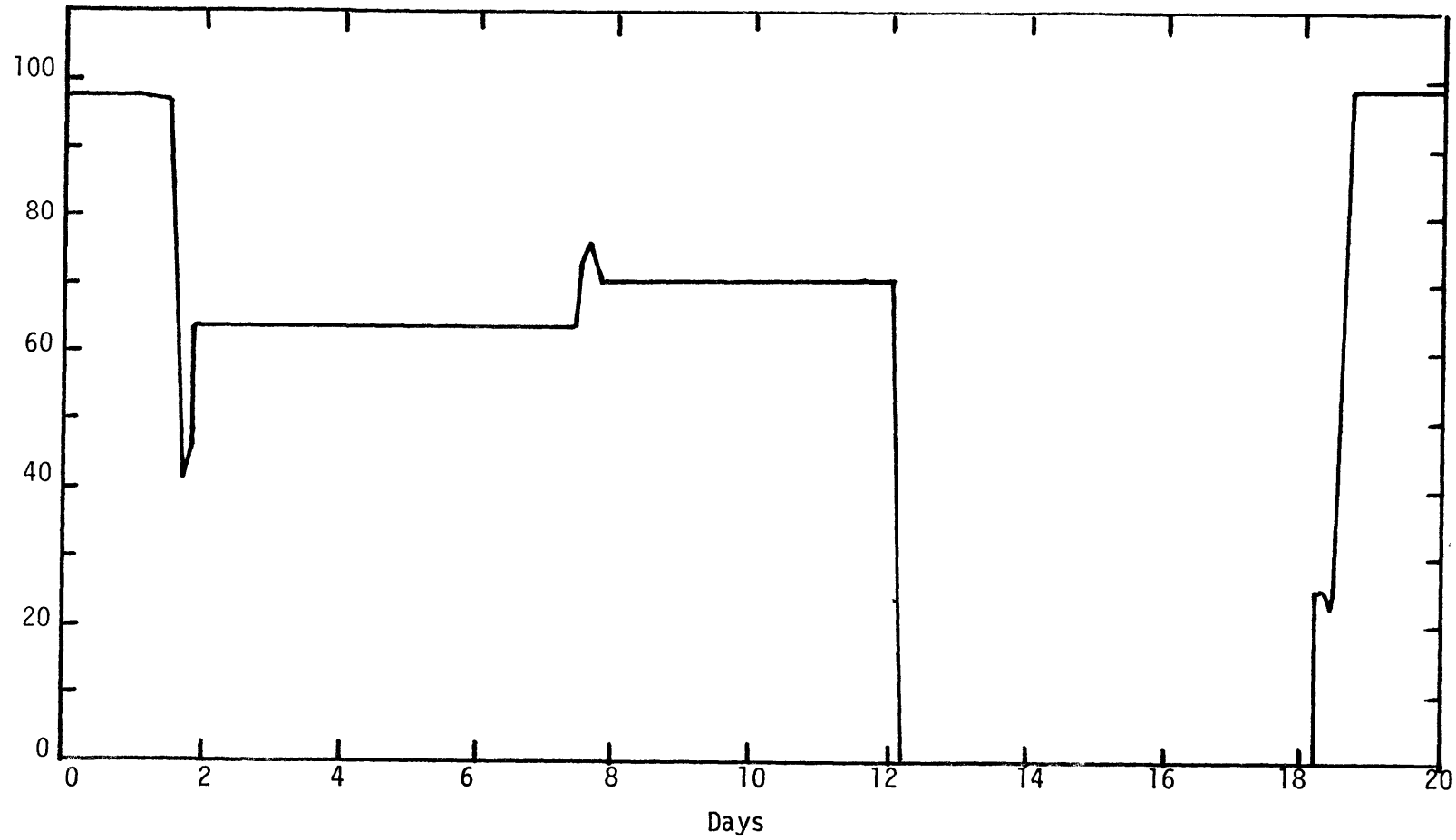

Figure 4-12 Connecticut Yankee power history from August 8 to August 28, 1977.

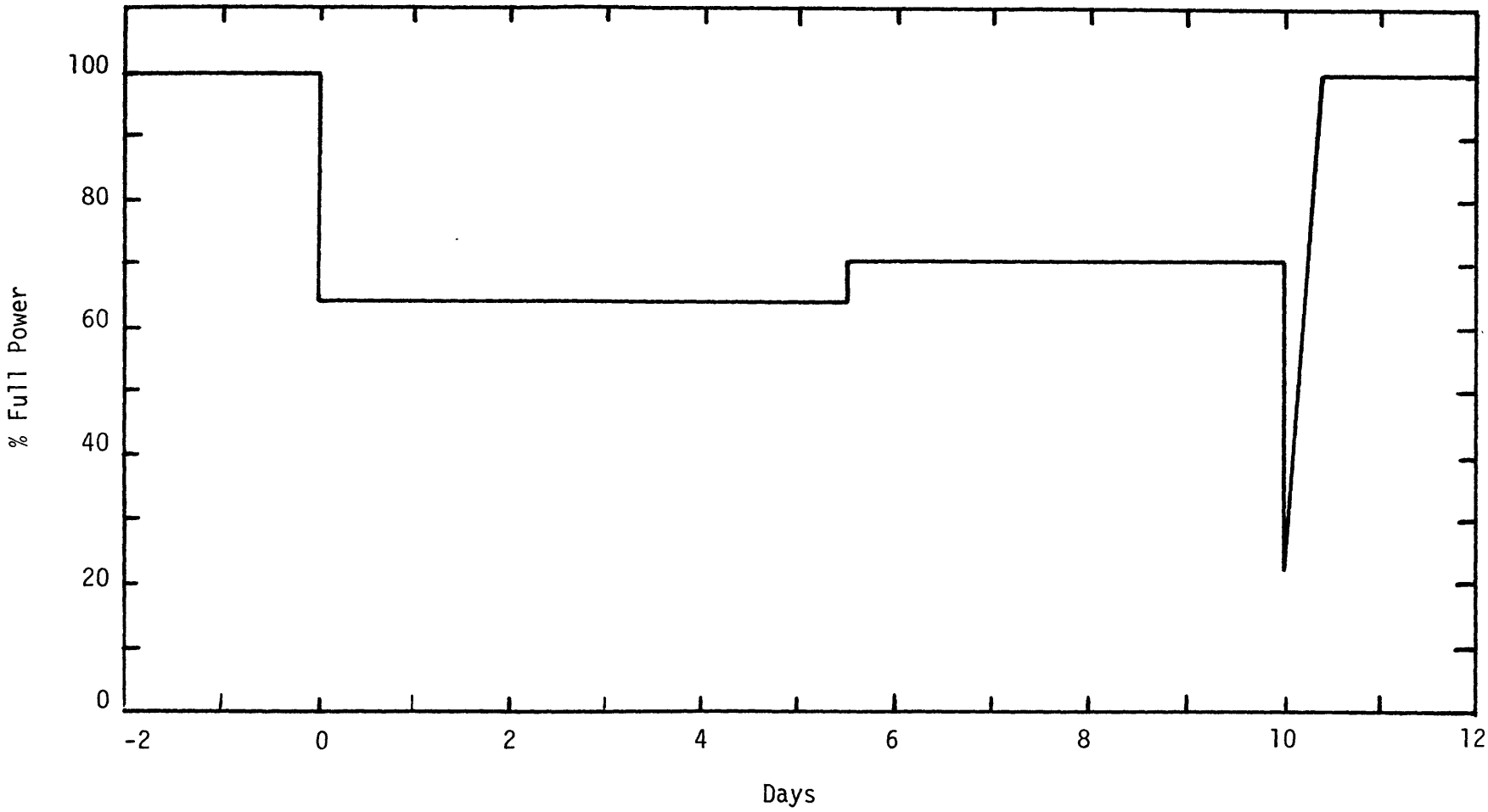

Figure 4-13 Connecticut Yankee Power Maneuver Representation for August 1977.

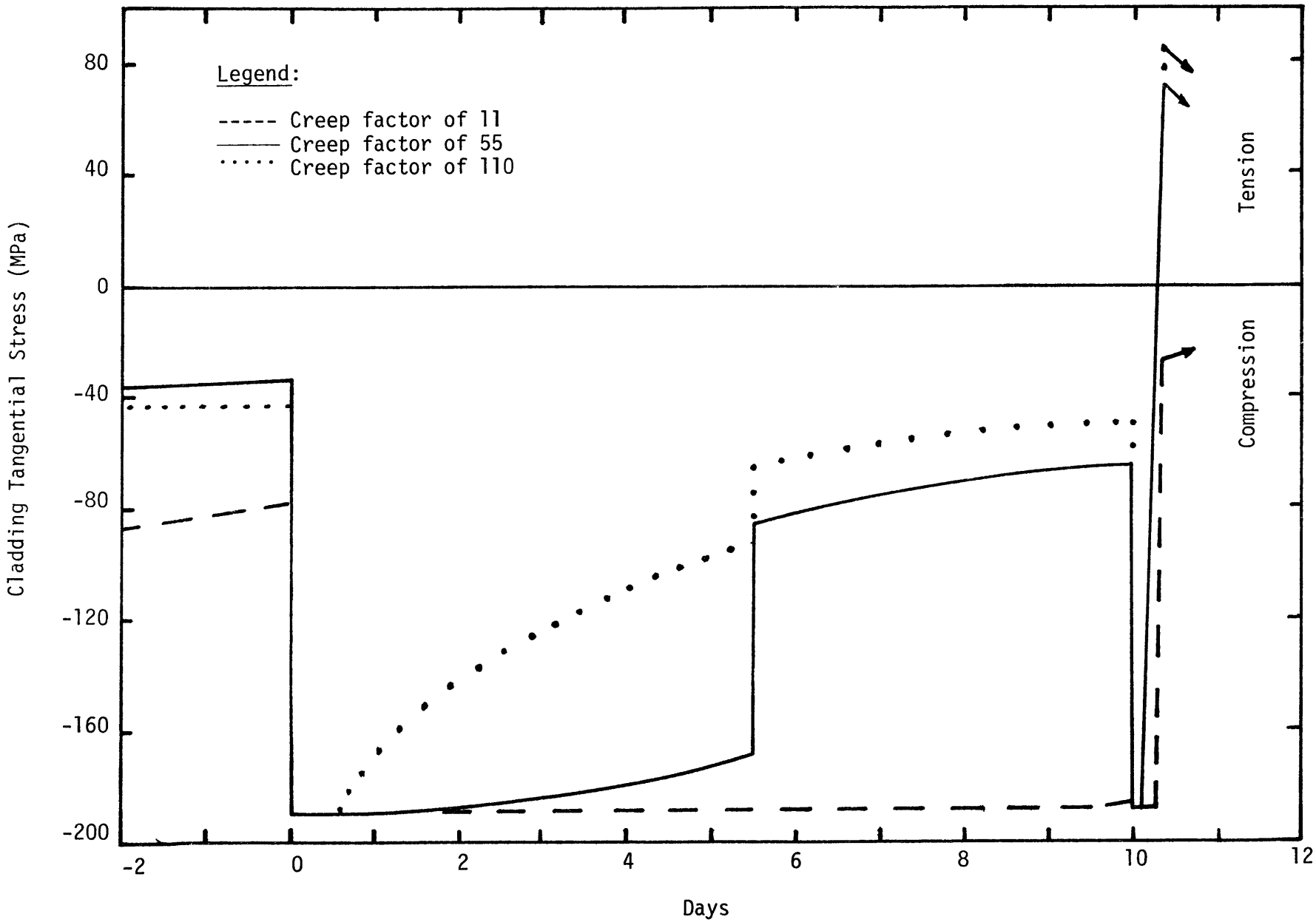

Figure 4-14 Unpressurized SS304 cladding hoop stress behavior for the August 1977 maneuver.

stainless steel pressurized case results, illustrated in Fig. 4-15, show similar behavior (the open gap hoop stress is -142.1 MPa). What is interesting to note is that pressurization has a minimal effect on the predicted end-of-maneuver hoop stress values. Improved behavior, from a stress state point of view, would be indicated by a reduction in these values. The pressurized Zircaloy case results for this maneuver are given in Fig. 4-16 for comparison. Tensile hoop stresses are not as great for this material. This is due to increased stress relaxation and elastic compliance.

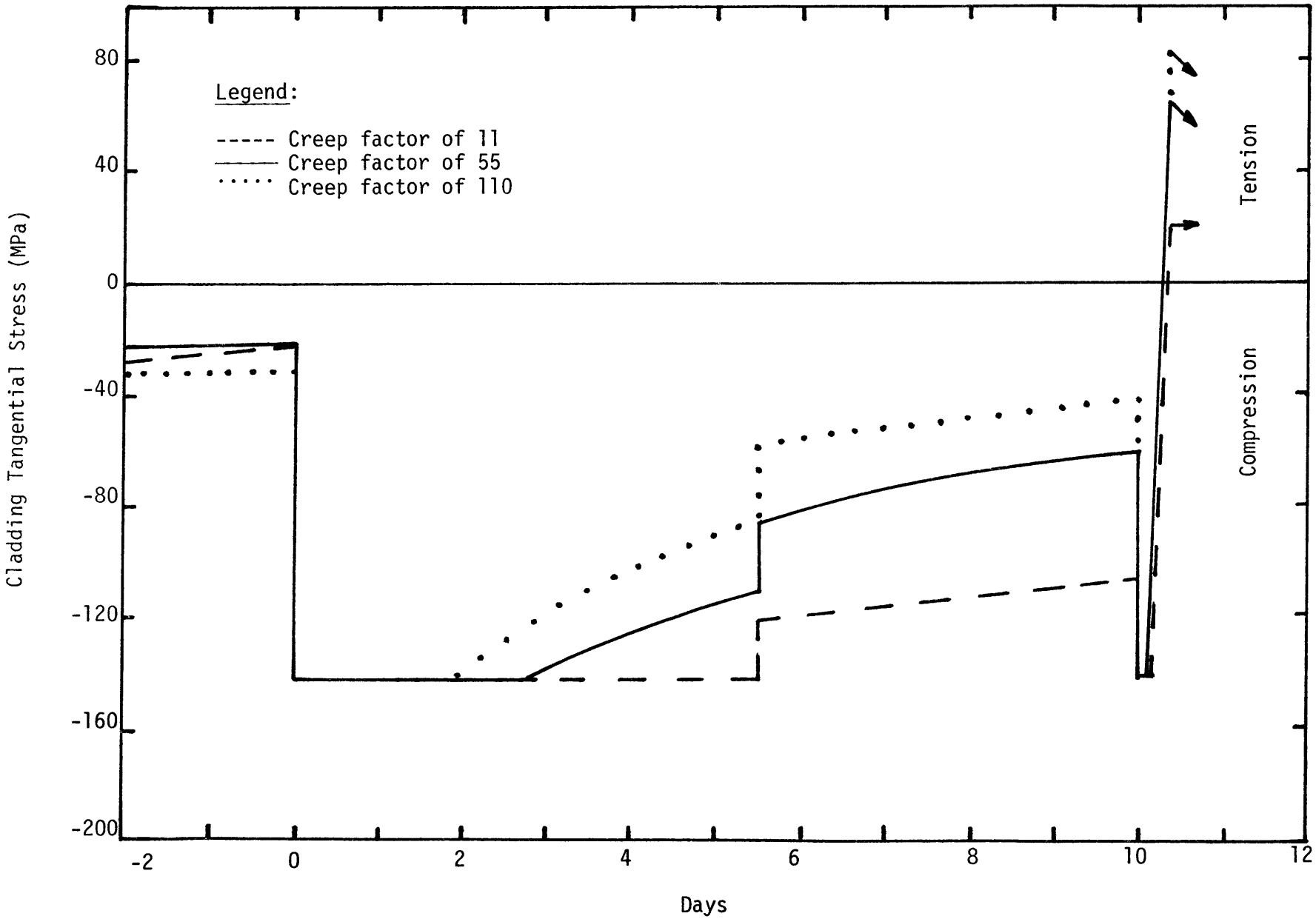

Figure 4-15 Pressurized SS304 cladding hoop stress behavior for the August 1977 maneuver.

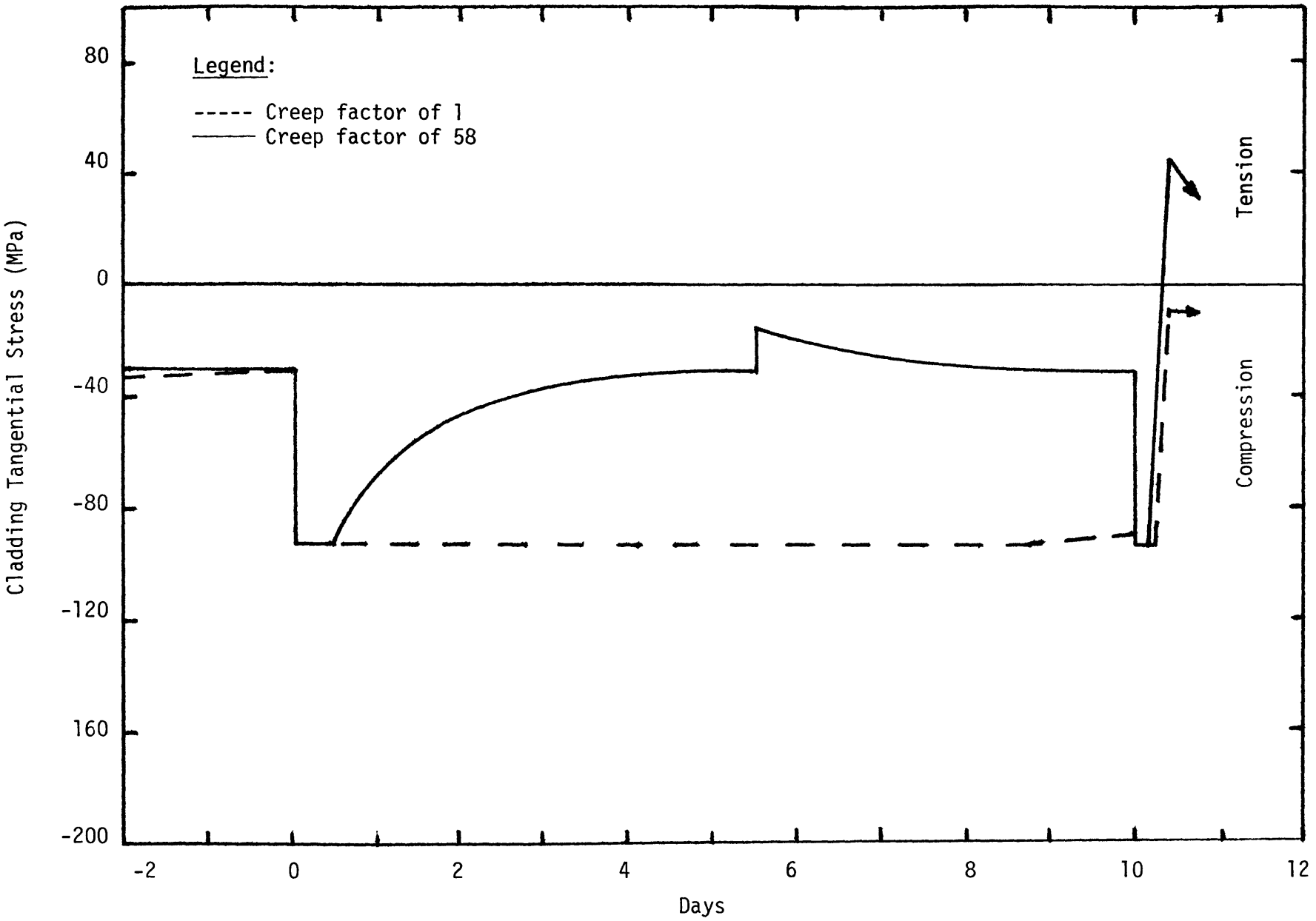

Figure 4-16 Pressurized Zircaloy cladding hoop stress behavior for the August 1977 maneuver.

4.5 Guideline Methodology

The first step in establishing ramp rate limitations is to define a cladding threshold stress (in this case tangential or hoop) which places an upper limit on stresses realized in a given up-power maneuver. The basis of this threshold stress may be one of stress corrosion cracking (SCC) or yield. In order to compensate for the effect of local stress concentrations which may not be considered in a code (such is the case for STRESS), a fractior of this threshold value may be used as the limiting value. For instance, daSilva (Ref. 13) uses a 296.4 MPa Zircaloy stress corrosion cracking threshold. In order to compensate for local stress concentrations, half this value was used as an upper limit on allowable hoop stresses. An estimation of hourglass local stress concentration values for both materials is presented below.

4.5.1 Stress Concentrations

An estimation of stress concentrations at fuel pellet ends due to pellet hourglassing may be made using the information supplied in Fig. 4-17 (Ref. 14 and references therein). This figure illustrates the difference between end and mid-pellet radial displacement (thermal expansion induced) as a function of pellet length to diameter ratio. The additional thermal radial displacement at the pellet end may be estimated by

$$\Delta u_F^T = A_F \, R_F \, \overline{\Delta\varepsilon^T}_F \quad ;$$

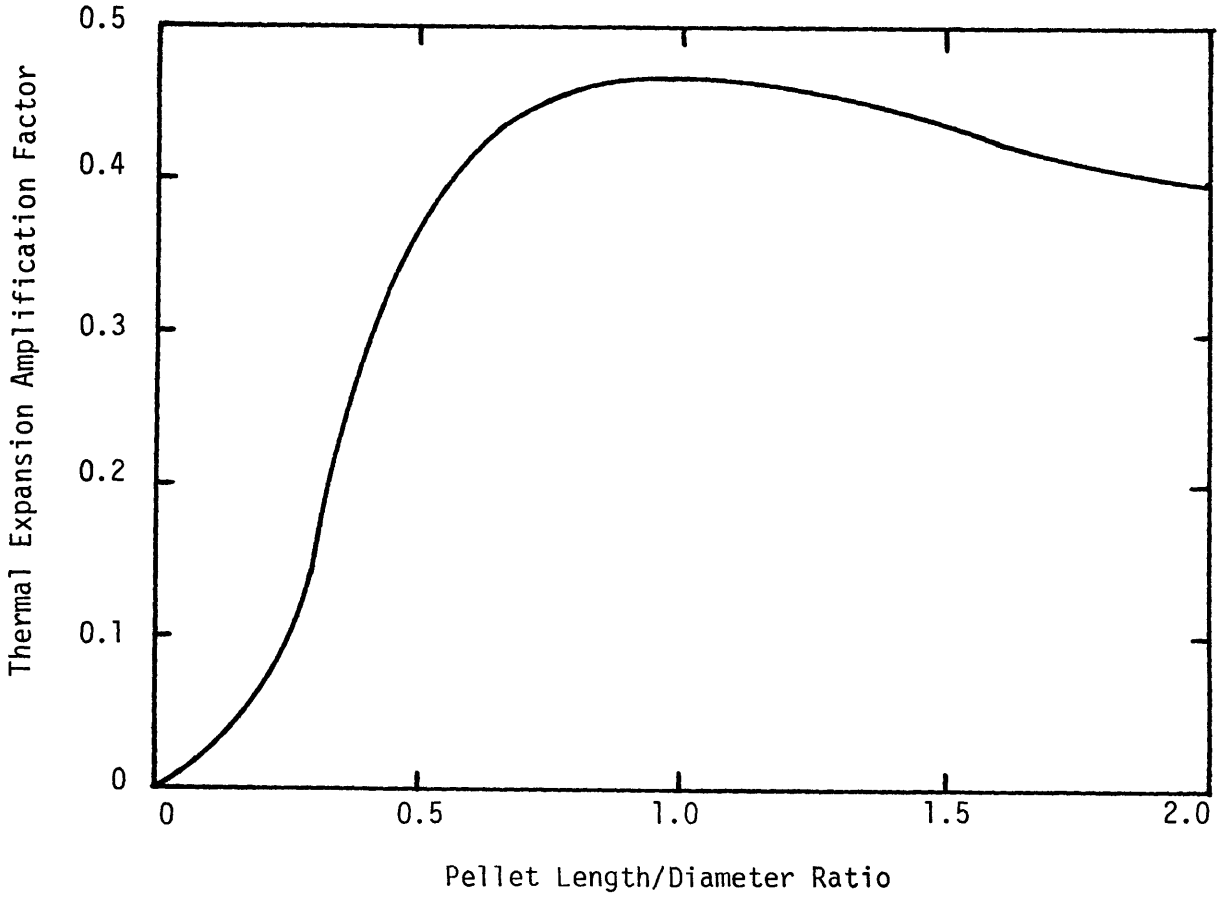

Figure 4-17 Difference Between End and Mid-Pellet Radial Displacement (from Ref. 14)

where

Δu_F^T = additional thermal radial displacement at the pellet ends due to hourglassing (mm);

A_F = fuel pellet amplification factor (from Fig. 4-1);

R_F = densified or swelled cold fuel radius as defined in Section 3.4 (mm); and

$\Delta\bar{\varepsilon}_F^T$ = change in fuel average thermal strain from "just contact" $(\frac{mm}{mm})$.

The increase in cladding hoop stress may be estimated on an elastic basis using the equations of Sections 3.3 and 3.4. The additional radial thermal displacement is compensated for by both cladding and fuel elastic deflections. For the cladding, the increase in deflection is

$$\Delta u_a^{e\ell} = \frac{(b+a)}{2}\varepsilon_\theta^{e\ell} - \frac{(b-a)}{2}\varepsilon_r^{e\ell}$$

$$= \frac{a\Delta P_c}{E}\left[\frac{b^2+a^2}{b^2-a^2} + \nu\right] \quad ;$$

and for the fuel,

$$\Delta u_F^{e\ell} = -\frac{R_F\Delta P_c}{E_F}(1-\nu_F) \quad ;$$

where

$\Delta u_a^{e\ell}$ = increase in inside cladding elastic deflection (mm);

$\Delta u_F^{e\ell}$ = increase in fuel radial elastic deflection (mm);

ΔP_c = increase in pellet-cladding contact pressure to produce these deflections (MPa); and

all other symbol definitions are as in Section 3.

Since the pellet and cladding are initially in contact and remain contacted, the increase in pellet-cladding contact pressure may be obtained by equating the fuel and inside cladding surface deflections. Thus,

$$\Delta u_a^{e\ell} = \Delta u_F^T + \Delta u_F^{e\ell}$$

and manipulation yields

$$\Delta P_c = \frac{\Delta u_F^T}{\left[\frac{(1-\nu_F)R_F}{E_F} + \frac{a}{E}\left(\frac{b^2+a^2}{b^2-a^2} + \nu\right)\right]} \quad ;$$

which may be directly related to an increase in hoop stress using

$$\Delta\sigma_\theta = \frac{a}{(b-a)} \Delta P_c$$

The results of this calculation for both stainless steel and Zircaloy are presented in Table 4-1. The very large increase in stainless steel cladding hoop stress (about 130 MPa) for the pellet hourglassing phenomenon alone, exemplifies the importance of considering the effects of stress concentrations when choosing a limiting stress value.* The additional cladding hoop stress for Zircaloy is much lower, demonstrating the greater elastic compliance (lower elastic modulus) of this material. Remember that these stresses are in addition to those predicted for the maneuver of Section 4.4.

*Other local stress concentrations may be caused by pellet cracks, pellet chips lodged within the gap, or even local power peaking. It should be mentioned that stress relaxation is not considered in the hourglassing example.

Table 4-1 Hourglassing Stress Concentration Results Due to the August 1977 Maneuver

Symbol	Definition	Value	
		Connecticut Yankee SS304	Maine Yankee Zircaloy-4
E	Cladding Elastic Modulus (GPa)	177.39	76.69
ν	Cladding Poisson Ratio	.318	.253
E_F	Fuel Elastic Modulus (GPa)	169.35	170.62
ν_F	Fuel Poisson Ratio	.301	.300
a	Cold BOL Cladding Inside Radius (mm)	4.940	4.877
b	Cold BOL Cladding Outside Radius (mm)	5.359	5.588
R_F	Cold Swelled Fuel Radius (mm)	4.890	4.808
L/D	Pellet Length to Diameter Ratio	1.158	1.158*
A_F	Hourglassing Amplification Factor	.46	.46
f_c	Creep Acceleration Factor	55.	58.
$\Delta\bar{\varepsilon}_F^T$	Increase in Fuel Average Thermal Strain After "Just Contact" (%)	.1767	.2503
$\Delta\sigma_\theta$	Additional Hoop Stress	126.0	75.0

*Assumed value

4.5.2 Possible Failure Modes

As mentioned previously, the threshold stress criterion may be based on stress corrosion cracking or yield. Yield in itself does not necessarily constitute failure, however, other possible failure modes may gain importance for stresses of this magnitude. Such is the case for irradiated stainless steel. Stress corrosion cracking has been observed in both stainless steel (chlorine SCC) and Zircaloy (iodine assisted SCC) but has only been established itself as a dominant failure mode in Zircaloy.

Figure 4-18 shows the effect of irradiation on the yield and ultimate tensile strengths of SS304. An estimate of fast fluence ($E > 0.1$ MeV n/m^2) experienced by a Connecticut Yankee assembly near the end of its second cycle (typical of batch 8 near the August 1977 maneuver) is also indicated on this graph. What is interesting to note is that although both the yield and ultimate tensile strengths increase with irradiation, the ultimate tensile stress does not increase in proportion to yield. This implies that very little strain hardening takes place after yield and a phenomenon known as plastic instability may occur (Ref. 12). If this high stress region is entered, high local cladding strain rates are expected.

Deformation channels have been observed in irradiated type 304 stainless steel (Ref. 15). This phenomenon produces deformation bands due to highly localized strain which may lead to fracture at lower engineering strains. Channel fracture is believed to occur from extensive slip (due to shear) with a possible contribution from irradiation produced voids.

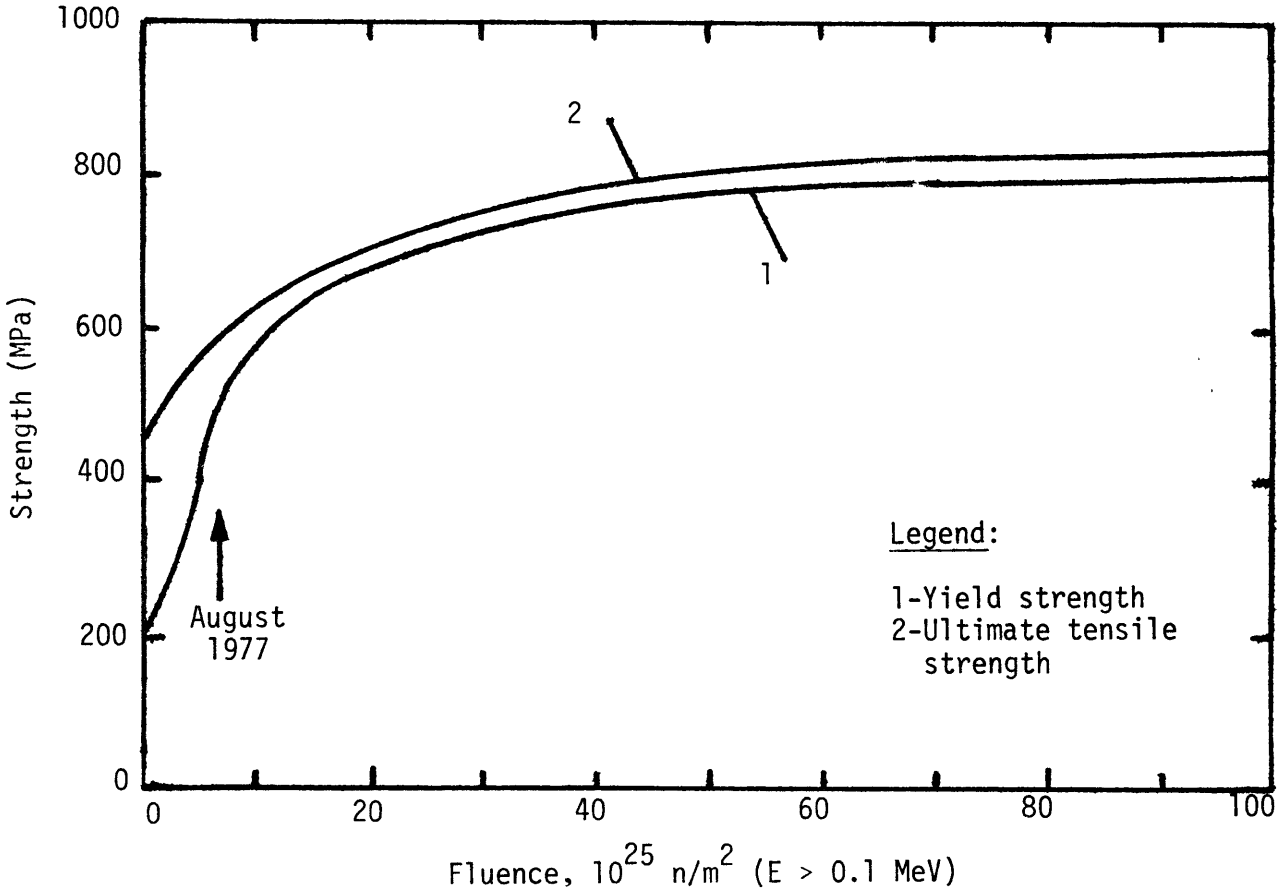

Figure 4-18 The Effect of Fast Neutron Fluence on the Strength of SS304 Irradiated and Tested at 370°C (from Ref. 15 and references therein)

5. CONCLUSIONS

The following concluding sections are based on the particular reactor/fuel element design investigated. The stainless steel clad fuel results are derived from operation/design characteristic of the Connecticut Yankee plant (assembly 8-H22), while the Zircaloy clad fuel results are primarily based on operation and design characteristic of Maine Yankee (hot rod assembly). The only design variation investigated is the fill gas pressurization level of the stainless steel clad fuel rods.

5.1 Effects of Fill Gas Pressure

Stainless steel pressurized rods (about 2 MPa Helium) have been shown to have at least two distinct advantages over unpressurized rods (atmospheric pressure Helium). The first is a time (burnup) extension for initial hard pellet-cladding contact due to long term cladding creepdown/fuel swelling. The STRESS code predictions show about a 4 MWD/kgU (local) extended contact burnup for two creep models investigated. The second and more significant advantage is lower fuel temperatures. It has been estimated that fuel centerline temperatures much greater than 1400°C are unlikely with pressurization, while temperatures in the 1700°C range may be expected without it. The higher temperatures predicted for the unpressurized case extend well into the fuel restructuring regimes over substantial periods of time (burnup).

Lack of pressurization does effect fuel behavior at initial pellet-cladding contact but has a minimal effect once good contact (contact pressure $\geq$ 1 MPa) has been established. This is the only

notable difference between the conditioning behavior for the pressurized and unpressurized cases. Up-power ramping and maneuvering results show no significant differences between the final hoop stresses realized in each case.

5.2. Effects of Creep Acceleration Factors

If no creep acceleration factor is used, long term stainless steel cladding creepdown to contact is expected to occur in the latter part of the third cycle. However, some experimental findings (Ref. 11) indicate that these creep rates may be multiplied by a factor of 11. Preliminary outside cladding measurements suggest that the higher creep factor may be more realistic. Initial hard contact is expected to occur in the latter part of the second cycle for this factor. If this is the case, cladding conditioning should be considered prior to up-power ramps or maneuvers at these burnups.

Higher creep acceleration factors (i.e., 55 and 110) are investigated for conditioning and ramping calculations. They are included as compensation for the effects of fuel restrained swelling, creep deformation, and cracked pellet relocation which has been ignored in the fuel pellet model. The cladding hoop stresses realized for up power ramping from a 60% preconditioned state are of the same magnitude for each creep factor, but more stress relaxation is exhibited for the higher ones. In these cases, the benefits of stress relaxation due to reduced ramp rates are insignificant until 5%/hr or less.

5.3 Zircaloy Differences

From a hoop stress behavior point of view, Zircaloy cladding appears to be the superior performer. The up-power ramping and maneuvering examples of Section 4 show much lower final hoop stresses for this material when compared to stainless steel. This reduction in stress is basically due to two factors. The first is the higher creep deformation (and therefore stress relaxation) exhibited by Zircaloy. This characteristic alone allows greater flexibility in power maneuvering since reduced ramp rates considerably increase stress relaxation. The second is the increase in elastic compliance for this material (much lower elastic modulus). This allows the Zircaloy cladding to elastically respond to a thermally expanding pellet by about a factor of two (for a given hoop stress) over stainless steel. In other words, if the inside cladding surface for each cladding material is elastically deflected outward the same amount, the increase in hoop stress for the Zircaloy cladding would be roughly half of that for stainless steel.

5.4 Connecticut Yankee Design/Operation Recommendations

Fill Gas Pressurization

The present Connecticut Yankee fuel rod fill gas pressurization level is approximately 101 kPa Helium (this corresponds to 1 atmosphere pressure - denoted "unpressurized" throughout this study). An alternate pressurization of about 2 MPa, indicative of rods presently in the San Onofre 1 station, has also been investigated. As stated in Section 5.1, pressurization extends the burnup for initial hard pellet-cladding contact. Also, it has been estimated that fuel

centerline temperatures much greater than 1400°C are not expected with pressurization while temperatures in the 1700°C range are quite likely without it. The higher temperatures predicted for the unpressurized case extend well into the fuel restructuring regimes over substantial period of time (burnup). There are at least two unfavorable effects associated with fuel restructuring. The first is a possible increase in fission gas release which would tend to augment fuel temperatures (a positive feedback effect). The second is a possible increase in fuel swelling. For these reasons, an increase in fill gas pressure to about 2 MPa Helium is recommended.

Ramp Rate Limitations

The up power ramping examples of Section 4.3 illustrate the "stubborn" nature of stainless steel cladding. Even the use of a creep multiplication factor of 110 does not show a large spread between final hoop stress values for the various ramp rates investigated. However, a much larger spread (increased creep deformation/stress relaxation) would be expected if stress concentrations were included in these calculations. In this case, the final hoop stresses would certainly be greater but creep deformation and stress relaxation would be enhanced since the generalized stress also increases in magnitude.* Regardless, what may be inferred from the results of the up power examples is that benefits of stress relaxation due to reduced ramp rates are minimal for a reduction from 50 to 5% of full

*The stainless steel creep rate equation of Section A-6 is directly proportional to generalized stress.

power (FP) per hour. However, a good deal of benefit may be realized for ramp rates less than this. In this light, an upper limit of 5% FP per hour is recommended for up power ramping.* This is approximately half the ramp rate used for return to full power at the end of the August 1977 maneuver discussed in Section 4.4.

Cladding Material Choice

As concluded in Section 5.3, from a "hoop stress behavior" point of view, Zircaloy cladding is the superior performer. This material has been shown to exhibit much more creep deformation/stress relaxation than stainless steel. It has also been shown to develop much lower cladding hoop stresses as it elastically responds to a thermally expanding pellet. However, it is not within the scope of this study to recommend a change in cladding material from stainless steel to Zircaloy. There are many other limiting criteria such as strain rate (from a ramp rate viewpoint) or Zircaloy hydriding (from a stress threshold viewpoint) which may render Zircaloy inferior. Material performance under accident conditions such as a loss of coolant occurrence (LOCA) must also be considered. Ultimate cladding material choice should be made only after all pros and cons have been carefully reviewed and weighed.

*In other words, the benefits of stress relaxation due to reduced ramp rates are only significant for rates below 5% FP/hr.

A. MATERIAL PROPERTIES

A.1 CLADDING THERMAL CONDUCTIVITY

The thermal conductivity for SS304 (Ref. 17) is calculated using a third order relation in temperature of the form

$$k_{SS} = 9.01748 + 1.62997\times10^{-2}T - 4.80329\times10^{-6}T^2 + 2.18422\times10^{-9}T^3 \quad ;$$

where

k_{SS} = SS304 thermal conductivity (W/m·K); and

T = cladding temperature (°K).

The Zircaloy-4 conductivity relation was taken from CENPD-218 (Refs.18 and 9) and assumes the linear form

$$k_{Zr} = 13.959 + 9.8522\times10^{-3}T \quad ;$$

where

k_{Zr} = Zircaloy-4 thermal conductivity (W/m·K); and

T = cladding temperature (°C).

The above two conductivity relations are shown in Fig. A-1, illustrating this thermal property difference between materials.

A.2 CLADDING THERMAL STRAIN

The cladding thermal strain correlation for SS304 was derived from the following average coefficient of thermal expansion relation (Ref. 17)

$$\bar{\alpha} = 1.7887\times10^{-5} + 2.3977\times10^{-9}T + 3.2692\times10^{-13}T^2 \quad ;$$

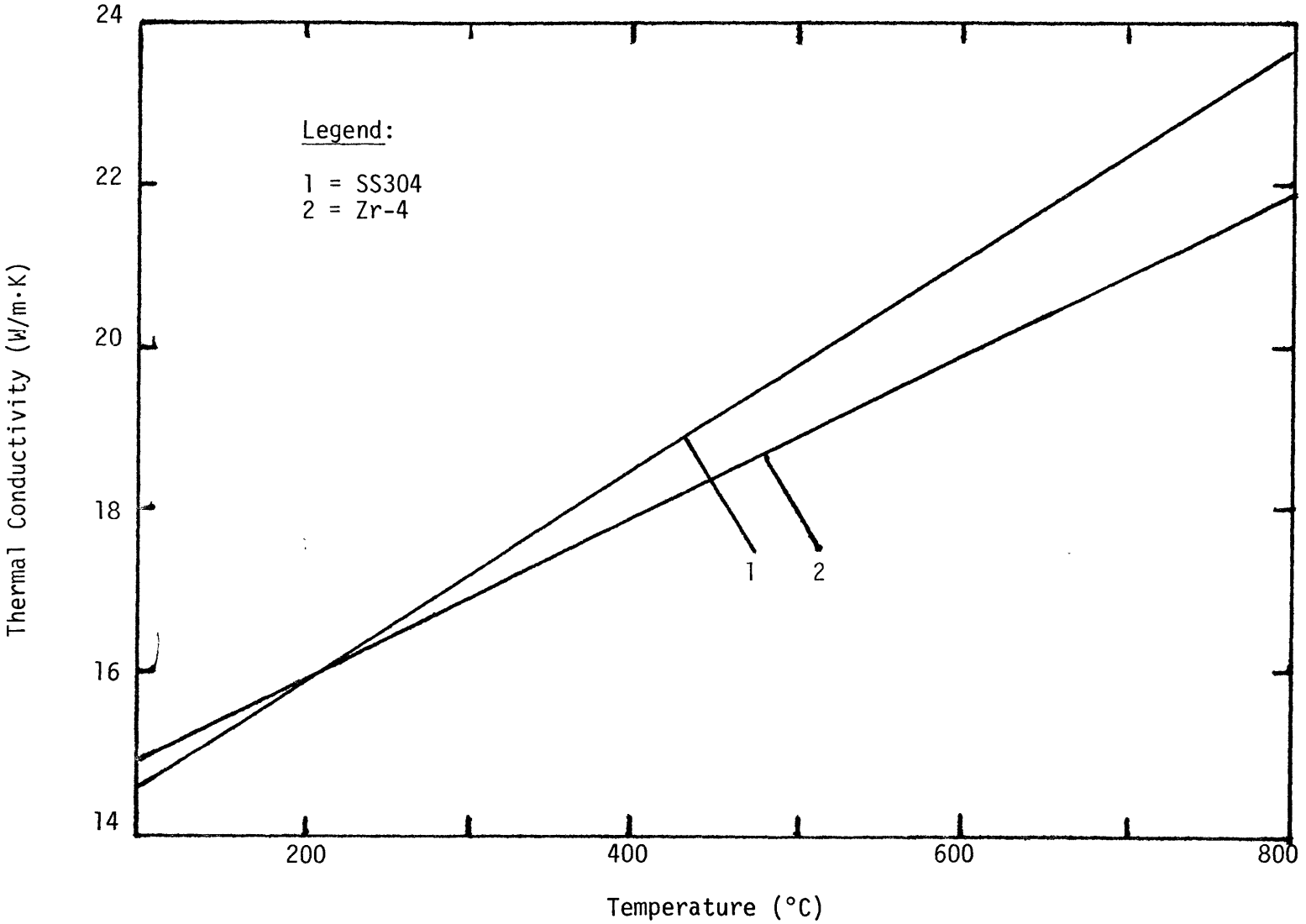

Figure A-1 Comparison of SS304 and Zircaloy-4 Thermal Conductivities.

where

$\bar{\alpha}$ = average coefficient of thermal expansion (m/m·K); and

T = temperature (°K).

The thermal strain was determined as follows

$$\varepsilon_T = \int_{T_o}^{T} \bar{\alpha}\, dT = \bar{\alpha}\,(T - T_o)$$

so

$$\varepsilon_T = (1.7887\text{x}10^{-3} + 2.3977\text{x}10^{-7}T + 3.2692\text{x}10^{-11}T^2)\,(T - T_o) \quad ;$$

where

ε_T = SS304 thermal strain (%);

T = cladding temperature (°K); and

T_o = 298.15 °K.

The Zircaloy-4 thermal strain relation was taken from MATPRO (Ref. 19) (applicable in the range 27 < T < 800°C) and is

$$\varepsilon_T = -2.373\text{x}10^{-2} + 6.721\text{x}10^{-4}T \quad ;$$

where

ε_T = Zircaloy-4 thermal strain (%); and

T = cladding temperature (°C).

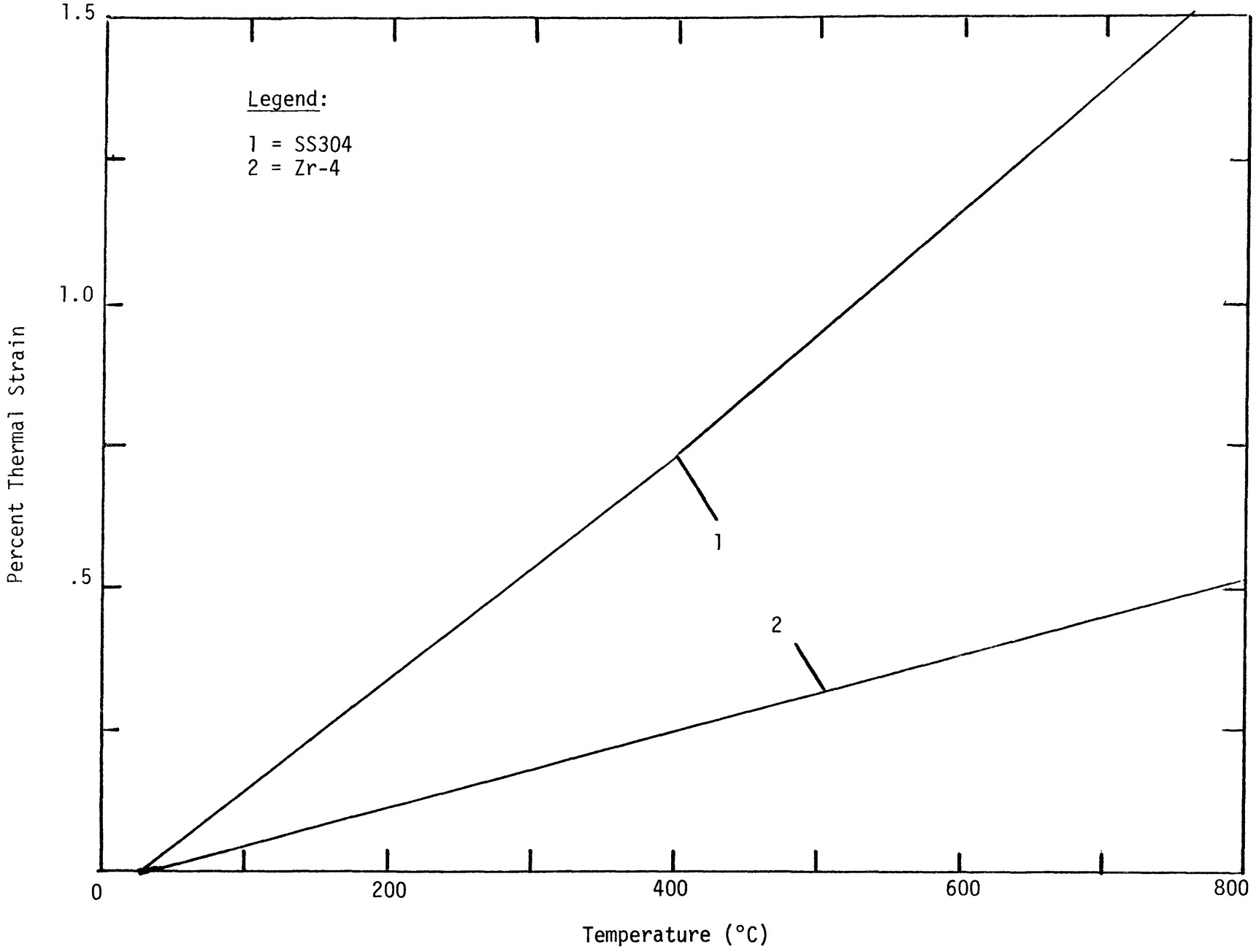

Figure A-2 Comparison of SS304 and Zircaloy-4 Thermal Strains

A.3 CLADDING MODULUS OF ELASTICITY

Young's modulus for SS304 was modeled using a linear approximation from data obtained in Ref. 20. This property was assumed to depend just on temperature as follows

$$E_{SS} = 202.82 - 7.4707 \times 10^{-2} T \quad ;$$

where

E_{SS} = SS304 modulus of elasticity (GPa); and

T = cladding temperature (°C).

The temperature dependent elastic modulus for Zircaloy-4 was taken from MATPRO. Although cladding temperatures above 862°C are not expected, it is included in the code.

For $T \leq 862$°C

$$E_{Zr} = 114.8 - 5.99 \times 10^{-2} (T + 273.15) \quad ;$$

and for $T > 862$°C

$$E_{Zr} = 100.5 - 4.725 \times 10^{-2} (T + 273.15) \quad ;$$

where

E_{Zr} = Zircaloy modulus of elasticity (GPa); and

T = cladding temperature (°C).

These relations are plotted in Fig. A-3. Since elastic strains are inversely proportional to these values, the elastic response to fuel-cladding contact pressures would be less for SS304.

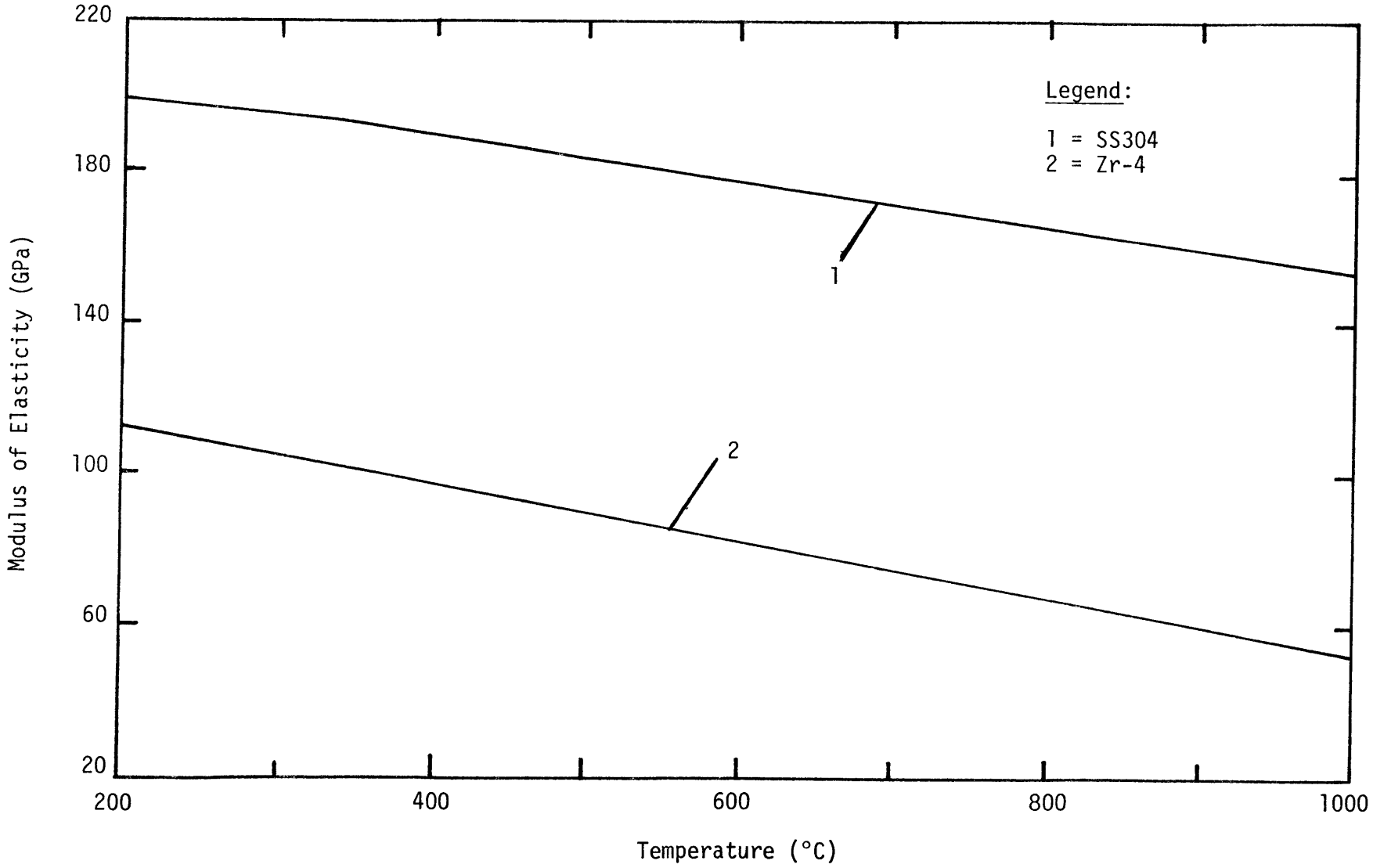

Figure A-3 Cladding Modulus of Elasticity for SS3-4 and Zircaloy-4.

A.4 POISSON RATIO FOR CLADDING

SS304 Poisson ratio is calculated using a temperature dependent linear fit through data supplied in Ref. 20. This relation is

$$\nu_{SS} = 0.304 + 1.7102 \times 10^{-4} (T - 260) \quad ;$$

where

ν_{SS} = Poisson ratio for SS304; and

T = cladding temperature (°C).

The Zircaloy relation was obtained from MATPRO and is

for $T \leq 397°C$

$$\nu_{Zr} = .333 - 1.26 \times 10^{-4} (T + 273.15) \quad ;$$

for $T > 397°C$

$$\nu_{Zr} = 0.248 \quad ;$$

where

ν_{Zr} = Poisson ratio for Zircaloy; and

T = cladding temperature (°C).

Values for both materials are plotted in Fig. A-4.

A.5 CLADDING MEYER HARDNESS

Meyer Hardness values are necessary for use in gap contact pressure conductance evaluation. The the SS304 case, this hardness number was found to be related to the Brinell Hardness number using

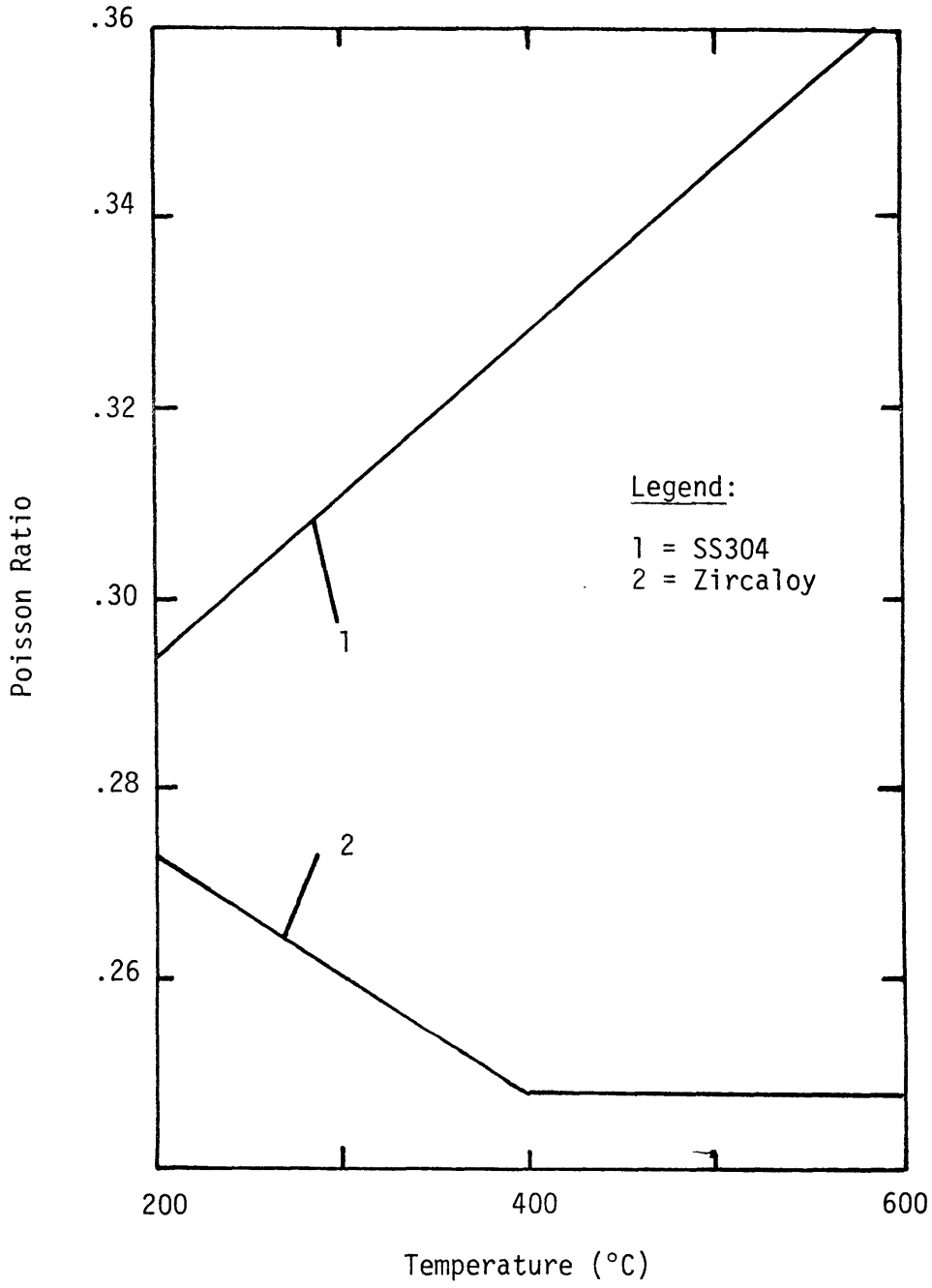

Figure A-4 Comparison of Poisson Ratios for SS304 and Zircaloy

$$MH = \frac{9.807\ (BH)}{(1 - \frac{9.5493}{BH})} \quad ;$$

where

MH = Meyer Hardness for SS304 (MPa); and

BH = Brinell Hardness for SS304 (Kg/mm^2).

Typical Brinell Hardness values for steels near 25°C are in the range of 150 Kg/mm^2 (Ref. 21). The corresponding Meyer Hardness number for this value is found to be about 1571 MPa and is assumed to vary with yield strength (Ref. 22) as follows

$$MH = 3.448 \times 10^{-3}\ (MH_o)\ S \quad ; \text{ and}$$

$$S = 290 - 0.245\ (T - 25) \quad ;$$

where

MH = Meyer Hardness for SS304 (MPa);

MH_o = MH at 25°C (MPa);

S = SS304 yield strength (MPa); and

T = cladding temperature (°C).

The variation in MH with temperature may be more accurately represented by tensile strength variation, but due to data scatter either appear appropriate.

The Zircaloy Meyer Hardness was obtained from MATPRO (see also Ref. 9) and is

for $T < 25°C$

$$MH = 1960 \quad ;$$

for 25°C < T < 727°C

$$MH = 6.48\times10^{3} - 23.6\,(T + 273.15) + 3.29\times10^{-2}\,(T + 273.15)^{2} - 1.568\times10^{-5}\,(T + 273.15)^{3} \quad ;$$

for T > 727°C

$$MH = 100 \quad ;$$

where

MH = Meyer Hardness for Zircaloy (MPa); and

T = cladding temperature (°C).

Comparison of these representations for both materials is shown in Fig. A-5.

A.6 CLADDING CREEP STRAIN RATE

The SS304 cladding creep relation was taken from Ref. 11 with some modifications and approximations. The correlation was obtained by differentiating the steady state representation for annealed SS304 and is

$$\dot{\varepsilon}_g^c = f_c\, C\, \phi\, \sigma_g \quad ; \text{ and}$$

$$C = 1.4504\times10^{-31}\,[1.25 - 2.2\times10^{-3}\,(T - 177)] \quad ;$$

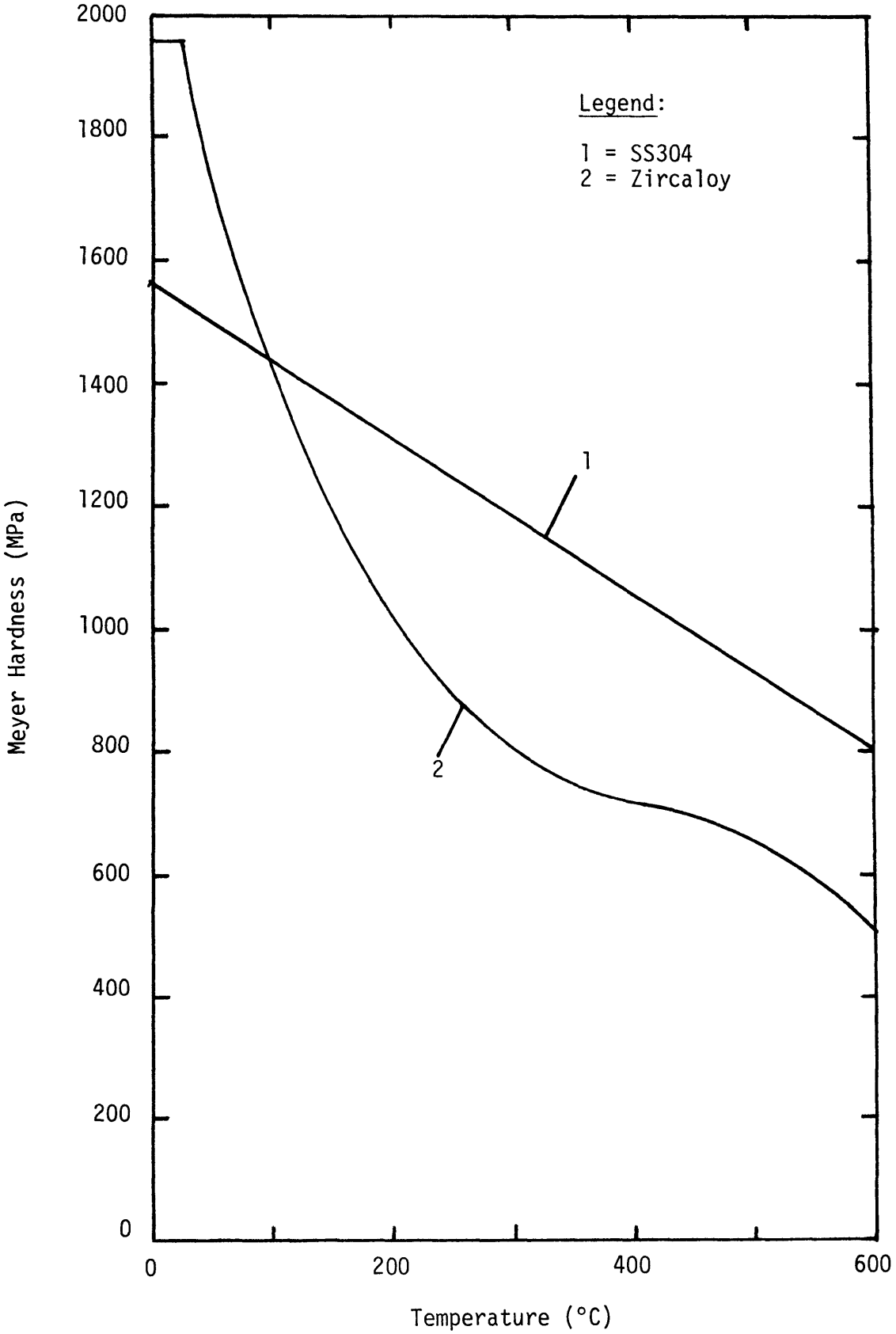

Figure A-5 Comparison of SS304 and Zircaloy Meyer Hardness Values

where

$\dot{\varepsilon}_g^c$ = generalized creep strain rate (s^{-1});

f_c = creep acceleration factor (dimensionless);

C = creep coefficient $(n \cdot MPa/m^2)^{-1}$;

ϕ = fast flux (E > 0.82 MeV $n/m^2 \cdot s$);

σ_g = cladding generalized stress (MPa); and

T = cladding temperature (°C).

The creep coefficient is represented as a linear approximation to graphical data supplied in the above reference.

The Zircaloy creep strain rate relation was obtained by modifying the tangential creep relation taken from Ref. 23. This relation was developed for 20% cold worked and stress relieved Zircaloy-2 and has the form

$$\dot{\varepsilon}_g^c = f_c \, K \, \phi^m \, \sigma_g^n \exp(B_s \sigma_g) \quad ;$$

where

$$K = 1.3585 \, \alpha \, \phi_o^{-m} \, u^{-n} \exp[-Q_o/R(T+273.15)] \quad ;$$

$$B_s = \frac{2 \, Q_o}{\sqrt{3} \, \tau \, R(T+273.15)} \quad ; \text{ and}$$

$$u = 6.8947 \, [4.77 \times 10^3 - 1.906 \, (1.8T + 32)]$$

and where

$\dot{\varepsilon}_g^c$ = generalized creep strain rate $(hr)^{-1}$;

f_c = creep acceleration factor (dimensionless);

ϕ = fast flux (for E > 1 MeV $n/m^2 \cdot s$);

σ_g = cladding generalized stress (MPa);

u = shear modulus for Zircaloy-2 (MPa); and

T = average cladding temperature (°C).

Constant values are

α = 0.020

m = 0.613

n = 1.130

$\phi_o = 0.05 \times 10^{17}$ $(n/m^2 \cdot s)$

Q_o = 8851.5 (cal/mole)

τ = 2697.9 (MPa)

A.7 FUEL THERMAL CONDUCTIVITY

The uranium dioxide thermal conductivity relation was taken from EPRI (Ref. 24; see also Ref. 9) and is of the form

$$k_F = PF \left\{ \frac{3.824}{(402.4+T)} + 6.12 \times 10^{-14} (T+273)^3 \right\} \quad ; \text{ and}$$

$$PF = \frac{1.1316(1-P)}{1+P+10P^2} \quad ;$$

where

k_F = UO_2 thermal conductivity (kW/m·K);

PF = porosity factor normalized to 95% TD (dimensionless);

P = fuel fractional porosity (dimensionless); and

T = fuel temperature (°C).

Fuel thermal conductivity and porosity factor are illustrated in Figs. A-6 and A-7, respectively.

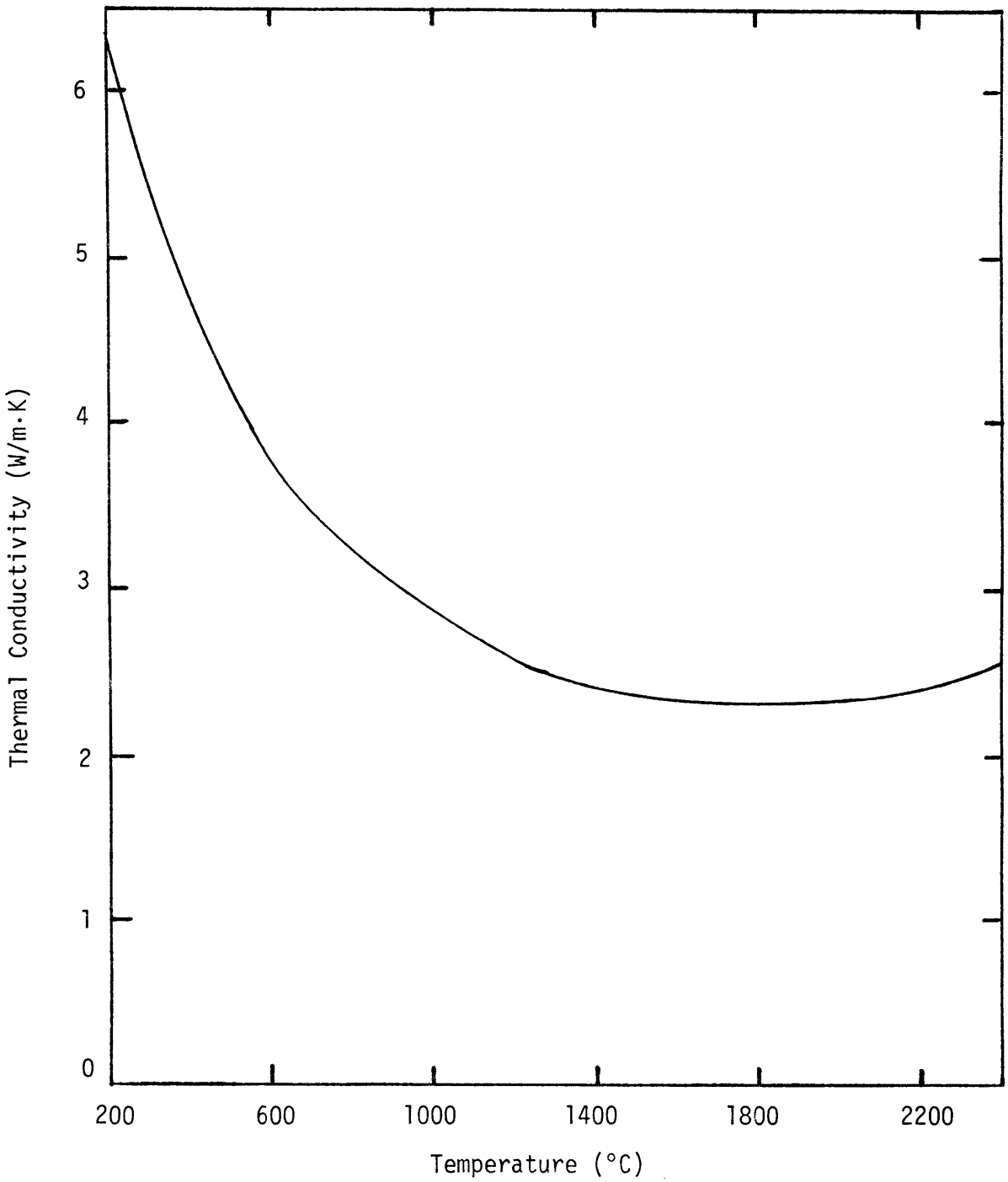

Figure A-6 Uranium Dioxide Thermal Conductivity

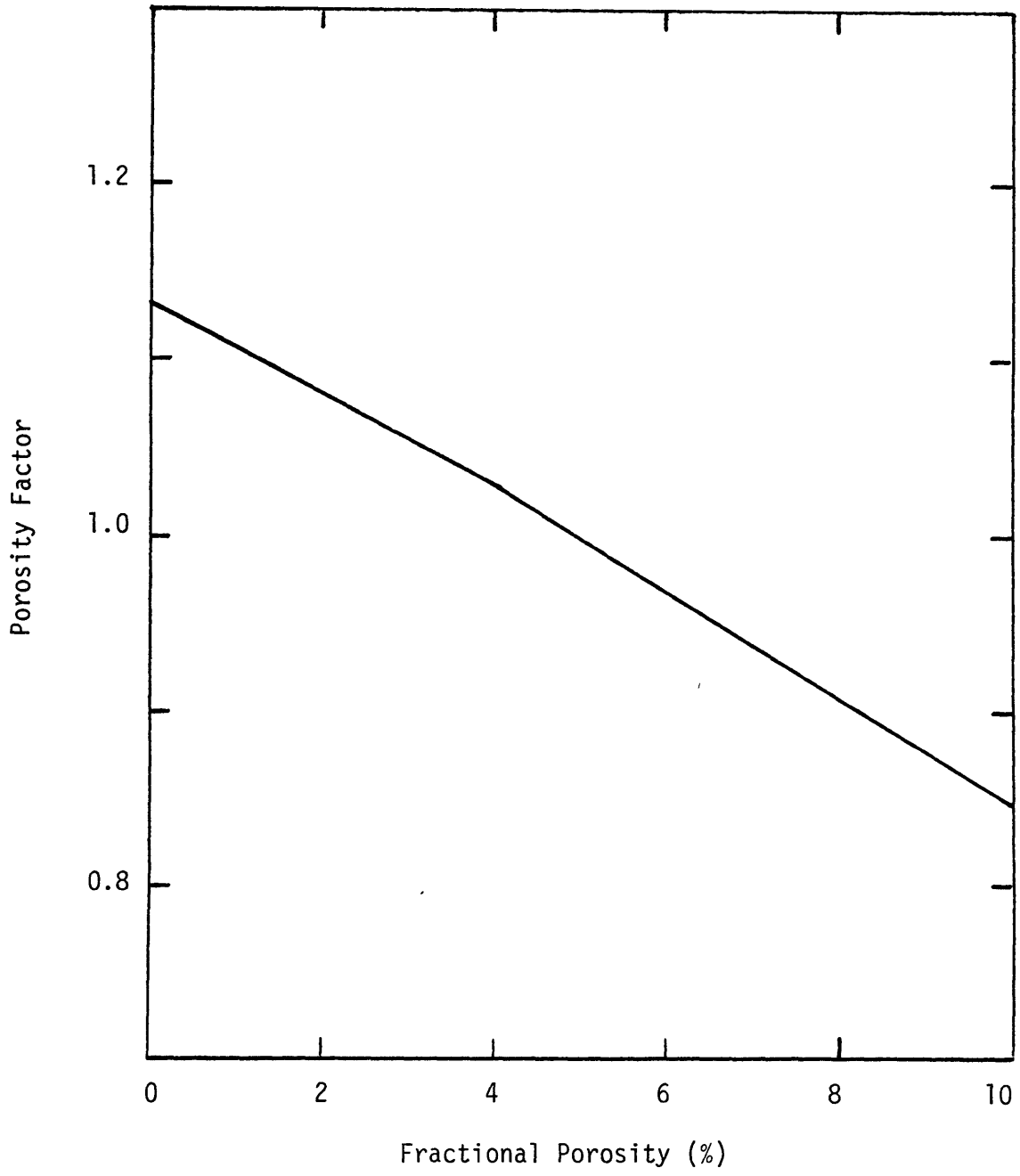

Figure A-7 Uranium Dioxide Thermal Conductivity Porosity Factor

The fuel conductivity integral was obtained using the above correlation and 0°C as a reference lower limit. Integration yields

$$\int_0^T k_F \, dT = PF \{3.824 \, \ell n(1 + \frac{T}{402.4}) + 1.53 \times 10^{-14} (T+273)^4 - 8.4985 \times 10^{-5}\} ;$$

where

$\int k_F \, dT$ = UO_2 conductivity integral (kW/m); and

T = fuel temperature (°C).

A graphic representation of this integral is given in Fig. A-8.

A.8 FUEL THERMAL STRAIN

The fuel thermal strain correlation for uranium dioxide was taken from MATPRO (Ref. 19; see also Ref. 9) and normalized for zero thermal strain at 25°C. This modified relation is

$$\varepsilon_F^T = 1.14 \times 10^{-11} T^3 + 2.581 \times 10^{-7} T^2 + 7.107 \times 10^{-4} T - 1.7929 \times 10^{-2} ;$$

where

ε_F^T = UO_2 thermal strain (%); and

T = fuel temperature (°C).

This relation is plotted in Fig. A-9. The original root of this equation existed at about 68°C yielding a negative 0.0318% strain at 25°C. The modification was just the simple addition of this value to the MATPRO relation.

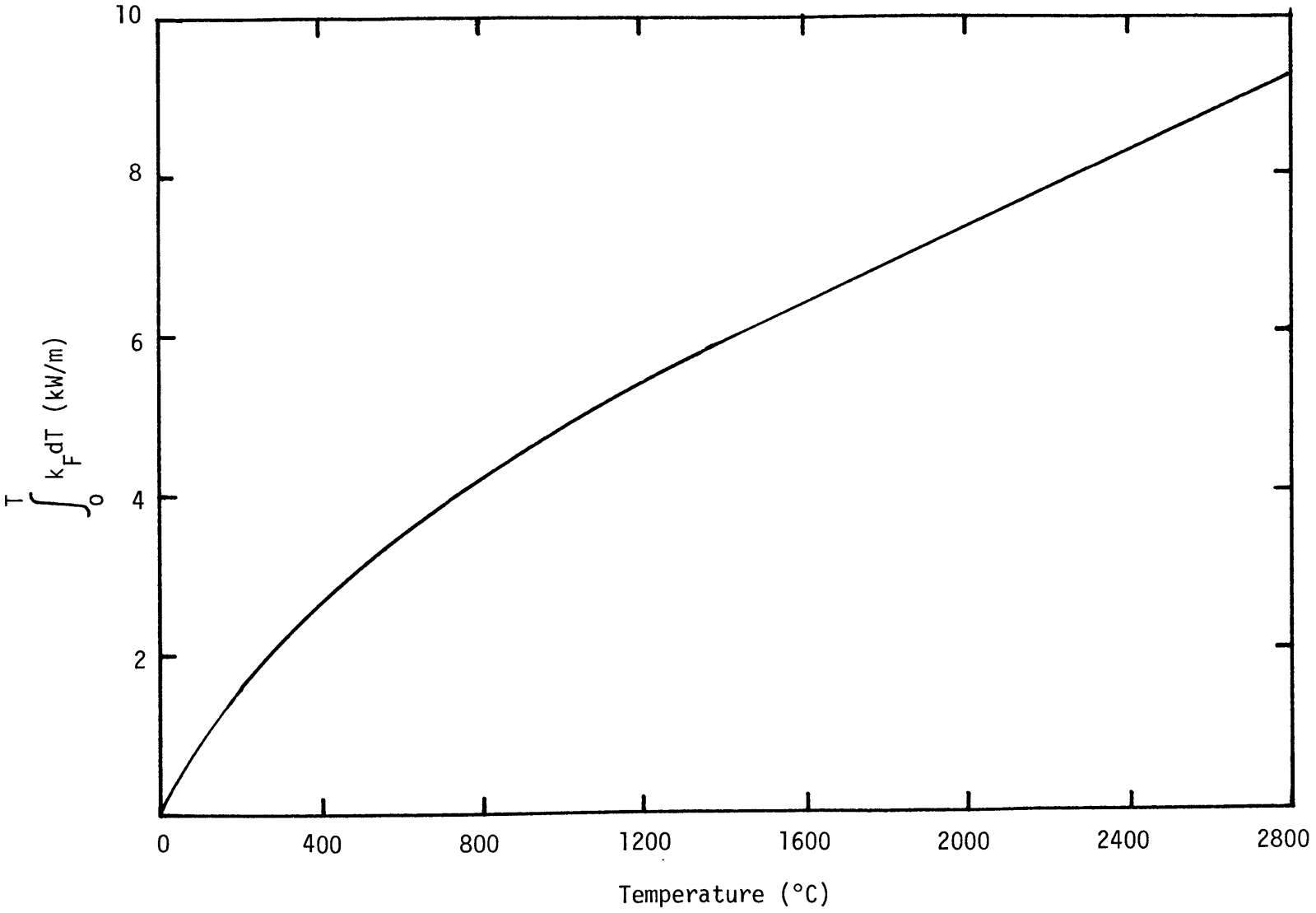

Figure A-8 Uranium Dioxide Conductivity Integral

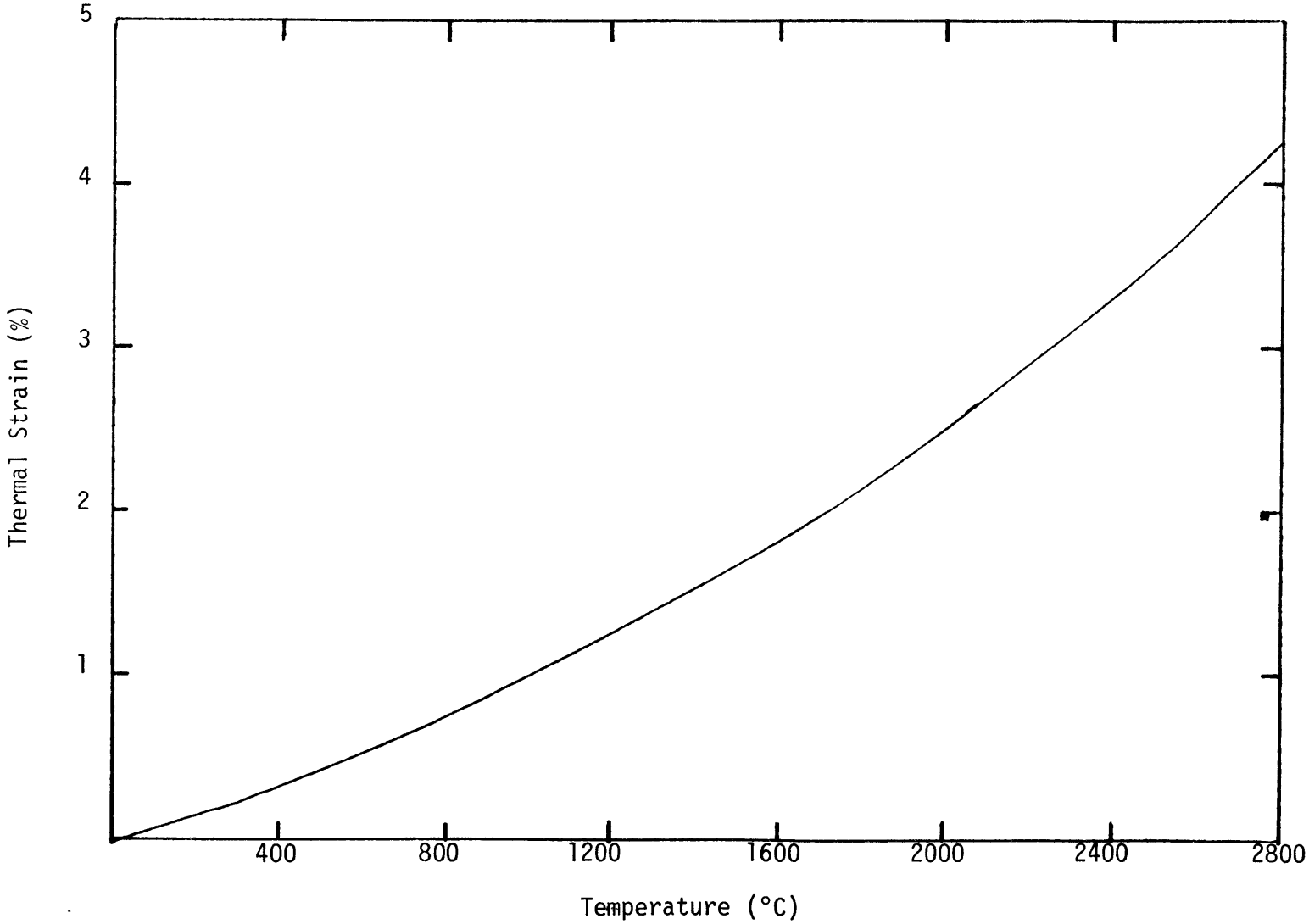

Figure A-9 Uranium Oxide Thermal Strain

A.9 FUEL MODULUS OF ELASTICITY

Uranium dioxide modulus of elasticity was taken from Ref. 25 and references therein. It is expressed as the product of a porosity dependent relation evaluated at 25°C times a temperature dependent correction factor. The model is

$$E_F = CF\ [223\ (1 - 1.92P)]\ ;$$

$$CF = \begin{cases} 1 - 1.6\times10^{-4}T - 2.0\times10^{-8}T^2 & \text{for } T < 2000°C \\ 0.6 - 0.35\ (\frac{T}{1000} - 2) & \text{for } T \geq 2000°C \end{cases}$$

where

E_F = UO_2 modulus of elasticity (GPa);

P = fuel fractional porosity (dimensionless);

CF = temperature dependent correction factor (dimensionless); and

T = fuel temperature (°C).

The correction factor was fit to graphical data obtained in the above reference and was found to be better represented by different segments for T < or > 2000°C. The fuel modulus of elasticity relation is shown in Fig. A-10 for 100% TD UO_2 (zero porosity).

A.10 FUEL POISSON RATIO

The Poisson ratio for uranium dioxide was calculated by first calculating the shear modulus (Ref. 25) and using the relation

$$\nu_F = \left(\frac{E_F}{2G_F} - 1 \right)\ ;$$

$$G_F = CF\ [84.2\ (1 - 1.66P)]\ ;$$

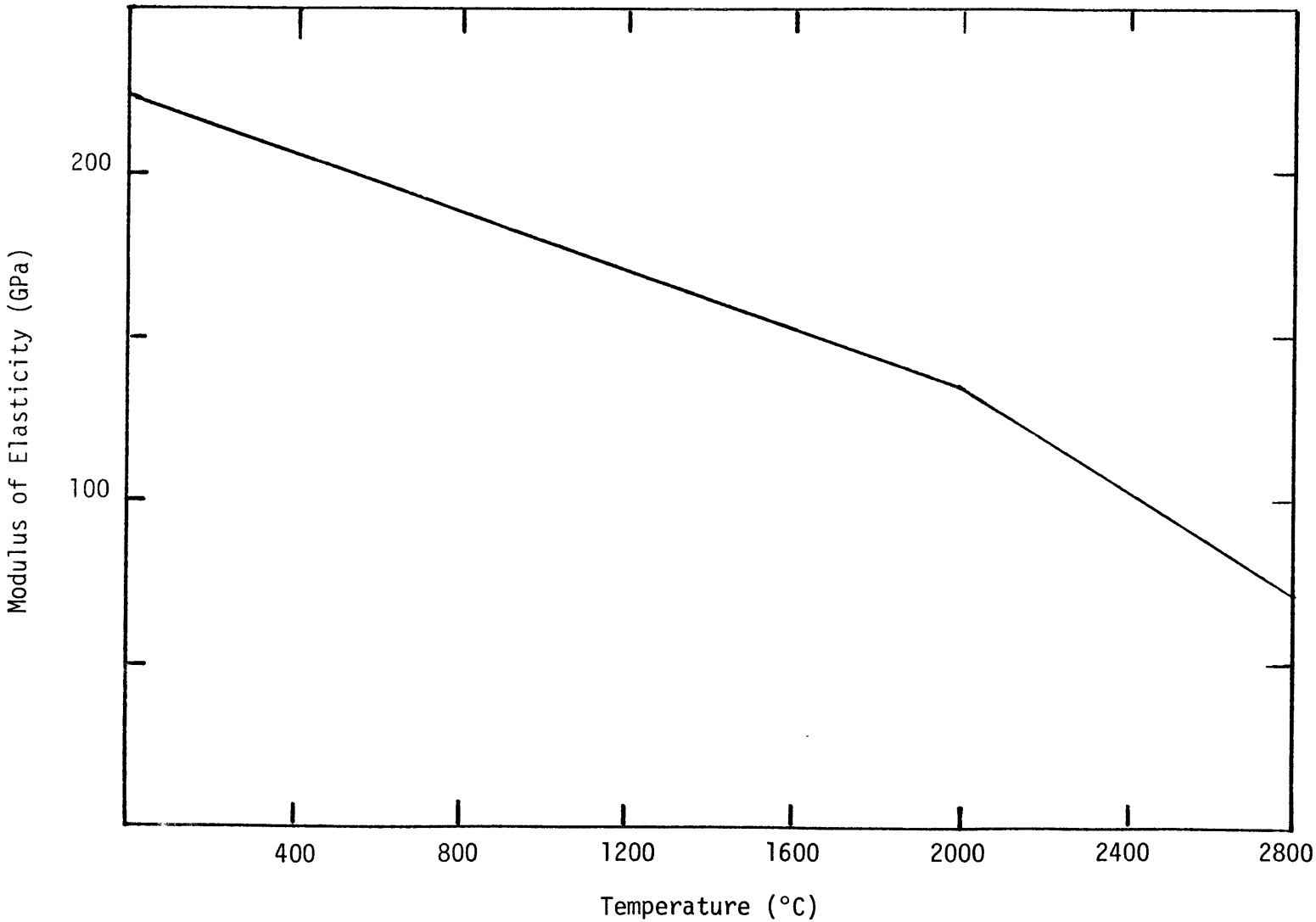

Figure A-10 Uranium Dioxide Modulus of Elasticity

where

ν_F = UO_2 Poisson ratio (dimensionless);

E_F = UO_2 modulus of elasticity (from A.10) (GPa);

G_F = UO_2 shear modulus (GPa);

CF = temperature correction factor (same as in A.10); and

P = fractional porosity.

Notice that the temperature dependent correction factor cancels, leaving only a porosity dependent relation. This is graphically illustrated in Fig. A-11.

A.11 FUEL DENSIFICATION AND SWELLING

Information on fuel densification and swelling was obtained from Ref. 26. The simple model assumes maximum densification to a value of 96.5% TD in the first 2 MWD/kgU local burnup. Half of this densification occurs linearly with burnup in the first 0.2 MWD/kgU and the remainder occurs in the next 1.8 MWD/kgU or

for $0 \leq B^L < 0.2$ (MWD/kgU)

$$d = 2.5\, B^L\, (96.5 - d_o) + d_o \quad ;$$

for $0.2 \leq B^L < 2.0$ (MWD/kgU)

$$d = \frac{(B^L - 0.2)}{3.6}\, (96.5 - d_o) + 0.5\, d_o + 48.25 \quad ;$$

where

d = fuel density (%TD);

d_o = beginning of life fuel density (%TD); and

B^L = local burnup (MWD/kgU).

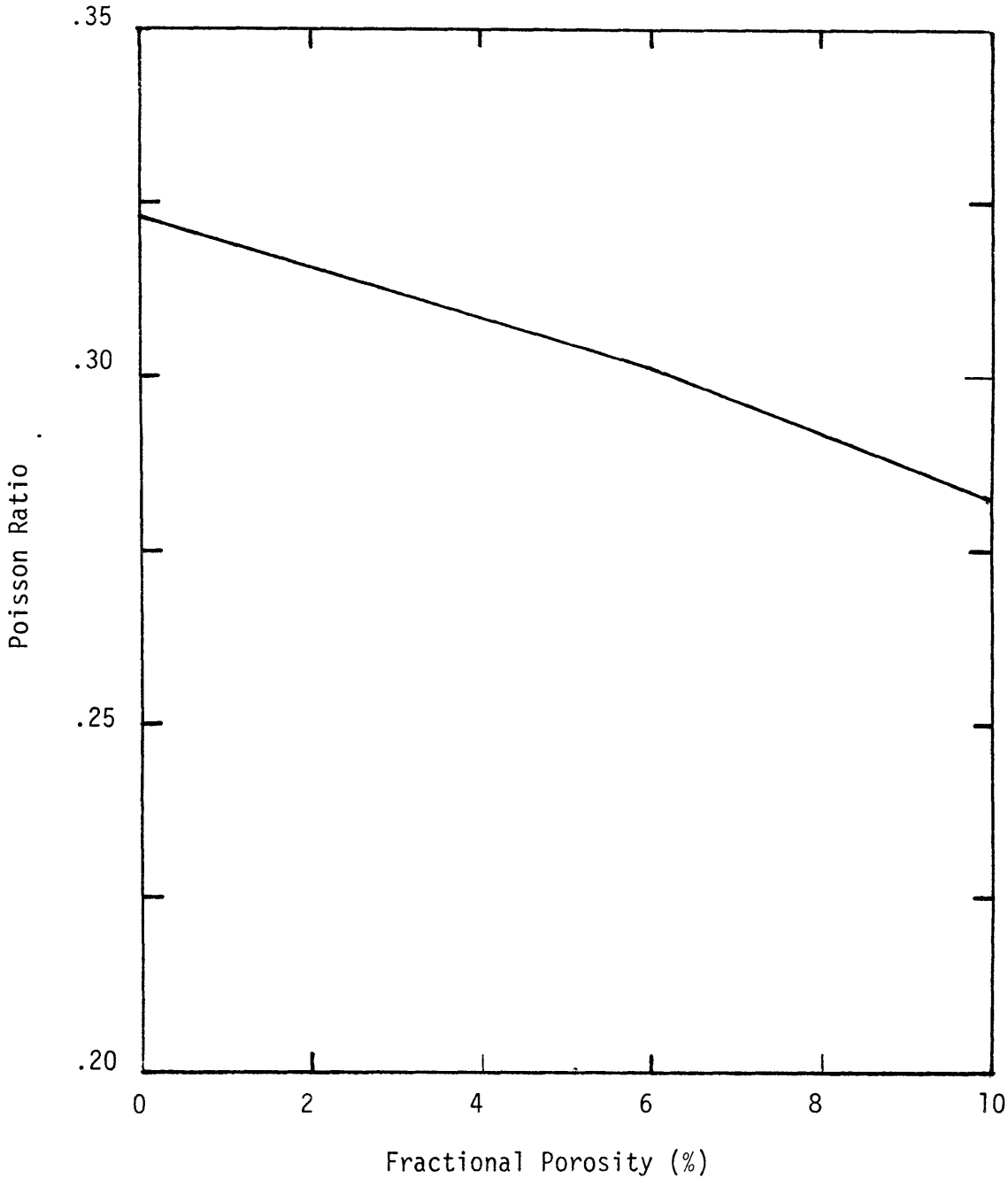

Figure A-11 Uranium Dioxide Poisson Ratio

The fuel density remains at this densified value (96.5% TD) until 10 MWD/kgU. Measurable fuel swelling, due to both solid and gaseous fission products, is assumed to initiate after this period. Density relations for burnups greater than 2 MWD/kgU are summarized as follows

for $2.0 \leq B^L < 10.0$ (MWD/kgU)

$$d = 96.5 \quad ;$$

for $10.0 \leq B^L < 20.0$ (MWD/kgU)

$$d = 96.5 - 0.148\,(B^L - 10);$$

for $20.0 \leq B^L < 30.0$ (MWD/kgU)

$$d = 95.02 - 0.145\,(B^L - 20); \text{ and}$$

for $B^L \geq 30.0$ (MWD/kgU)

$$d = 93.57 - 0.141\,(B^L - 30).$$

All symbols and units are as above.

It is assumed that both densification and swelling occur isotropically. The above relations are plotted in Fig. A-12 depicting both phenomenological effects on fuel density with burnup.

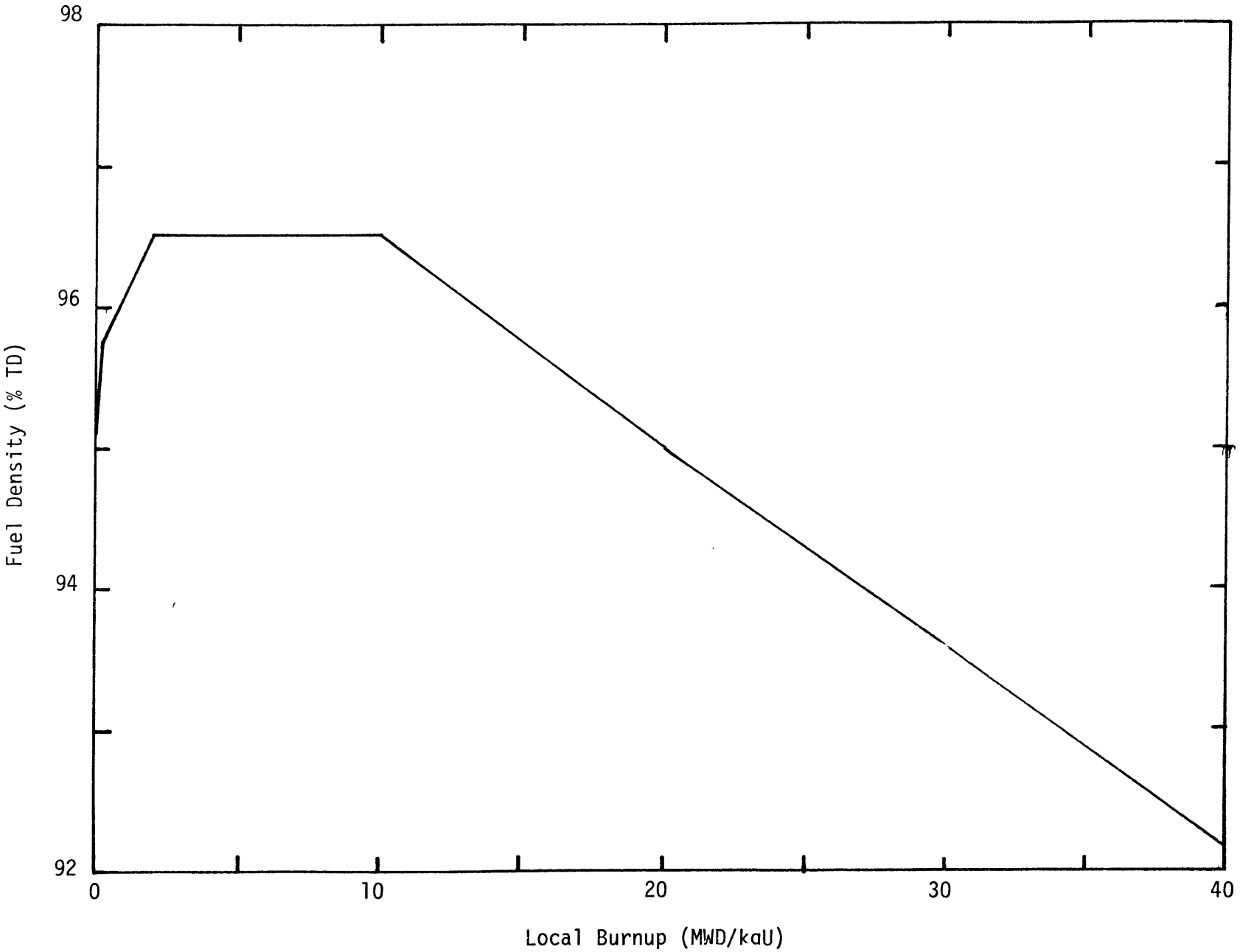

Figure A-12 Uranium Dioxide Fuel Density Variation (initial density = 95% TD)

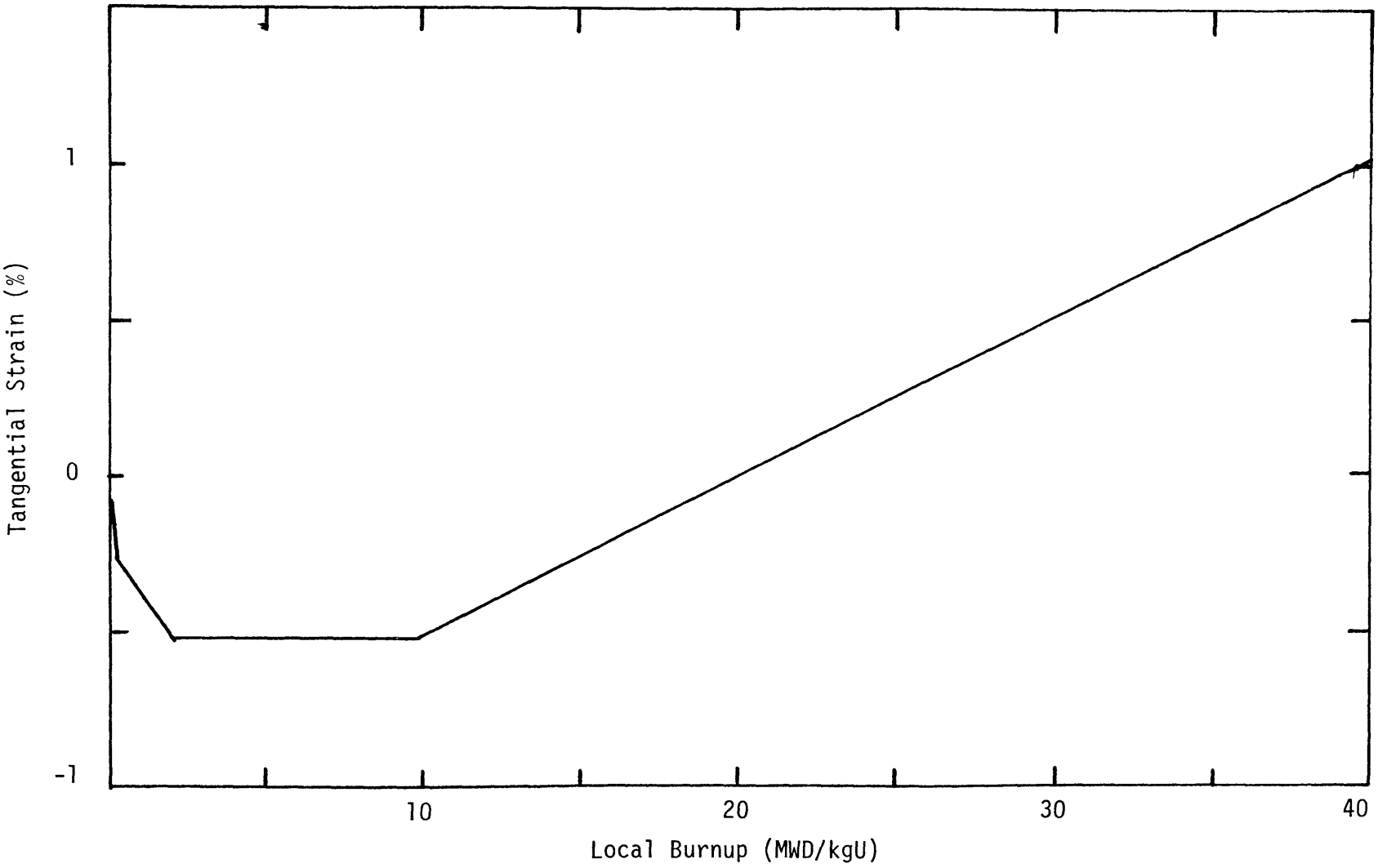

Figure A-13 Fuel Tangential Volume Strain Component

A.12 FUEL VOLUME STRAIN

Fuel tangential volume strain, with respect to a prescribed reference value at some point in burnup, is calculated using the following linearized approximation

$$\varepsilon_v = \frac{100}{3}\left[\frac{d_o}{d} - 1\right] - \varepsilon_{vref} \quad ; \text{ and}$$

$$\varepsilon_{vref} = \frac{100}{3}\left[\frac{d_o}{d_{ref}} - 1\right] \quad ;$$

where

ε_v = incremental or decremental fuel tangential volume strain (%);

ε_{vref} = reference fuel tangential volume strain (%);

d_o = BOL fuel density (%TD);

d_{ref} = fuel density at some prescribed reference burnup (%TD); and

d = fuel density for burnup values greater than reference burnup (%TD).

This relation is shown graphically in Fig. A-13 for a reference strain equal to zero at beginning of life (BOL).

A.13 FILL AND FISSION GAS CONDUCTIVITIES

Individual and mixed fuel-cladding gap gas conductivities were taken from MATPRO (Ref. 19). The overall thermal conductivity for a monatomic gas mixture is calculated from

$$k_{mix} = \sum_{i=1}^{n}\left[k_i/\left(1 + \sum_{\substack{j=1 \\ j\neq i}}^{n} \psi_{ij}\,\frac{X_j}{X_i}\right)\right] \quad ;$$

$$\psi_{ij} = \phi_{ij}\left[1 + 2.41\,\frac{(M_i - M_j)(M_i - 0.142M_j)}{(M_i + M_j)^2}\right] \quad ;$$

$$\phi_{ij} = \frac{[1 + (k_i/k_j)^{0.5}(M_i/M_j)^{0.25}]^2}{2^{1.5}(1 + M_i/M_j)^{0.5}} \quad ;$$

where

k_{mix} = gas mixture thermal conductivity (kW/m·K);

n = number of gas components in mixture;

X = component mole fraction;

M = component molecular weight; and

k = thermal conductivity of individual component (kW/m·K).

The three gas components considered in this study are

$k_{He} = 3.366 \times 10^{-6}\ T^{0.668}$;

$k_{Xe} = 4.0288 \times 10^{-8}\ T^{0.872}$; and

$k_{Kr} = 4.726 \times 10^{-8}\ T^{0.923}$;

where

k = gas thermal conductivity (kW/m·K); and

T = gas temperature (°K).

The above three conductivities are shown in Fig.A-14 illustrating the superior conductivity of helium.

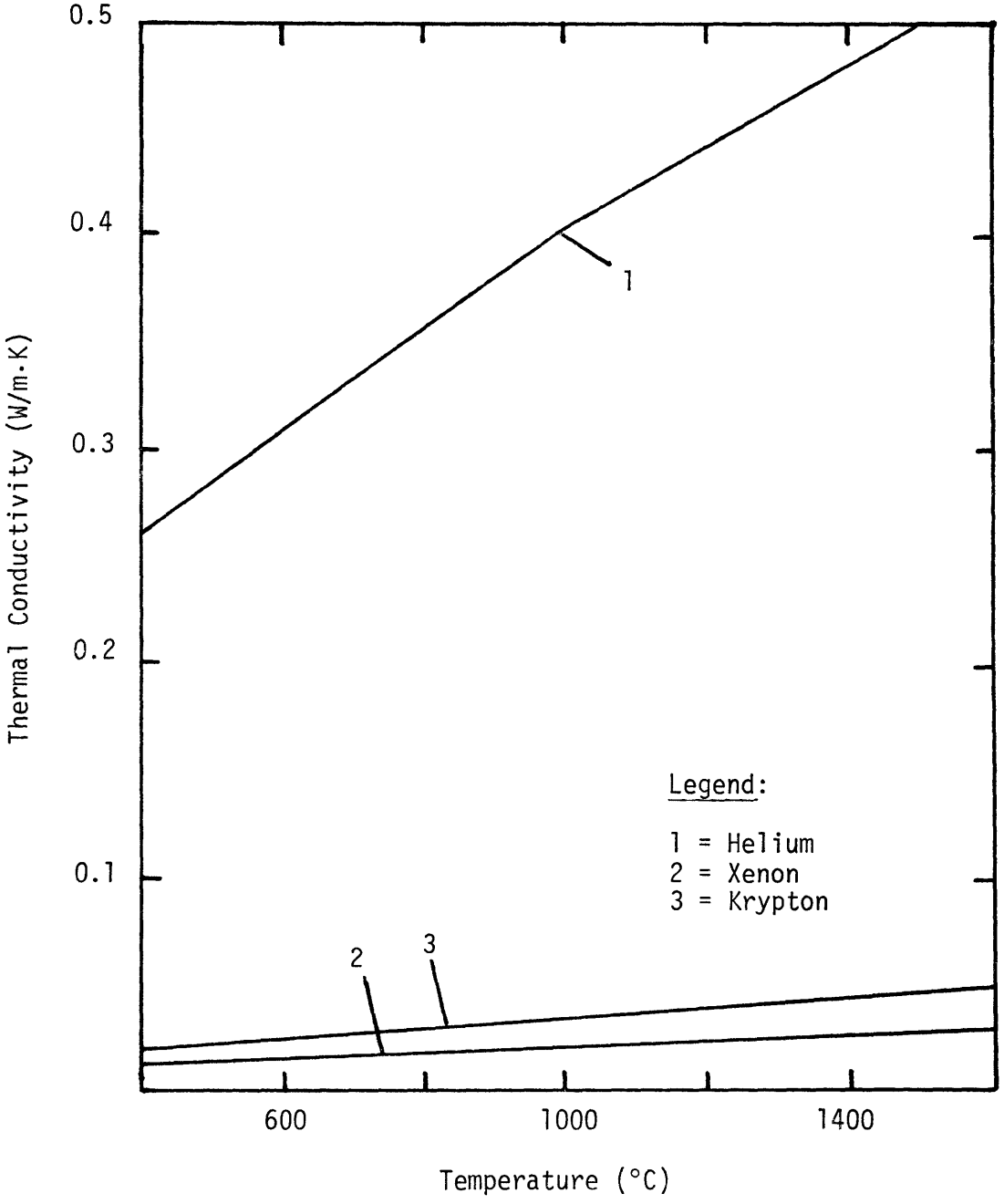

Figure A-14 Comparison of pure gas thermal conductivities (from Ref. 26).

A.14 FUEL-CLADDING CONTACT CONDUCTANCE

Pellet-cladding mechanical interaction (PCMI) requires an additional conductance term. The relation used in this study for fuel-cladding contact conductance was taken from Ref. 27 and is

$$h_c = \frac{k_m \lambda}{R} \left(\frac{P_c}{H}\right)^{0.5} \quad ;$$

$$k_m = \frac{2\, k_f\, k_c}{k_f + k_c} \quad ; \text{ and}$$

$$\lambda = \exp[0.5825\ \ell n(R \cdot 10^6) - 3.598] \quad ;$$

where

h_c = fuel-cladding contact conductance $(\frac{kW}{m^2 \cdot K})$;

k_F = fuel thermal conductivity at fuel surface (kW/m·K);

k_c = cladding thermal conductivity at inside surface (kW/m·K);

R = fuel surface roughness (m);

P_c = fuel-cladding contact pressure (MPa); and

H = Meyer Hardness of inside cladding surface (MPa).

The variation of contact conductance with fuel surface temperature is shown in Fig. A-15. Other data used to obtain this graph was taken from assembly 8-H22 operating at 100% full power at an average core burnup of 18.6 MWD/kgU. The contact pressure is set to unity so that variations with this parameter can be found if multiplied by $\sqrt{P}_c$. It should be noted that contact pressure and fuel surface temperature may be strongly coupled, especially for poor gas conductance values.

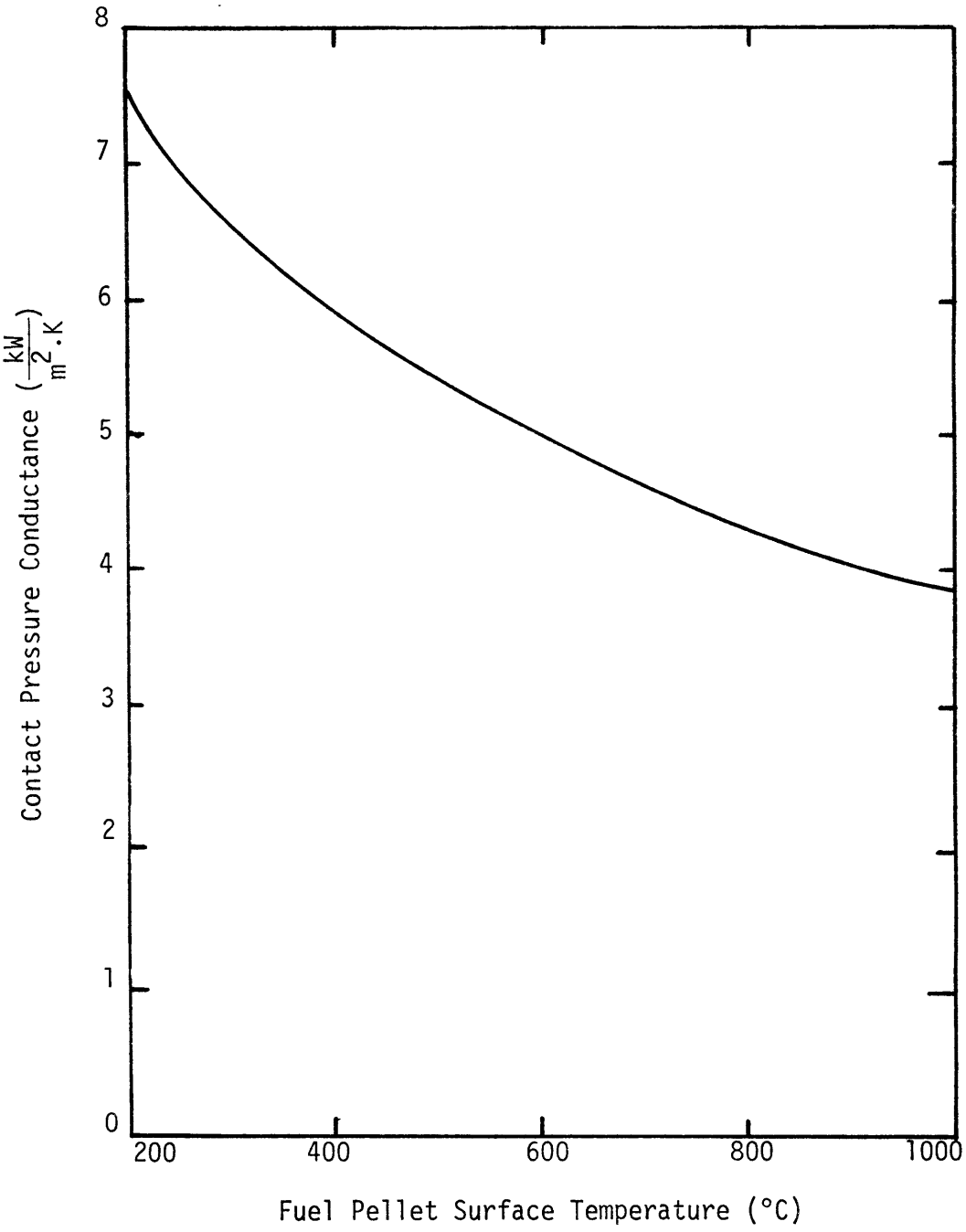

Figure A-15 Variation in pellet-cladding contact conductance with fuel pellet surface temperature for 1 MPa contact pressure.

B.1 FUEL ROD DESIGN PARAMETERS

The Connecticut Yankee fuel rod design parameters used in this study (listed below) were supplied by Northeast Utility Service Company. The lower pressurization value for the stainless steel case is specific to Connecticut Yankee (Haddem Neck) while the higher value is an estimate for rods in the San Onofre 1 plant. Fuel and cladding roughness values for both cases, as well as Zircaloy case design values (specific to Maine Yankee), were taken from Ref. 26.

Design Parameter	Connecticut Yankee	Maine Yankee
Cladding Material	SS304	Zircaloy-4
Fill Gas	Helium	Helium
Fill Pressure (kPa)	101.35, 2068.4	2068.4
Fuel Density (%)	95.17	95.00
Fuel Surface Roughness (μm)	0.991	0.991
Cladding Surface Roughness (μm)	1.500	1.500
Fuel Pellet Radius (mm)	4.870	4.782
Cladding Inside Radius (mm)	4.940	4.877
Cladding Outside Radius (mm)	5.359	5.588

B.2 OUTSIDE CLADDING TEMPERATURE REPRESENTATION

Thermal hydraulic and heat transfer calculations necessary to obtain outside cladding temperature are by-passed by the development of a simple piece-wise linear relation dependent on local linear heat generation rate (LHGR) value alone. A more detailed prediction of this temperature at a particular axial location along a rod requires a great deal of unavailable data. Therefore, a simple model based on obtainable data is deemed appropriate and allows straightforward and reasonable prediction of outside rod temperature essential for further fuel rod performance calculations.

Development of the simplified model can be viewed as a two-part procedure. The first goal is to calculate, as realistically as possible, actual LHGR and corresponding outside cladding temperature for a given rod at various power levels. The piece-wise linear model is then extracted from these results. Both nominal and hot rod cases are developed, providing some information on model sensitivity and the nature of the final steps in model formulation.

This representation has been utilized in a past fuel performance study (Ref. 9), the results of which serve as the Zircaloy case predictor. A summary of this work is provided in Section B.2.2.

B.2.1 Connecticut Yankee Outside Cladding Temperature

The outside cladding temperature model developed for Connecticut Yankee incorporates a good deal of data characteristic of this unit (supplied by Northeast Utility Service Company (NUSCO)). Pertinent information and methods for its interpretation are summarized below. Actual data from cycle 8 was used in place of design values if major differences exist.

Thermal-hydraulic Data	Value
Core heat output at 100% power (MW)	1825
Coolant system nominal pressure (MPa)	13.89
Core effective flow rate (10^3 kg/s)	11.22
Average coolant velocity along rods (m/s)	3.97
Core average LHGR (kW/m)	18.22
Core average temperature rise (°C)	29.28

Mechanical data - hot	Value
Fuel rod outside diameter (mm)	10.77
Fuel rod pitch (mm)	14.36

The coolant inlet temperature at different power levels is shown in Fig. B.1. The inlet temperature at 100% FP was changed to 276.6°C and held constant for core powers greater than this. Core powers ranging from 60 to 140% FP were investigated to produce sufficient data for model extraction.

Actual axial flux profile information during cycle 8 (core position J09, 11/15/78) was utilized as axial power profile data. This is graphically illustrated in Fig. B-2 and assumes the 35 axial nodes are located at the center of 35 axial sections of active fuel length. Grid spacer locations are depicted by flux depressions along the essentially flat profile. It is assumed that this axial power distribution function is applicable at other core powers.

Bulk coolant temperature and linear heat generation rate (LHGR) calculations rely on integrated values of this profile. Numerical techniques, namely Simpson's three-eighths and one-third rules, were applied with the following assumptions:

- the profile curve may be extrapolated at the beginning and end of active length as shown in Fig. B-2; and
- values at nodes 1 and 35 are taken as the midpoint between measured and extrapolated curves and held constant from these nodes to respective rod ends.

With this information, the bulk coolant temperature at an axial height, Z, may be expressed as

$$T_B = T_I + f\ \Delta T \quad ;$$

and

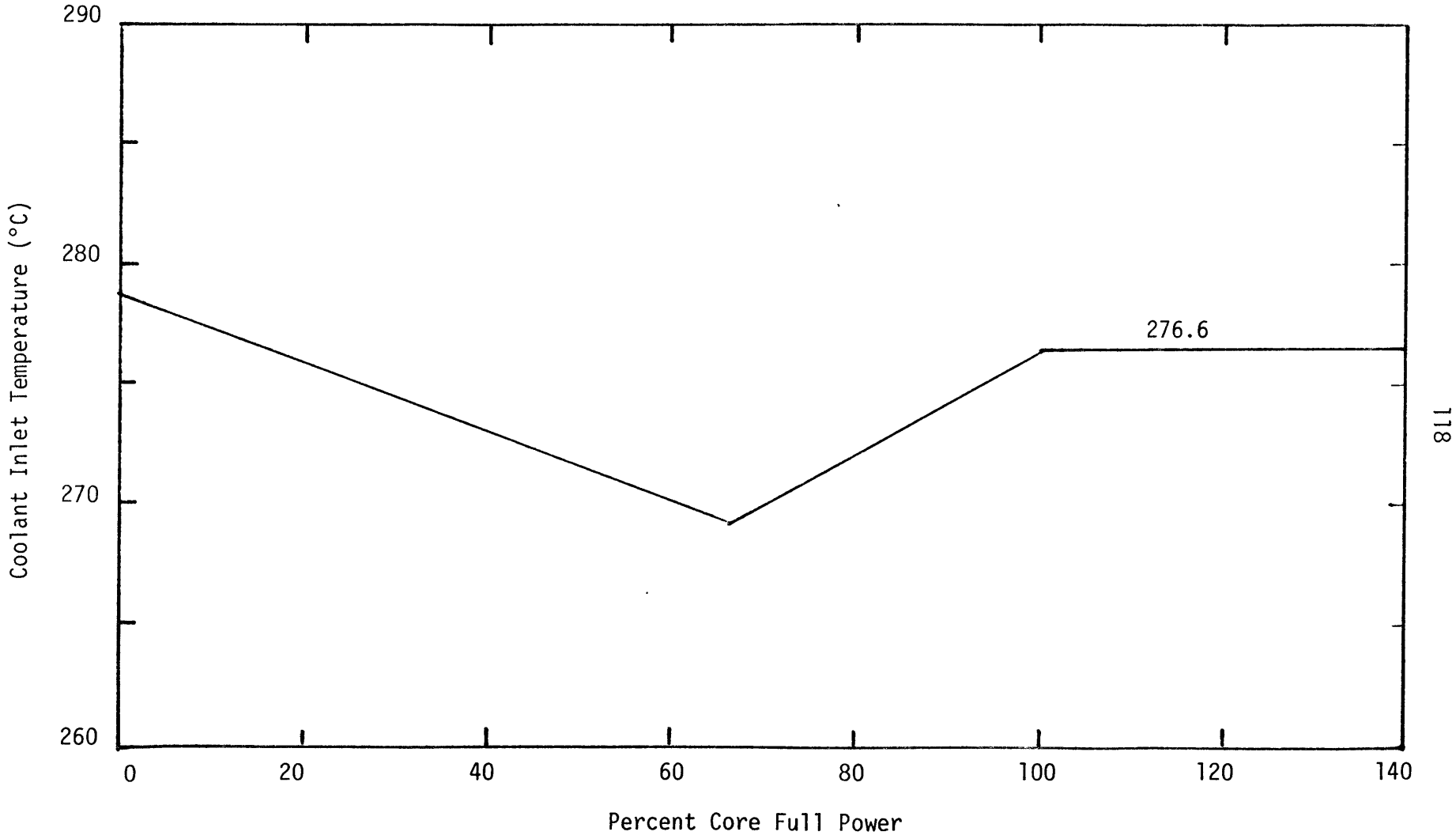

Figure B-1 Coolant Inlet Temperature for Various Core Powers

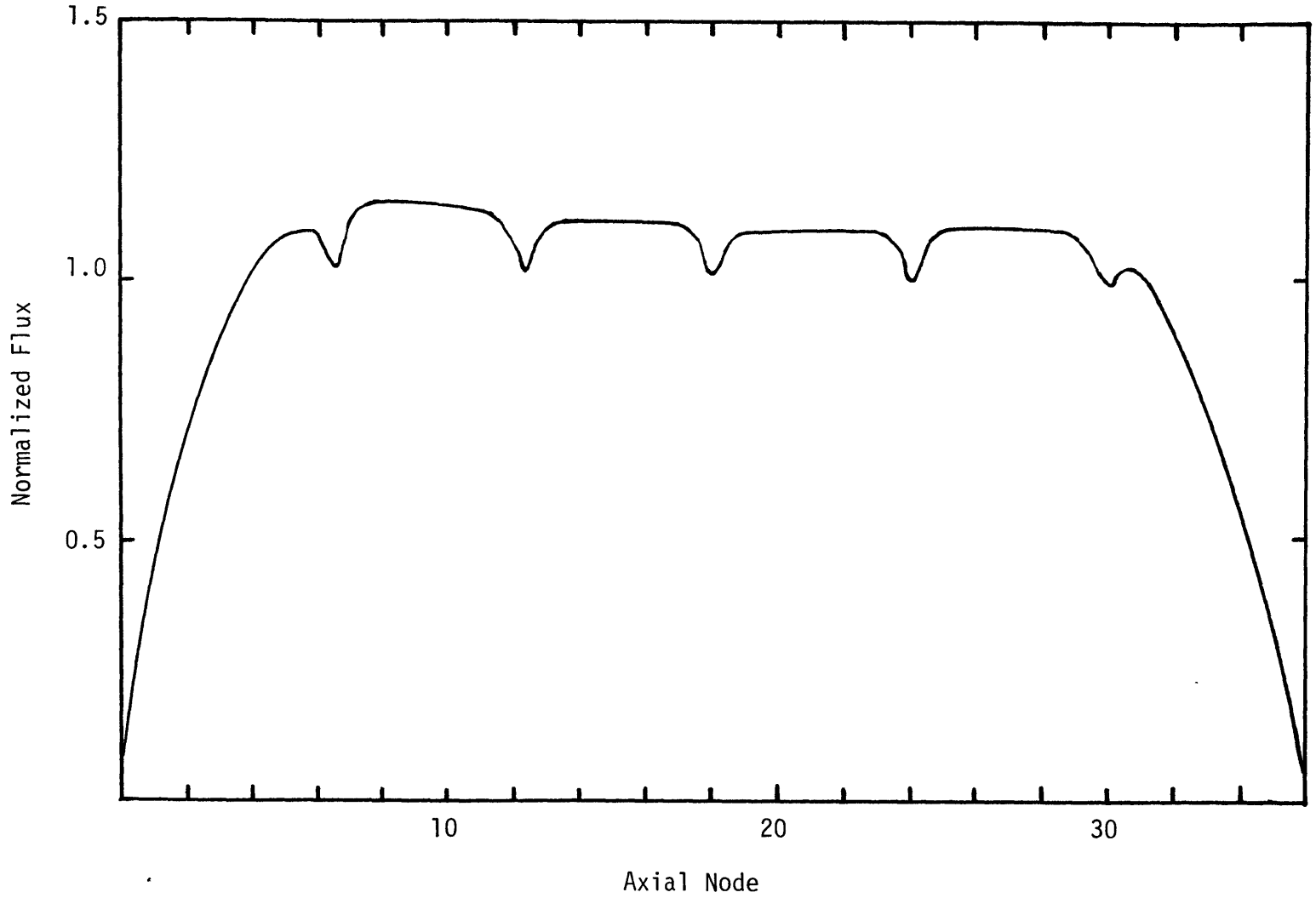

Figure B-2 Connecticut Yankee Axial Flux Profile (core position J09, 11/15/78)

$$f = \frac{\int_0^Z F\,dz}{\int_0^L F\,dz} \quad ;$$

where

T_B = bulk coolant temperature at channel height Z (°C);

T_I = inlet coolant temperature (°C);

ΔT = temperature rise for given rod (°C);

f = linear integral fraction of total integrated axial power distribution;

F = axial power distribution function; and

L = active fuel length (# of axial sections).

With the knowledge of coolant inlet temperature and temperature rise, the bulk coolant temperature depends only on the function f which is shown in Fig. B-3.

A linear heat generation rate (LHGR) correlation for this power distribution may be simply defined as

$$q' = \bar{q}'\ f'\ F_{x\text{-}y} \quad ;$$

$$\bar{q}' = \pi\ D_o\ \bar{q}'' \quad ; \text{ and}$$

$$f' = \frac{F}{\frac{1}{L}\int_0^L F\,dz} \quad ;$$

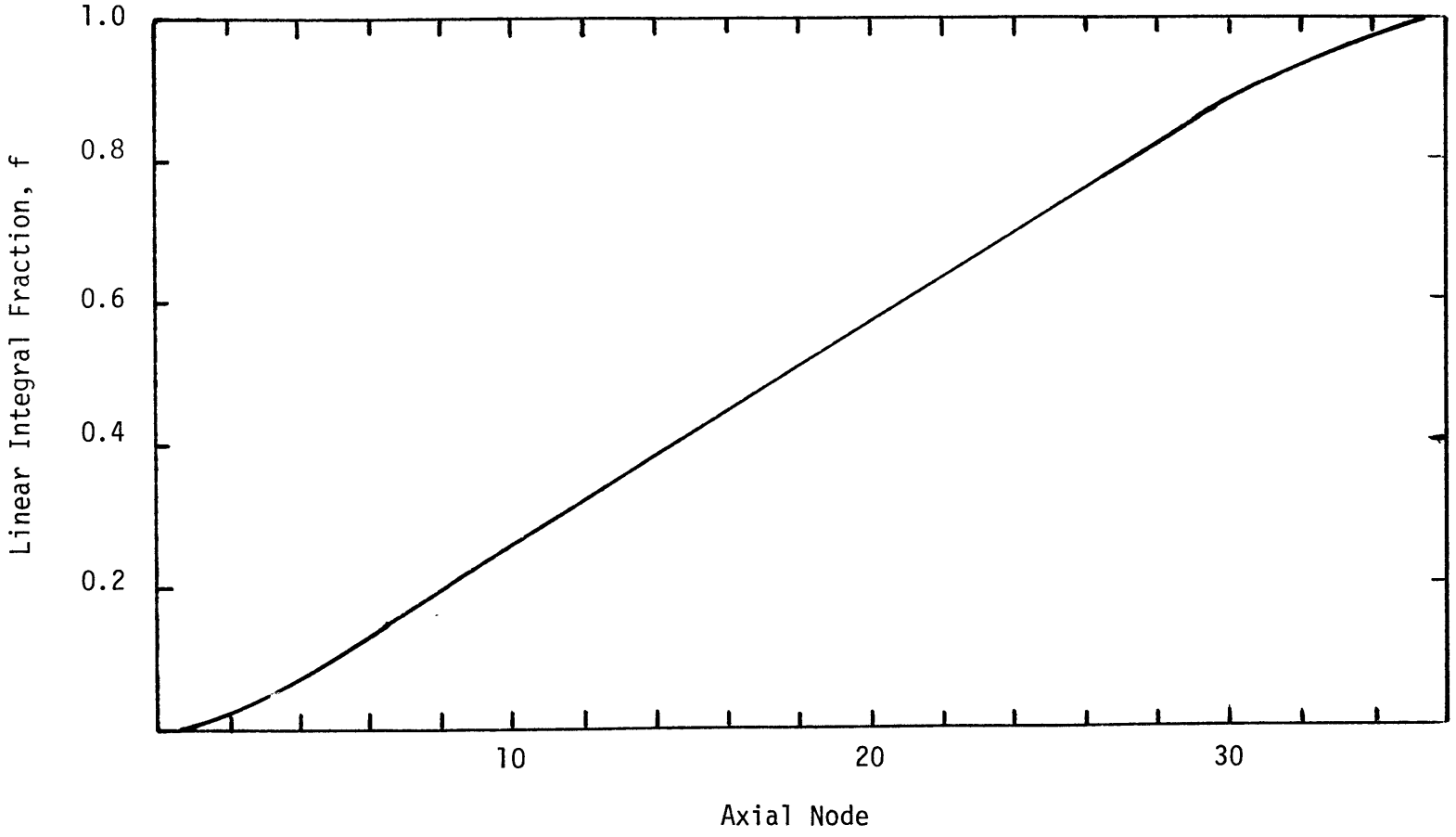

Figure B-3 Fraction of Total Integrated Axial Power

where

q' = local (at height Z) LHGR (kW/m);

$\bar{q}'$ = core average LHGR (kW/m);

$\bar{q}''$ = core average heat flux (kW/m^2);

D_o = fuel rod outside diameter (hot) (m);

f' = local to average power factor (see Fig. B-2); and

F_{x-y} = radial peaking factor (1 for nominal rod; 1.28 for hot rod)

It is assumed that the radial peaking factor used in the hot rod case remains constant in the axial direction.

The 100% FP enthalpy rise for both the nominal and hot rod cases were obtained using available temperature information and thermodynamic data (Refs. 28, 29). The average core temperature rise was used for enthalpy calculations in the nominal case, which served as a base for generating all other temperature/enthalpy rise data using

$$\Delta h = (\Delta h)_o \, f_p \, F_{x-y} \quad ;$$

where

Δh = bulk coolant enthalpy rise (kJ/kg);

$(\Delta h)_o$ = bulk coolant enthalpy rise for 100% FP nominal case (kJ/kg);

f_p = fraction of core full power; and

F_{x-y} = radial peaking factor as above.

Inlet enthalpy values were obtained using inlet temperatures supplied in Fig. B-1, thus, exit enthalpy and corresponding temperature values could be determined. The previously tabulated value of bulk

coolant nominal system pressure was used in the above and remaining analysis (i.e., inlet pressure variations and core pressure drop ignored).

With coolant pressure and inlet/exit temperatures, all other necessary bulk coolant inlet/exit properties are characterized. Further calculations are simplified by employing average property values defined as

$$\overline{C}_p = \frac{\Delta h}{\Delta T}$$

where

$\overline{C}_p$ = average specific heat (kJ/kg·K);

Δh = enthalpy rise (defined above) (kJ/kg); and

ΔT = temperature rise (°K).

Also,

- density, ρ (kg/m^3);
- thermal conductivity, k (kW/m·K); and
- dynamic viscosity, μ (kg/m·s);

use the following general form

$$y = \frac{y_i + y_e}{2}$$

where

y, y_i, y_e = ρ, K, or μ average, inlet, and exit values, respectively.

Computed property values for all investigated power levels are given in Table B-1 for the nominal rod case and Table B-2 for the hot rod.

Table B-1 Nominal Rod Averaged Properties

Percent Full Power	ΔT_{core} (°C)	Δh_{core} (kJ/kg)	$\overline{C}_p$ (kJ/kg°K)	$\overline{\rho}$ (kg/m^3)	$\overline{k}$ (W/m°K)	$\overline{\mu}$ (10^{-5} $\frac{kg}{m \cdot s}$)
60	18.5	93.5	5.06	760.9	0.587	10.00
80	24.3	124.6	5.14	751.7	0.578	9.84
100	29.3	155.8	5.32	737.1	0.565	9.63
120	34.8	186.9	5.38	731.1	0.558	9.51
140	40.1	218.1	5.44	725.0	0.551	9.42

Table B-2 Hot Rod Averaged Properties

60	23.6	119.6	5.07	757.2	0.583	9.96
80	30.4	159.5	5.25	744.6	0.572	9.76
100	36.9	199.4	5.40	728.7	0.555	9.47
120	43.1	239.3	5.55	720.6	0.547	9.34
140	48.9	279.1	5.71	712.4	0.538	9.26

All the above information is integrated into the final expressions for outside cladding temperature and are (Ref. 30) for $T_o < T_{sat}$ (336°C)

$$T_o = \frac{q'}{\pi D_o h_C} + T_B \quad ; \quad \text{and}$$

$$h_C = .023 \frac{K}{D_C} R_e^{.8} P_r^{.4} \quad \text{(Dittus-Boilter)} \quad ;$$

and for $T_o > T_{sat}$

$$T_o = \frac{60\left[\frac{q'}{3.155 \times 10^{3} \pi D_o}\right]^{.25}}{1.8 \exp[P/6.205]} + T_{sat} \quad \text{(Jens-Lottes)} \quad ;$$

where

T_o = outside cladding temperature (°C);

T_{sat} = bulk coolant saturation temperature (°C);

T_B = bulk coolant temperature (°C);

q' = local LHGR (kW/m);

h_C = Dittus-Boelter convective heat transfer coefficient ($kW/m^2 \cdot k$);

D_o = hot fuel rod outside diameter (m);

D_e = hydraulic diameter (using hot dimensions) (m);

R_e = Reynolds number (dimensionless);

P_r = Prandlt number (dimensionless); and

P = nominal system pressure (MPa).

Axial variation of bulk coolant and outside rod temperatures are shown in Figs. B-4 and B-5 for the 100% full power nominal and hot rod cases.

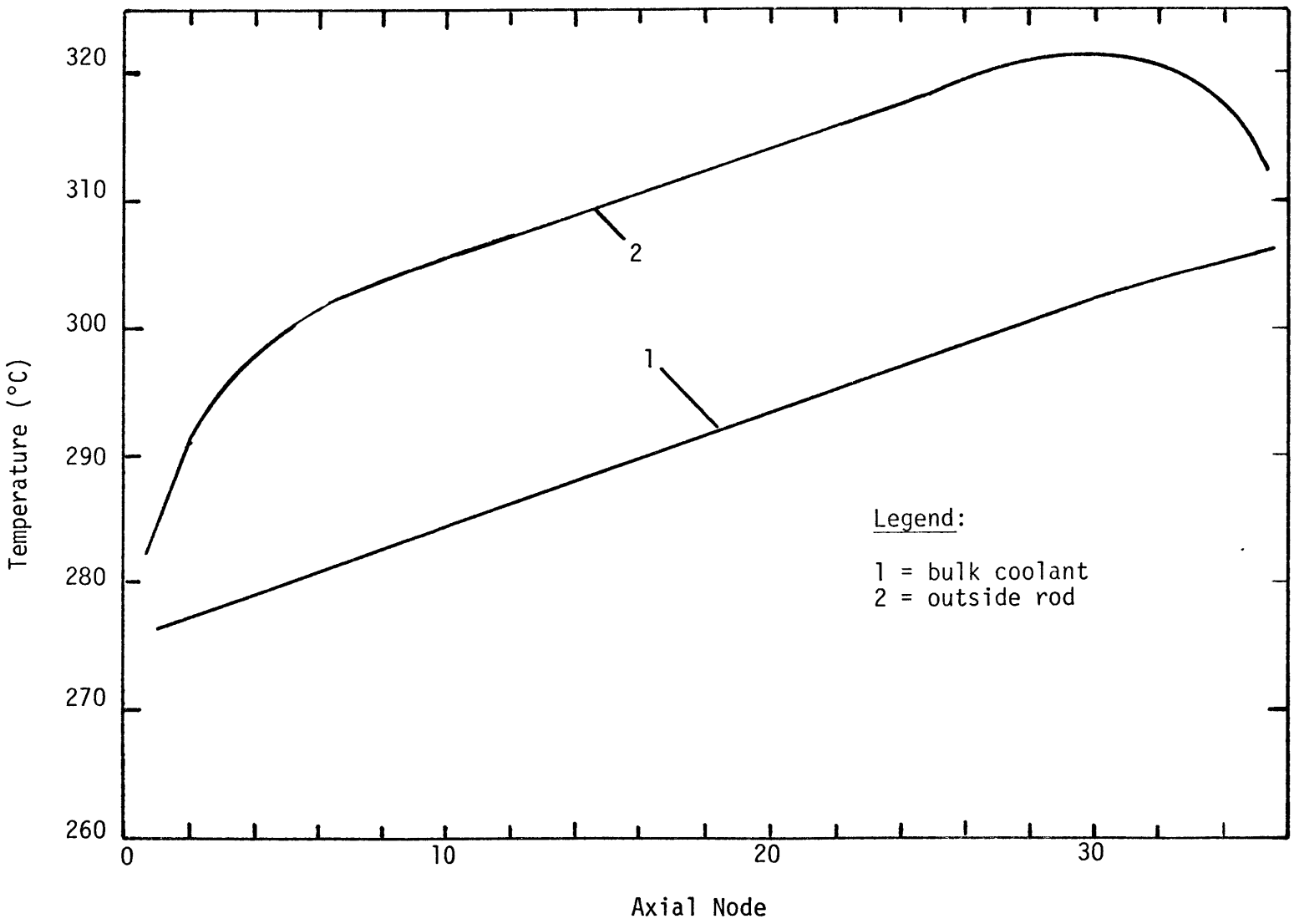

Figure B-4 Bulk Coolant and Outside Rod Axial Temperature Profiles for Nominal Rod (100% full power)

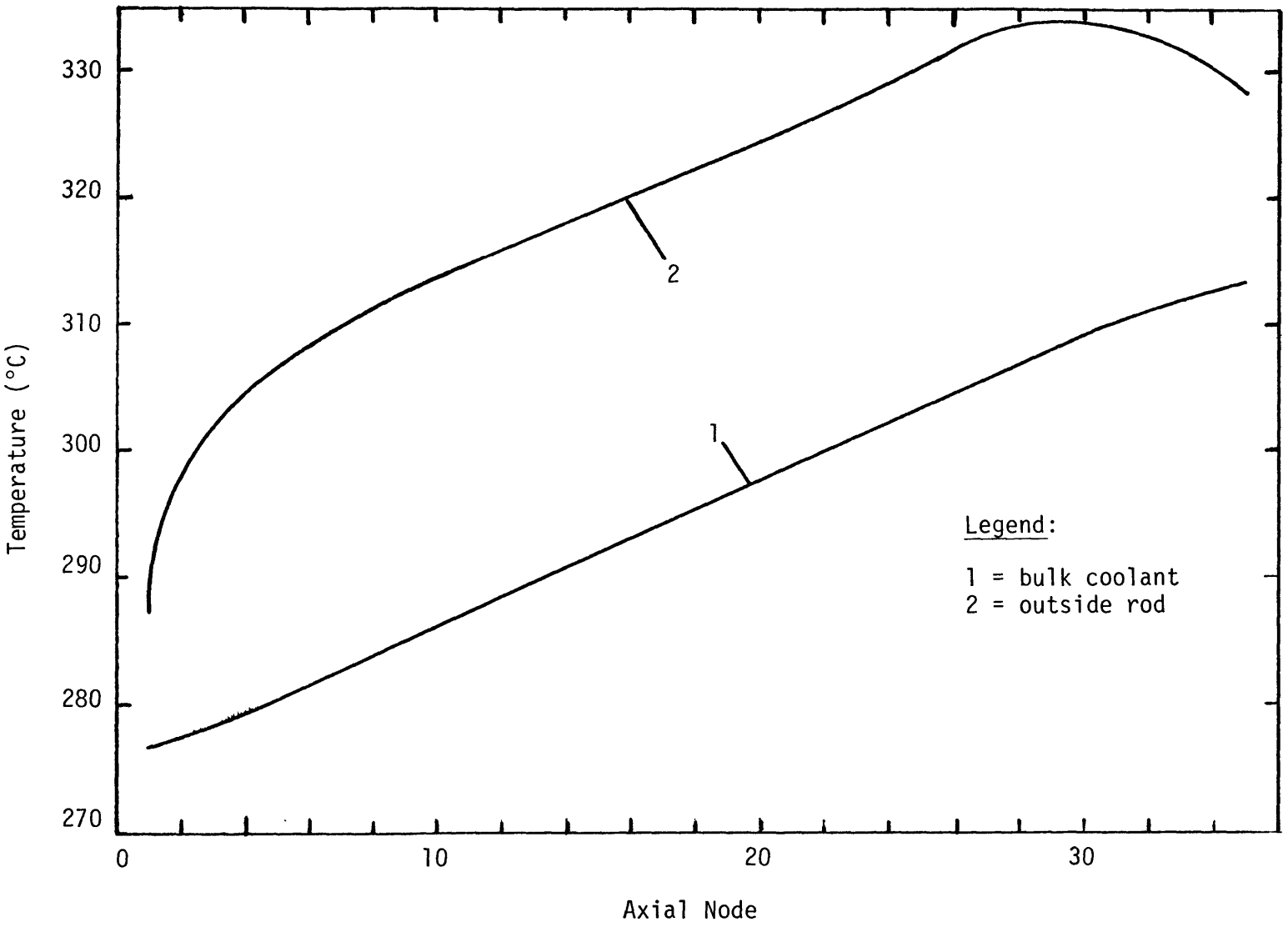

Figure B-5 Bulk Coolant and Outside Rod Axial Temperature Profile for Hot Rod

The final step in model formulation is shown in Fig. B-6 for the nominal case. The profiles illustrate outside cladding temperature and corresponding LHGR values along the nominal rod for various core power levels. The simplified model involves "compressing" this information into the piece-wise representation indicated by the heavier lines. Thus,

for $q' \leq 18$ (kW/m)

$$T_o = 279 + 1.61\ q' \quad ;$$

for $18 < q' \leq 29$ (kW/m)

$$T_o = 308 + 2.73\ (q' - 18) \quad ;$$

and for $q > 29$ (kW/m)

$$T_o = 338$$

where

T_o = outside cladding temperature (°C); and

q' = local LHGR (kW/m).

Although the ultimate model choice seems quite arbitrary, its design reflects the general trend of actual data. The same representation may be used for the hot rod case (Fig. B-7) and illustrates the insensitive nature of this model.

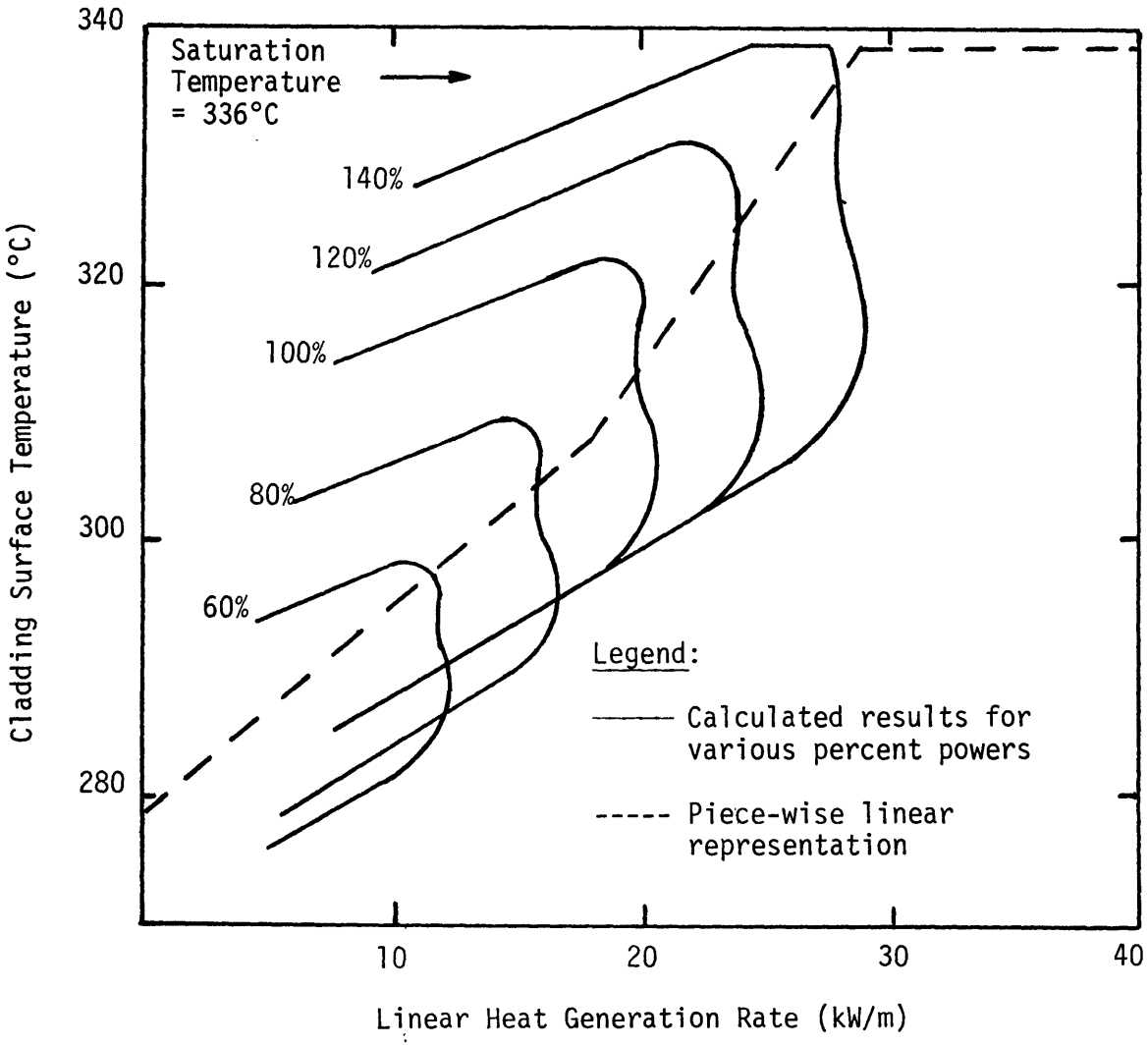

Figure B-6 Comparison of Connecticut Yankee nominal fuel rod outside cladding temperature to modeled outside cladding temperature correlation.

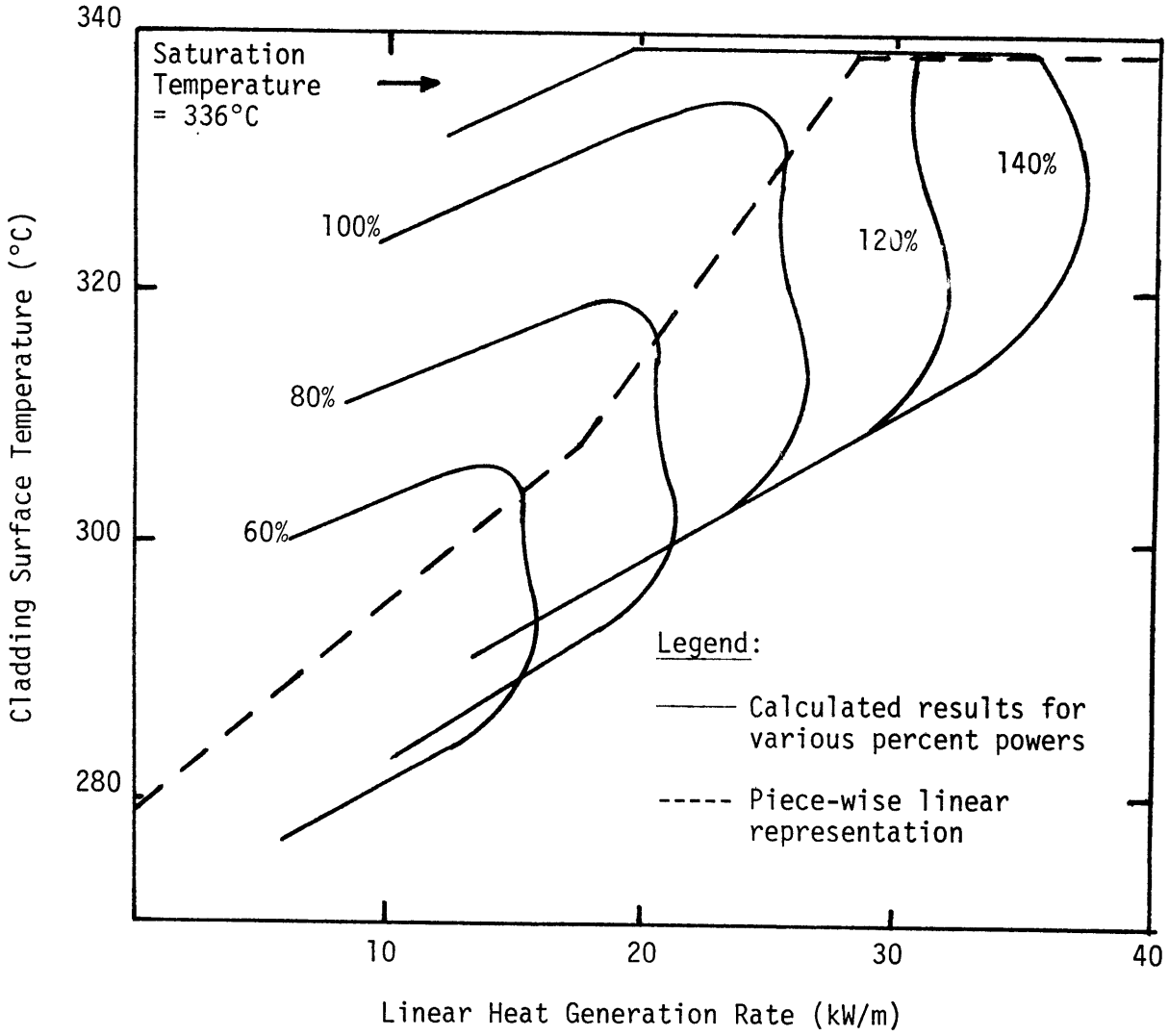

Figure B-7 Comparison of Connecticut Yankee hot fuel rod outside cladding temperature to modeled outside cladding temperature correlation.

B.2.2 Maine Yankee Outside Cladding Temperature

The model used as the Zircaloy outside rod temperature predictor was taken from a fuel performance study done by Maki and Meyer for Maine Yankee (Ref. 9). Since axial power profile data was unavailable, a chopped cosine distribution was used. The remaining analysis was done in a fashion similar to that presented in the prior section. The results are graphically displayed in Figs. B-8 and B-9 and may be summarized as

$$T_o = 282 + 2.6\ q' \text{ for } 0 \leq q' \leq 25 \text{ (kW/m); and}$$

$$T_o = 347 \text{ for } q' > 25 \text{ (kW/m);}$$

where

T_o = outside cladding temperature (°C); and

q' = local LHGR (kW/m).

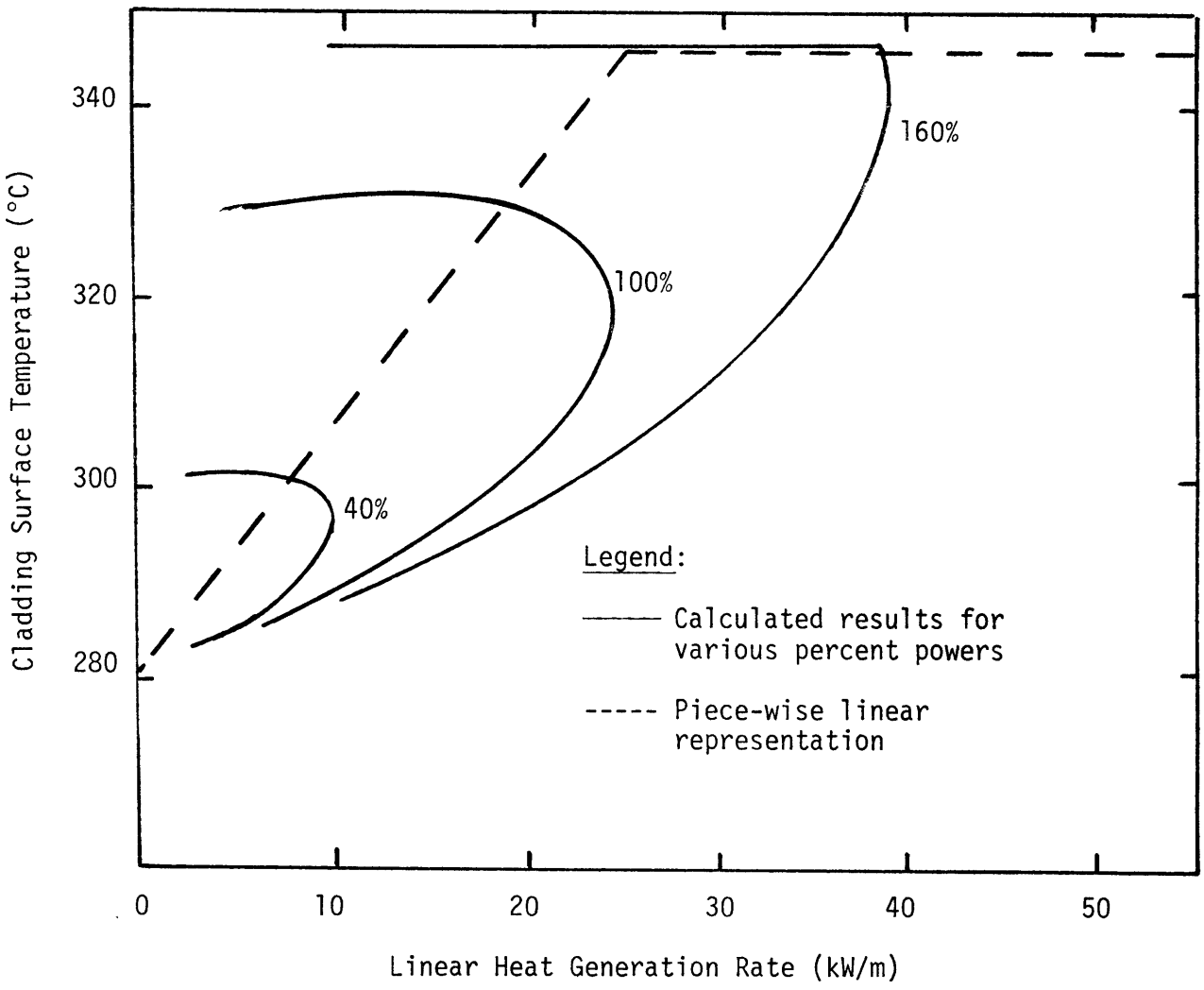

Figure B-8 Comparison of Maine Yankee nominal fuel rod outside cladding temperature to modeled outside cladding temperature correlation (from Ref. 9).

C ANALYTIC CONDITIONING MODEL

A closed form solution for fuel-cladding contact pressure (and therefore cladding stresses) is derived for stainless steel. The concept of constant power "conditioned" adopted in this study represents a state in which the contact pressure has attained a steady state value (i.e., the fuel and inside rod surfaces deflect at a constant rate). The model provides a desirable analytic solution which predicts stress behavior after "just contact" for constant power operation in the region of fuel swelling (burnup > 10 MWD/kgU). Conditioning time and differences due to parameter variations may be investigated without detailed computation. Comparison to code results and discussion of model approximations/limitations are also given.

C.1 Stainless Steel Conditioning Model

Using the single element model discussed in Section 3.3.1, the inside cladding deflection from its "just contact" position may be represented as

$$u_a = \frac{1}{2}\left[\varepsilon_\theta^c(b+a) - \varepsilon_r^c(b-a)\right] + \frac{P_c}{2}\left[C_\theta(b+a) - C_r(b-a)\right] \quad ;$$

and

$$C_\theta = \frac{1}{E}\left[\frac{a}{(b-a)} + \frac{\nu a}{(b+a)}\right]$$

$$C_r = -\frac{1}{E}\left[\frac{a}{(b+a)} + \frac{\nu a}{(b-a)}\right]$$

where

u_a = inside cladding radial deflection (mm);

a = cold BOL inside cladding radius (mm);

b = cold BOL outside cladding radius (mm);

P_c = fuel-cladding contact pressure (MPa);

$\varepsilon_\theta^c, \varepsilon_r^c$ = tangential and radial creep strains, respectively (mm/mm);

ν = cladding Poisson ratio;

E = cladding modulus of elasticity (MPa).

Further analysis requires an expression for deflection rate since the creep strain values depend on an integrated time dependent contact pressure. Thus,

$$\dot{u}_a = \frac{1}{2}\left[\dot{\varepsilon}_\theta^c(b+a) - \dot{\varepsilon}_r^c(b-a)\right] + \frac{\dot{P}_c}{2}\left[C_\theta(b+a) - C_r(b-a)\right]$$

where time differentiation is represented by a dot above the appropriate symbols.

The creep strain rate relations incorporate single element stress expressions from Section 3.3.1 and component relations of Section 3.3.2 (symbols defined therein). Factoring out contact pressure yields

$$\dot{\varepsilon}_\theta^c = f_c \frac{C(f_p\phi_o)}{2}\left[P_c\left(\frac{2a}{(b-a)} - \frac{a}{(b+a)}\right) + (2\sigma_\theta^o - \sigma_r^o - \sigma_z^o)\right] \quad ; \text{ and}$$

$$\dot{\varepsilon}_r^c = -f_c \frac{C(f_p\phi_o)}{2}\left[P_c\left(\frac{2a}{(b+a)} + \frac{a}{(b-a)}\right) - (2\sigma_r^o - \sigma_\theta^o - \sigma_z^o)\right] \quad ;$$

where

$\dot{\varepsilon}_\theta^c, \dot{\varepsilon}_r^c$ = tangential and radial creep strain rate components (s^{-1});

f_p = fraction of core full power;

ϕ_o = 100% full power fast flux ($E > 0.82$ MeV $n/m^2 \cdot s$);

$\sigma_r^o, \sigma_\theta^o, \sigma_z^o$ = zero contact pressure cladding stress components (MPa).

The above deflection rate may now be written in the simplified form of

$$\dot{u}_a = K_o P_c + K_1 f_c \dot{P}_c + K_2 f_c$$

where

$$K_o = [C_\theta(b+a) - C_r(b-a)]/2 \quad ;$$

$$K_1 = f_t \frac{C f_p \phi_o}{2} \left[\frac{a(3b^2 + a^2)}{b^2 - a^2} \right] \quad ;$$

$$K_2 = f_t \frac{C f_p \phi_o}{4} \left[(b+a)(2\sigma_\theta^o - \sigma_r^o - \sigma_z^o) - (b-a)(2\sigma_r^o - \sigma_\theta^o - \sigma_z^o) \right] \quad ;$$

$$f_t = 8.64 \times 10^4 \text{ (s/day)} \quad ;$$

and all symbol definitions are as above.

Under the assumption that the fuel thermal strain remains essentially unchanged (i.e., constant power, negligible contact conductance effect) and the radial component of volume strain is one-third of the total volume strain, the fuel surface deflection may be expressed as

$$u_F = R_F \frac{\varepsilon_v}{3} - R_F \frac{(1-\nu_F)}{E_F} P_c$$

where

u_F = fuel surface radial deflection (mm);

R_F = cold swelled fuel radius (mm);

ε_v = fuel volume strain (mm/mm);

P_c = fuel-cladding contact pressure (MPa);

ν_F = fuel Poisson ratio; and

E_F = fuel modulus of elasticity (MPa).

The time dependent relation for volume strain may reduce complexity if linearized as

$$\varepsilon_v = \left[\frac{d_o}{C_1 - C_2 t} - 1 \right]$$

$$\approx \left[\left(\frac{d_o}{C_1} - 1 \right) + \frac{d_o C_2}{C_1^2} t \right]$$

where

d_o = beginning of life (BOL) fuel density (%TD); and

t = real time after contact (days).

The coefficients C_1 and C_2 are determined from the appropriate density relation supplied in Section A.11 (applicable in the fuel swelling region). The general form is

$$d = d_1 - A(B^L - B) \quad ;$$

where

d = local fuel density (%TD);

B^L = local fuel burnup (MWD/kgU); and

d_1,A,B = constants as defined in Section A.11.

By using the following two relations

$$B^L = B^L_o + F^N_Q \, \Delta B_C \quad ;$$

and core burnup after "just contact" (MWD/kgU)

$$\Delta B_C = 2.825 \times 10^{-2} \, f_P \, t$$

the burnup dependent form may be redefined as

$$d = C_1 - C_2 \, t$$

$$= [d_1 - A(B^L_o - B)] - [2.825 \times 10^{-2} \, f_P \, A \, F^N_Q] \, t$$

where

B^L_o = local burnup at "just contact" (MWD/kgU);

F^N_Q = local nuclear heat flux hot channel factor at 100% full power; and

f_P = fraction of core full power;

and all other symbol definitions are as above.

The constant power assumption also restricts F^N_Q to remain constant over the conditioning interval. It should also be noted that the coefficient in the core burnup expression converts core EFPD to MWD/kgU.

Taking the time derivative of fuel surface deflection and equating it to the inside cladding deflection rate results in the following differential equation

$$\dot{P}_c + \frac{K_1 f_c}{K_o + F_o} P_c = \frac{F_1 - K_2 f_c}{K_o + F_o} \quad ;$$

where

$$F_o = R_F (1-\nu_F)/E_F \quad ;$$

$$F_1 = R_F d_o C_2/3 C_1^2 \quad ;$$

and all other symbols are as previously defined in this section.

Using the boundary condition of zero contact pressure at a "just contact" reference time of zero, contact pressure behavior takes the form

$$P_c = \frac{(F_1/K_1) - (K_2/K_1) f_c}{f_c} (1 - e^{-t/\tau}) \quad ;$$

where the time constant is

$$\tau = (K_o + F_o)/K_1 f_c \quad ;$$

and where

P_c = fuel cladding contact pressure (MPa);

τ = "conditioning" time constant (days); and

t = real time after contact (days).

Variation in cladding hoop stress may now be simply calculated using the relations of Section 3.3.1, thus

$$\sigma_\theta = \sigma_\theta^o + \frac{a}{(b-a)} P_c \quad .$$

The results of this equation for creep acceleration factors of 11, 55, and 110 are given in Fig. C-1 for a non-pressurized rod and in Fig. C-2 for the pressurized case. The values used to generate these curves are given in Table C-1.

While analytic and computational results agree well for the pressurized case (see Fig. 4-5), notable differences exist without pressurization (see Fig. 4-4). The complex thermal behavior, encountered when contact conductance appreciably alters overall gap conductivity, has not been accounted for in the above model. However, once the gap thermal characteristics "stabilize" (i.e., increased contact pressure has minimal impact on fuel surface temperature), the model predicts curve shape and steady state pressure values reasonably well. A more detailed discussion of code results is found in Section 4.

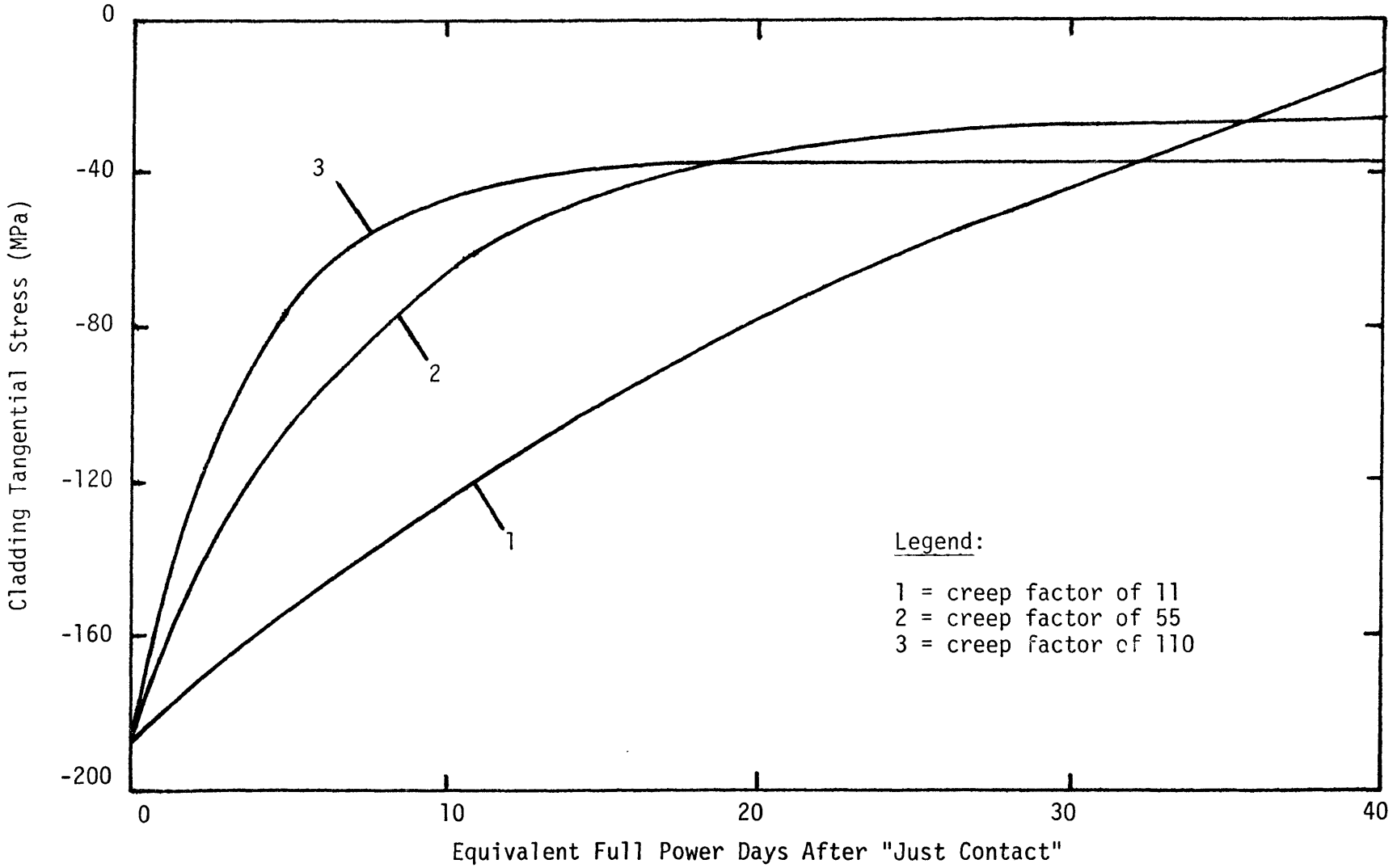

Figure C-1 Hoop stress variation for unpressurized SS304 as predicted by the analytic conditioning model.

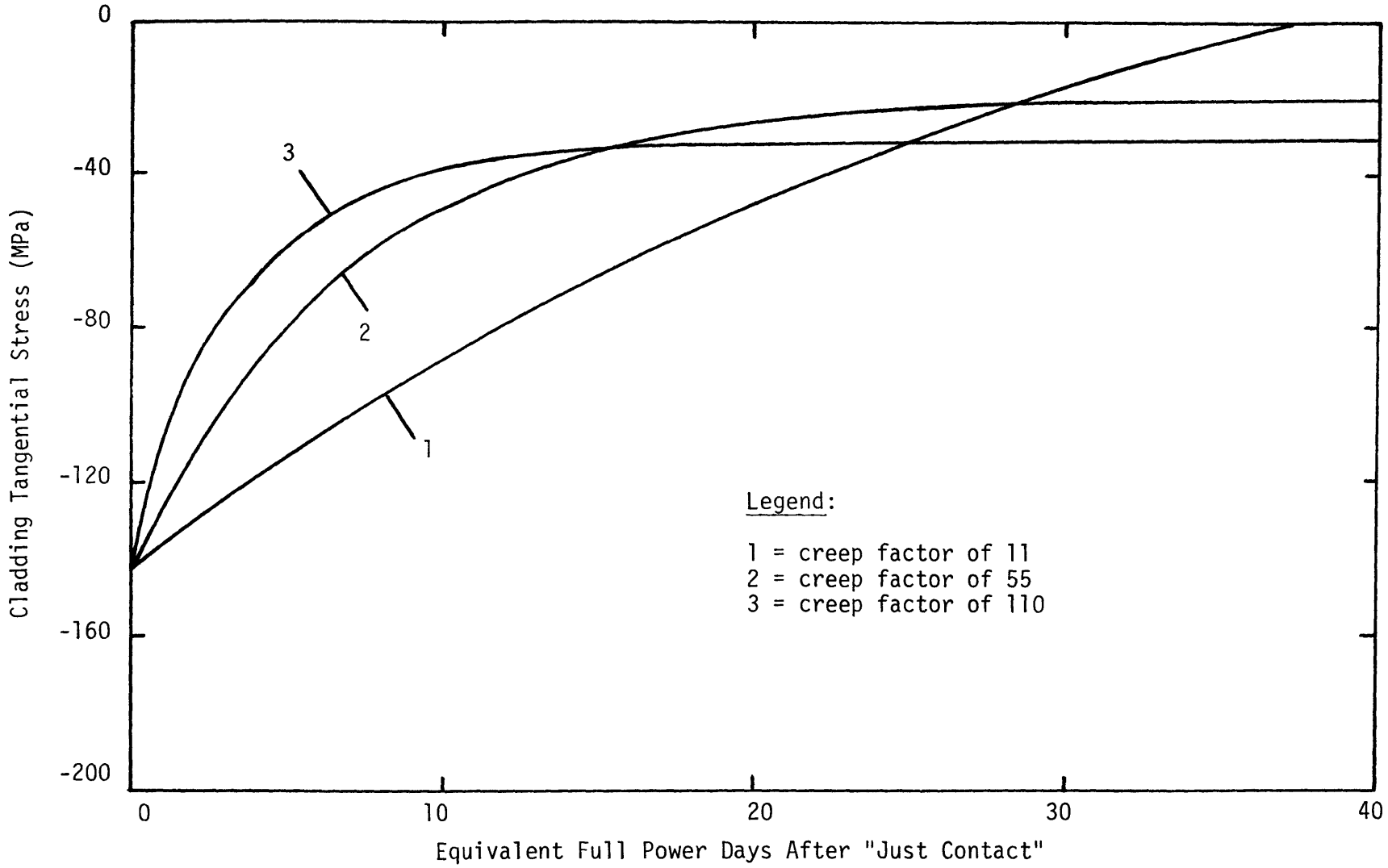

Figure C-2 Hoop stress variation for pressurized SS304 as predicted by the analytic conditioning model.

Table C-1

Symbol	Definition	Value	
		No Prepress.	Prepress.
E_c	Cladding Elastic Modulus (GPa)	177.39	177.39
ν_c	Cladding Poisson Ratio	.318	.318
E_f	Fuel Elastic Modulus	169.35	173.19
ν_f	Fuel Poisson Ratio	.301	.301
σ_r^o	Zero Contact Cladding Radial Stress (MPa)	-7.86	-9.75
σ_θ^o	Zero Contact Cladding Tangential Stress (MPa)	-188.50	-142.12
σ_z^o	Cladding Axial Stress (MPa)	-98.18	-75.93
ϕ_o	Fast Flux ($E > 0.1$ MeV $\frac{n}{m \cdot s^2}$)	1.379×10^{18}	1.379×10^{18}
T_{avc}	Cladding Average Temperature (°C)	340.4	340.4
R_F	Cold Swelled Fuel Radius (mm)	4.890	4.890
B_L	Local Burnup (MWD/kgU)	27.16	27.16

Unpressurized case results:

$$\sigma_\theta(\text{MPa}) = \left[\frac{140.8\ f_c + 1317.2}{f_c}\right](1 - e^{-tf_c/397.4}) - 188.5$$

Pressurized case results:

$$\sigma_\theta(\text{MPa}) = \left[\frac{99.1\ f_c + 1269.8}{f_c}\right](1 - e^{-tf_c/381.4}) - 142.1$$

D. STRESS COMPUTER CODE

The following section reviews the input format and procedure for use of the STRESS code. As stated in Section 3.1, the code capabilities are versatile and two-fold. However, some changes may improve its versatility and allow parametric studies made more readily. Computation time may also be reduced by use of the stainless steel analytic conditioning model of Section C.1.1. Sample output is given in Section D.2 and a listing is supplied in Section D.3.

D.1 Input Procedure and Format

The STRESS code listing supplied in Section D.3 is designed to run on the Multics System (Honeywell Fortran compiler). The input is entered entirely from an interactive on-line terminal (for long term cladding creepdown/fuel swelling to initial hard contact behavior) or accompanied by file input (designated FILE 7 for conditioning, ramping, and maneuvering calculations). The first input data is the program selection,

$$\text{nprog} = \begin{cases} 1 \text{ for condition and ramp.} \\ 2 \text{ for creepdown to contact.} \end{cases}$$

The second input data value designates the desired creep factor, f_c, as mentioned in Section A.6. These options are given in Table D-1 for each material. Since these factors are prescribed, one improvement to the code would be to enter the actual creep multiplication factor desired. This could be done by changing the input format to read a floating point variable designated "accel" (changed from "mod") and the variable list and logic of Subroutine Creep.

Table D-1 Creep Acceleration Factor Options

Input Value	Creep Factor	
	SS304	Zircaloy
1	1	1
2	11	2.3
3	22	5.8
4	55	11.5
5	220	23.1
6	110	57.7
7	---	115.5*

*Not recommended for use due to accuracy criteria.

If the program selection "nprog" is equal to 2,* the only other interactive data input is for cladding material selection, or

$$\text{mat} = \begin{cases} 1 \text{ for SS304.} \\ 2 \text{ for Zircaloy.} \end{cases}$$

No information is required from file 7 and program execution begins. All other information is supplied internally in program statements or block data. These must be edited if alternate values are necessary.

If the program selection."nprog" is equal to 1, information from file 7 is read. This file contains the following variables:

mat	= cladding material;
number	= number of ramping or maneuvering cases;
pow	= fraction of full power (%);
bc	= prescribed cumulative core burnup (MWD/kgU); and
days	= EFPD to condition cladding prior to ramping or maneuvering.

The remaining input from file 7 is the number of ramps in each case, the initial and final power of each ramp or maneuver, and the time between these power levels. The input format for this information may be found in the program listing.

*This option is not available for Zircaloy.

D.2 Sample Output

This section illustrates the output for an unpressurized stainless steel fuel rod conditioned at 100% fuel power. As mentioned previously, these results pertain to operation characteristic of Connecticut Yankee assembly 8-H22.

```
-----------------------------------------------------------------------------------------------
!!!!!!!!!!!!!!!!!!!!!!!!!!!!!!!!!!!!!!!!!!!!!!!!!!!!!!!!!!!!!!!!!!!!!!!!!!!!!!!!!!!!!!!!!!!!!!!!
-----------------------------------------------------------------------------------------------


                 * *   FUEL/CLADDING 'JUSTCONTACT' DATA   * *

        -----------------------------------------------------------------
        !                     OPERATING CONDITIONS                      !
        !---------------------------------------------------------------!
        !  Bulk coolant pressure (MPa)          !       14.925          !
        !  Helium fill pressure  (MPa)          !   0.101 (0.203 HOT)   !
        !  Clad-fuel contact pressure (MPa)     !        0.000          !
        !  % Full power operation               !        100.0          !
        !  Local LHGR (kW/m)                    !        26.44          !
        !  Core average burnup  (MWD/kgU)       !        18.60          !
        !  Rel. assembly burnup (MWD/kgU)       !        18.42          !
        !  Local/max FQN burnup (MWD/kgU)       !        27.16          !
        !---------------------------------------------------------------!
        !               FILL AND FISSION GAS RELEASE DATA               !
        !---------------------------------------------------------------!
        !  Fraction released                    !       0.1669          !
        !  Helium mole fraction                 !        0.130          !
        !  Xenon mole fraction                  !        0.739          !
        !  Krypton mole fraction                !        0.131          !
        !---------------------------------------------------------------!
        !                AVERAGE HOT MATERIAL PROPERTIES                !
        !---------------------------------------------------------------!
        !                                       !  SS 304  !   FUEL     !
        !                                       !----------+------------!
        !  Young's modulus (GPa)                ! 177.390  ! 169.350    !
        !  Poisson ratio                        !   0.318  !   0.301    !
        !  Inside clad Meyer hardness (MPa)     ! 1139.26  !            !
        !  Surface roughness (um)               !    1.50  !    0.99    !
        !---------------------------------------------------------------!
        !                       DIMENSIONS/VALUES                       !
        !---------------------------------------------------------------!
        !                                       ! BOL COLD ! HOT/COND   !
        !                                       !----------+------------!
        !  Outside clad radius (mm)             !  5.3590  !  5.3478    !
        !  Inside clad radius  (mm)             !  4.9400  !  4.9226    !
        !  Outside fuel radius (mm)             !  4.8700  !  4.9226    !
        !  Clad-fuel gap (um)                   !  70.000  !   0.000    !
        !  Fuel density (% TD)                  !  95.170  !  93.982    !
```

Fuel/cladding "just contact" data continued.

ELEMENT STRESS/STRAIN/TEMPERATURE VALUES	
Radial stress (MPa)	-7.86
Tangential stress (MPa)	-188.50
Axial stress (MPa)	-98.18
Thermal strain (%)	0.6145
Elastic strain - R (%)	0.0469
Elastic strain - T (%)	-0.0873
Creep strain - R (%)	0.8053
Creep strain - T (%)	-0.8053
Total strain - R (%)	1.4667
Total strain - T (%)	-0.2780
Outside radial deflection (um)	-11.244
Inside radial deflection (um)	-17.390
Inside mech. deflection (um)	-43.156
Outside clad temperature (C)	331.02
Inside clad temperature (C)	350.35
Average clad temperature (C)	340.44
FUEL STRESS/STRAIN/TEMPERATURE VALUES	
Radial stress (MPa)	-0.20
Tangential stress (MPa)	-0.20
Axial stress (MPa)	-0.20
Thermal strain (%)	0.6581
Elastic strain (%)	-0.0000
Total strain (%)	0.6580
Outside radial deflection (um)	32.179
Outside fuel temperature (C)	447.74
Fuel centerline temperature (C)	1075.35

* * TRANSIENT DATA FOR CONSTANT POWER AT 100.00 (% FP) * *

CREEP MODEL : 4 CLAD MATERIAL : SS304			STRAIN (%) CLAD-R,T/FUEL			DEFLECT (um)	TEMP (C)	STRESS (MPa)
STEP TIME % POWER LHGR	FLUX FLUENCE U1mech Pc	EFPD BU-C BU-R BU-L	THERMAL ELASTIC CREEP/SWELL TOTAL			U0 U1 U2 HOT GAP	T0 T0 T2 TCL	SR ST SZ SG
0	1.379	658.50	0.6145	0.6145	0.6406	-11.23	331.0	-7.89
0.00	6.10	18.60	0.0468	-0.0870	-0.0001	-17.37	350.4	-187.97
100.00	-43.16	18.42	0.8053	-0.8053	-0.0000	31.33	435.9	-98.18
26.44	0.05	27.16	1.4666	-0.2777	0.6406	0.00	1055.8	155.95
9	1.379	661.87	0.6144	0.6144	0.6127	-12.95	331.0	-8.11
3.38	6.14	18.70	0.0457	-0.0838	-0.0003	-19.25	350.3	-182.35
100.00	-45.20	18.53	0.8437	-0.8434	0.0072	30.30	417.0	-98.18
26.42	0.52	27.30	1.5037	-0.3127	0.6197	0.00	1023.7	150.93
18	1.379	665.25	0.6143	0.6143	0.5709	-12.64	330.9	-10.59
6.75	6.19	18.79	0.0334	-0.0490	-0.0023	-19.03	350.2	-121.57
100.00	-46.78	18.64	0.8775	-0.8728	0.0145	28.51	388.1	-98.18
26.40	5.68	27.44	1.5251	-0.3076	0.5830	0.00	974.9	101.34
27	1.379	668.62	0.6142	0.6142	0.5637	-12.29	330.8	-12.01
10.13	6.23	18.89	0.0263	-0.0291	-0.0035	-18.76	350.1	-86.68
100.00	-47.54	18.76	0.9029	-0.8865	0.0217	28.46	383.3	-98.18
26.38	8.64	27.57	1.5434	-0.3015	0.5819	0.00	966.2	81.04
36	1.379	672.00	0.6140	0.6140	0.5604	-11.92	330.8	-12.88
13.50	6.27	18.98	0.0220	-0.0169	-0.0043	-18.46	350.1	-65.24
100.00	-47.88	18.87	0.9241	-0.8922	0.0289	28.61	381.1	-98.18
26.36	10.45	27.71	1.5602	-0.2950	0.5851	0.00	962.0	74.51
45	1.379	675.37	0.6139	0.6139	0.5585	-11.55	330.7	-13.41
16.88	6.31	19.08	0.0193	-0.0094	-0.0047	-18.15	350.0	-52.06
100.00	-47.95	18.98	0.9427	-0.8929	0.0362	28.85	380.0	-98.18
26.34	11.57	27.85	1.5759	-0.2883	0.5899	0.00	959.5	73.51

Transient conditioning data continued.

54	1.379	678.75	0.6138	0.6138	0.5573	-11.16	330.7	-13.74
20.25	6.35	19.17	0.0177	-0.0047	-0.0050	-17.83	349.9	-43.97
100.00	-47.87	19.09	0.9597	-0.8905	0.0434	29.13	379.3	-98.18
26.32	12.26	27.99	1.5912	-0.2815	0.5957	0.00	957.9	74.10
63	1.379	682.12	0.6136	0.6136	0.5564	-10.77	330.6	-13.95
23.63	6.39	19.27	0.0167	-0.0019	-0.0052	-17.50	349.9	-38.99
100.00	-47.68	19.21	0.9757	-0.8863	0.0506	29.43	378.9	-98.18
26.30	12.68	28.13	1.6060	-0.2746	0.6019	0.00	956.6	74.92
72	1.379	685.50	0.6135	0.6135	0.5558	-10.38	330.6	-14.07
27.00	6.43	19.37	0.0161	-0.0002	-0.0053	-17.17	349.8	-35.94
100.00	-47.44	19.32	0.9910	-0.8809	0.0578	29.75	378.6	-98.18
26.28	12.94	28.27	1.6206	-0.2676	0.6083	0.00	955.5	75.59
80	1.379	688.50	0.6134	0.6134	0.5553	-10.04	330.5	-14.14
30.00	6.46	19.45	0.0157	0.0008	-0.0053	-16.88	349.7	-34.24
100.00	-47.19	19.42	1.0044	-0.8756	0.0643	30.04	378.4	-98.18
26.26	13.08	28.39	1.6335	-0.2614	0.6142	0.00	954.7	76.01

All units as in previous table
FLUX in 10E18 (n/m**2 s)
FLUENCE in 10E25 (n/m**2)

* * CONDITIONED ROD DATA - 30.0 CORE EFPD AFTER CONTACT * *

OPERATING CONDITIONS	
Bulk coolant pressure (MPa)	14.925
Helium fill pressure (MPa)	0.101 (0.203 HOT)
Clad-fuel contact pressure (MPa)	13.084
% Full power operation	100.0
Local LHGR (kW/m)	26.26
Core average burnup (MWD/kgU)	19.45
Rel. assembly burnup (MWD/kgU)	19.42
Local/max FQN burnup (MWD/kgU)	28.39

FILL AND FISSION GAS RELEASE DATA	
Fraction released	0.1699
Helium mole fraction	0.122
Xenon mole fraction	0.746
Krypton mole fraction	0.132

AVERAGE HOT MATERIAL PROPERTIES	SS 304	FUEL
Young's modulus (GPa)	177.432	172.798
Poisson ratio	0.318	0.301
Inside clad Meyer hardness (MPa)	1140.08	
Surface roughness (um)	1.50	0.99

DIMENSIONS/VALUES	BOL COLD	HOT/COND
Outside clad radius (mm)	5.3590	5.3490
Inside clad radius (mm)	4.9400	4.9205
Outside fuel radius (mm)	4.8700	4.9205
Clad-fuel gap (um)	70.000	0.000
Fuel density (% TD)	95.170	93.804

Conditioned rod data continued.

ELEMENT STRESS/STRAIN/TEMPERATURE VALUES	
Radial stress (MPa)	-14.14
Tangential stress (MPa)	-34.24
Axial stress (MPa)	-98.18
Thermal strain (%)	0.6134
Elastic strain - R (%)	0.0157
Elastic strain - T (%)	0.0008
Creep strain - R (%)	1.0044
Creep strain - T (%)	-0.8756
Total strain - R (%)	1.6335
Total strain - T (%)	-0.2614
Outside radial deflection (um)	-10.036
Inside radial deflection (um)	-19.533
Inside mech. deflection (um)	-47.191
Outside clad temperature (C)	330.52
Inside clad temperature (C)	349.73
Average clad temperature (C)	339.89
FUEL STRESS/STRAIN/TEMPERATURE VALUES	
Radial stress (MPa)	-13.29
Tangential stress (MPa)	-13.29
Axial stress (MPa)	-0.20
Thermal strain (%)	0.5553
Elastic strain (%)	-0.0053
Inc. volume strain (%)	0.0643
Total strain (%)	0.6142
Outside radial deflection (um)	30.036
Outside fuel temperature (C)	378.44
Fuel centerline temperature (C)	954.75

```
      common/ramo/aramc(10,2),tramo(10)
      common/burnup/bu(6,6),bia(12,6),btot(2,24)
      common/fisgas/wt(3),cd(3),fm(3),frel
      common/spline/sol(9,5)
      common/fluence/fx(6,4),tfx(7),ffcon
      common/zgas/fmz(7,3)
c
      common/stress1/mat,mod,nit,pg,nc,pfl,pfill,pbulk,
     * bur,bui,bc,bcc,bcon,conv,fx,flx,fnf,fxx,ffxx,days
      common/stress2/emc,emf,vc,vf,cruff,fruff,
     * hn,hard,r0,r1,r2,rfo,ui,gap,der,dn,dnew
      common/stress3/sr,st,sz,sg,elr,elt,tsc,ecr,ect,esf,
     * tsf,evf,evold,etotf,ecrer,ecret,ecrtran,ecttran
      common/stress4/gc,gi,gfo,pow,powi,delpow,
     * deltim,cramp1,t0,t1,t2,tavc,eccrr,econt,cf
      common/prog/nprog
c
c
c*************************************************
c
      nit=11
c
      read(5,25)nprog
      read(5,25)mod
      if(nprog.eq.2)goto 40
 10   read(7,20,end=1400)mat,number,ccw,bc,days
 20   format(i1,i2,f11.2,2f7.2)
 25   format(i1)
c
      goto 45
 40   read(5,25)mat
 45   if(mat.eq.2)goto 50
c
c     SS304 rod data
c
      r0=5.359
      r1=4.940
      r2=4.870
      den=95.17
      cruff=1.5
      fruff=.991
      pfill=2068.4
      pbulk=14.925
      hard=1571.1
      conv=2.825e-2
      goto 60
c
c     Zirc rod data
c
 50   r0=5.588
      r1=4.877
      r2=4.782
      den=95.00
      cruff=.508
      fruff=.991
      pfill=2068.4
      pbulk=15.50
      conv=2.994e-2
 60   continue
      if(nprog.eq.2)goto 1500
```

```
c
c       nit = number of bi-sections
c       nprog = program selection
c               1 = condition and ramp
c               2 = creepdown to contact
c       mod = creep acceleration factor selection (see subroutine cree
c       mat = cladding material selection (1 = SS304, 2 = Zircaloy)
c       number = number of cases
c       days = EFPD to "condition" cladding
c       pow = fraction of full power  (%)
c       bc = core burnup  (MWD/kgU)
c       r0 = BOL cold outside clad radius (mm)
c       r1 = BOL cold inside clad radius (mm)
c       r2 = BOL cold outside fuel radius (mm)
c       den = BOL fuel density  (%TD)
c       cruff = clad surface roughness (um)
c       fruff = fuel surface roughness (um)
c       pfill = BOL fill gas pressure (kPa)
c       pbulk = operating nominal coolant pressure (MPa)
c
c
c
c
c
c
c       Main program for fuel/cladding "just contact" conditions
c
        bc=bc-days*conv
        call qcond(mat,bc,qfo)
        qc=qfo*pow/100.
        call burn(0,mat,bc,bul,bur)
        call rfuelc(r2,den,bul,rfo,dn)
        call gas(mat,bul,bur,pfill)
        t0=temp0(mat,qc)
        call cts(mat,qc,r0,r1,t0,t1,tavc,emc,tsc)
        hn=hardn(mat,t1,hard)
        pfl=pfill*(1.e-3)
        pg=2.*pfl
        pgn=-pg
        pc=0.
        call ces(mat,r0,r1,pc,pg,pbulk,tavc,emc,vc,elr,elt,
     * sr,st,sz,econr,econt)
        gap=0.
        t2=t1
  100   told=t2
        call temp2(mat,qc,rfo,t1,t2,cruff,fruff,pc,gap,dr,hn)
        diff=told-t2
        if(diff)200,700,300
  200   t2=told+100.
        goto 100
  300   j=0
        tl=told-100.
        tr=told
  400   tmid=(tl+tr)/2.
        t2=tmid
        call temp2(mat,qc,rfo,t1,t2,cruff,fruff,pc,gap,dr,hn)
        j=j+1
        if(j.eq.nit)goto 700
        diff=tmid-t2
        if(diff)500,700,600
```

```
 500    t1=tmid
        goto 400
 600    tr=tmid
        goto 400
 700    call ftes(qc,rfo,t2,bc,pq,dn,emf,vf,tsf,esf,cf)
        evf=0.
        evold=(qen/dn-1.)/3.
        call out1(0)
c
c
c       Main program for fuel/conditioned cladding dimensions
c
        call flux(mat,0,bc,fix,tnf)
        icase=0
        bcon=bc
        ecrtran=ecr
        ecttran=ect
        cramp1=pow
        delpow=0.
        deltim=days*2400./pow
        ival=5.*(1.+days*50./pow)
        call solve(icase,deltim,ival,1,r5,t5)
        ecr=ecr+r5
        ect=ect+t5
        bc=bco
        qc=qi
        call out1(1)
c
c
c       Main program for transient values
c
        if(number.eq.0)goto 10
        call flux(mat,1,bc,fix,tnf)
        do 900 icase=1,number
        read(7,1000)nramp
        read(7,1100)((cramp(m,n),n=1,2),m=1,nramp),
     * (tramp(r),n=1,nramp)
        bnew=bc
        do 900 iramp=1,nramp
        bcon=bnew
        if(iramp.ne.1)goto 800
        ecrtran=ecr
        ecttran=ect
 800    cramp1=cramp(iramp,1)
        delpow=(cramp(iramp,2)-cramp1)
        deltim=tramp(iramp)
        ival=10.*(1.+tramp(iramp)/48.)+abs(delpow)
        call solve(icase,deltim,ival,iramp,r5,t5)
        ecrtran=ecrtran+r5
        ecttran=ecttran+t5
        bnew=bcc
 900    continue
 1000   format(i1)
 1100   format(11f7.2)
        goto 10
 1400   continue
        goto 1700
c
c
c       Main program for cladding creepdown to contact
```

```
c
 1500   pc=0.
        pfi=pfill*(1.e-3)
        pg=2.*pfi
        pgn=-pg
        evoid=0.
        ecr=0.
        ect=0.
        pow=100.
        pramoi=pgw
        delpow=0.
        rfo=r2
        dn=den
        call burn(0,mat,1.0,nul,bur)
        call flux(mat,0,0.0,flx,tnf)
        do 1600 ib=1,3
        jb=ib+(mat-1)*3
        bc=bu(jb,1)
        bcon=bc
        ecrtran=ecr
        ecttran=ect
        kb=4+2*(mat-1)
        days=(bu(jb,kb)-bu(jb,1))/conv
        celtim=days*24.
        ival=days*conv*4.
        call solve(0,celtim,ival,ib,r5,t5)
        ecr=ecr+r5
        ect=ect+t5
 1600   continue
        stop
 1700   continue
        end
c
c
c
c
c
c       Solution to differential equation
c
        subroutine solve(icase,deltim,ival,iramp,r5,t5)
        dimension csrr(4),csrt(4)
        common/prog/nprog
        nramp=ival+1
        div=ival
        celtx=deltim/div
        if(nprog.eq.2)goto 500
        a=ival
        b=a/9.
        c=int(b)
        iskip=c
        iad=(b-c)*10.
        ia=1
        if(iad.eq.0)ia=0
        ib=1
  500   tim=0.
        sro=0.
        sto=0.
        do 900 k=2,5
        ic=k-1
        call cladsr(tim,sro,sto,cr1,ct1)
```

```
      csrr(ic)=cr1
      csrt(ic)=ct1
      if(k.eq.2)call cut2(icase,iramp,mramp,0)
      if(noroc.eq.2)goto 700
      io=ib+iskip+ia
      if(io.ne.ic)goto 800
      istep=ic-1
      call cut2(icase,iramp,mramp,istep)
      ib=io
      iad=iad-1
      if(iad.le.0)ia=0
      goto 800
700   call cut2(icase,iramp,mramp,1000000)
800   if(k.eq.5)goto 900
      rkr1=deltx*cr1
      rkt1=deltx*ct1
      tt=tim+deltx/2.
      rss=sro+rkr1/2.
      tss=sto+rkt1/2.
      call cladsr(tt,rss,tss,cr2,ct2)
      rkr2=deltx*cr2
      rkt2=deltx*ct2
      rss=sro+rkr2/2.
      tss=sto+rkt2/2.
      call cladsr(tt,rss,tss,cr3,ct3)
      rkr3=deltx*cr3
      rkt3=deltx*ct3
      tt=tim+deltx
      rss=sro+rkr3
      tss=sto+rkt3
      call cladsr(tt,rss,tss,cr4,ct4)
      rkr4=deltx*cr4
      rkt4=deltx*ct4
      tim=tt
      sro=sro+(rkr1+2.*rkr2+2.*rkr3+rkr4)/6.
      sto=sto+(rkt1+2.*rkt2+2.*rkt3+rkt4)/6.
900   continue
      cr1=csrr(1)
      cr2=csrr(2)
      cr3=csrr(3)
      cr4=csrr(4)
      ct1=csrt(1)
      ct2=csrt(2)
      ct3=csrt(3)
      ct4=csrt(4)
      r4=sro
      t4=sto
      do 1100 k=5,mramp
      r5=r4+deltx*(55.*cr4-59.*cr3+37.*cr2-9.*cr1)/24.
      t5=t4+deltx*(55.*ct4-59.*ct3+37.*ct2-9.*ct1)/24.
      tt=tt+deltx
      call cladsr(tt,r5,t5,cr5,ct5)
      r5=r4+deltx*(9.*cr5+19.*cr4-5.*cr3+cr2)/24.
      t5=t4+deltx*(9.*ct5+19.*ct4-5.*ct3+ct2)/24.
      call cladsr(tt,r5,t5,cr5,ct5)
      if(noroc.eq.2)goto 950
      io=ib+iskip+ia
      if(io.ne.k)goto 1000
      istep=ic-1
      call cut2(icase,iramp,mramp,istep)
```

```
      ib=ip
      iad=iad-1
      if(iad.le.0)ia=0
      goto 1000
  950 call out2(icase,iramp,mramp,100(300)
 1000 cr1=cr2
      cr2=cr3
      cr3=cr4
      cr4=cr5
      ct1=ct2
      ct2=ct3
      ct3=ct4
      ct4=ct5
      r4=r5
      t4=t5
 1100 continue
      return
      end
c
c
c     Clad strain rate and transient values
c
c
      subroutine cladsr(txx,srx,stx,crx,ctx)
      common/stress1/mat,mod,nit,pg,pc,pfl,pfill,pbulk,
     * bur,bul,bc,bcc,bcon,conv,tx,flx,tnf,fxx,tfxx,days
      common/stress2/emc,emf,vc,vf,cruff,fruff,
     * hn,hard,r0,r1,r2,rfo,ul,gap,der,dn,dnew
      common/stress3/sr,st,sz,sg,elr,elt,tsc,ecr,ect,esf,
     * tsf,evf,evold,etotf,ecrer,ecret,ecrtran,ecttran
      common/stress4/qc,qi,qfp,pow,powi,delpow,
     * deltim,cramp1,t0,t1,t2,tavc,ecorr,econt,cf
      common/prog/ncrog
      tx=txx
      powi=delpow*tx/deltim+cramp1
      bcc=bcon+(conv*tx*powi/100./24.)
      call qccrd(mat,bco,qfp)
      qi=qfp*powi/100.
      call burn(1,mat,bco,bul,bur)
      call rfuelc(rfo,dn,bul,rdum,dnew)
      evf=(den/dnew-1.)/3.-evold
      call gas(mat,bul,bur,pfill)
      if(nprog.eq.1)goto 50
      call flux(mat,1,bco,flx,tnf)
      fxx=flx
      tfxx=tnf
      goto 60
  50  fxx=flx*powi/100.
      tfxx=tx*(fxx+flx*cramp1/100.)/2.+tnf
  60  t0=temp0(mat,qi)
      call cts(mat,qi,r0,r1,t0,t1,tavc,emc,tsc)
      call ces(mat,r0,r1,pc,pg,pbulk,tavc,emc,vc,elr,elt,
     * sr,st,sz,econr,econt)
      eac=(econt*(r0+r1)-econr*(r0-r1))/2.
      ecrer=ecrtran+srx
      ecret=ecttran+stx
      ear=(tsc+elr+ecrer)
      eat=(tsc+elt+ecret)
      ua=eat*(r0+r1)/2.-ear*(r0-r1)/2.
      hn=hardn(mat,t1,hard)
```

```
      klump=0
      if(pc.lt.1.5)klump=1
      tad=100.
      t2=t1
  100 told=t2
      call ftes(qi,rfo,t2,pc,pg,dn,emf,vf,tsf,esf,cf)
      etotf=(tsf+esf+pc*cf+evf)
      rfh=rfo*(1.+etotf)
      u1=ua+pc*eac
      gap=((r1+u1)-rfh)*(1.e+3)
      if(gap)200,300,300
  200 pc=(rfo*(1.+tsf+esf+evf)-r1-ua)/(eac-rfo*cf)
      gap=0.
      goto 400
  300 pc=0.
  400 call temp2(mat,qi,rfo,t1,t2,cruff,fruff,pc,gap,dr,nn)
      diff=told-t2
      if(diff)500,1300,600
  500 t2=told+tad
      goto 100
  600 if(klump.eq.0)goto 650
      if(tad.le.10.)goto 650
      t2=told-tad
      tad=tad/10.
      goto 100
  650 j=0
      tl=told-tad
      tr=told
  700 tmid=(tl+tr)/2.
      t2=tmid
      call ftes(qi,rfo,t2,pc,pg,dn,emf,vf,tsf,esf,cf)
      etotf=(tsf+esf+pc*cf+evf)
      rfh=rfo*(1.+etotf)
      u1=ua+pc*eac
      gap=((r1+u1)-rfh)*(1.e+3)
      if(gap)800,900,900
  800 gap=0.
      pc=(rfo*(1.+tsf+esf+evf)-r1-ua)/(eac-rfo*cf)
      goto 1000
  900 pc=0.
 1000 call temp2(mat,qi,rfo,t1,t2,cruff,fruff,pc,gap,dr,hr)
      j=j+1
      if(j.ge.nit) goto 1300
 1050 diff=tmid-t2
      if(diff)1100,1300,1200
 1100 tl=tmid
      goto 700
 1200 tr=tmid
      goto 700
 1300 if(j.eq.nit.and.pc.eq.0.0)goto 1050
      call ces(mat,r0,r1,pc,pg,pbulk,tavc,emc,vc,elr,elt,
     * sr,st,sz,econr,econt)
      call ftes(qi,rfo,t2,pc,pg,dn,emf,vf,tsf,esf,cf)
      etotf=(tsf+esf+pc*cf+evf)
      rfh=rfo*(1.+etotf)
      u1=ua+pc*eac
      sq=(((sr-st)**2+(st-sz)**2+(sz-sr)**2)/2.)**.5
      call creep(mat,mcd,sr,st,sz,sq,fxx,tavc,crx,ctx)
      return
      end
```

```
c
c
c*************************************************************
c
c       Data declaration subprogram
c
        block data
        common/burnup/bu(6,6),bla(12,6),btot(2,24)
        common/fisgas/wt(3),cd(3),fm(3),frel
        common/spline/spl(9,5)
        common/fluence/fx(6,4),ffx(7),ffcon
        common/zgas/fmz(7,3)
c
c       FQN values for assembly 8-H22
c
        data ((bla(m,n),n=1,4),m=1,3)/
     * 1.372,1.330,1.333,1.324,1.740,1.597,
     * 1.485,1.428,1.361,1.263,1.187,1.193/
c
c       Relative assembly power values
c
        data ((bla(m,n),n=1,4),m=4,6)/
     * 0.697,0.731,0.752,0.787,1.248,1.224,
     * 1.188,1.171,1.089,1.066,1.028,1.024/
c
c       Corresponding core burnup values
c
        data ((bu(m,n),n=1,4),m=1,3)/
     * 0.0,2.940,6.252,8.729,8.729,12.086,16.325,
     * 21.131,21.131,24.365,27.657,30.199/
c
c       Fill and fission gas molecular weight values
c
        data (wt(n),n=1,3)/4.003,131.30,83.80/
c
c       Fuel integral kdT vs temperature curve fit constants
c
        data ((spl(m,n),n=1,5),m=1,3)/
     * 1.6410,12.9620,105.6370,0.0,0.0,1.6410,12.9620,
     * 105.6370,0.0,0.0,2.0556,22.8077,177.1768,276.25,2.0/
        data ((spl(m,n),n=1,5),m=4,6)/
     * 1.9768,28.9744,228.9538,478.29,3.0,0.3472,34.9046,
     * 292.8380,738.20,4.0,-4.6456,35.9464,363.6892,1066.29,5.0/
        data ((spl(m,n),n=1,5),m=7,9)/
     * -9.7949,22.0097,421.6452,1461.28,6.0,-5.0250,-7.3749,436.2799,
     * 1895.14,7.0,-5.0250,-7.3749,436.2799,1895.14,7.0/
c
c       Fast flux (10E+18 n/m**2/s) and corresponding core EFPD values
c
        data ((fx(m,n),n=1,2),m=1,6)/
     * 1.222,1.336,1.336,1.379,2.618,2.551,
     * 2.551,2.534,2.352,2.302,2.302,2.324/
        data ((fx(m,n),n=3,4),m=1,6)/
     * 0.0,200.0,200.0,309.3,309.3,509.0,509.0,
     * 748.0,748.0,948.0,948.0,1141.0/
c
c       Fast flux conversion factor (1.85eV to 0.1MeV)
c
        data ffcon/0.543/
c
```

```
c       Corresponding burnup values for Zirc case
c
        data ((bu(m,n),n=1,6),m=4,6)/
     * 0.0,2.0,4.0,6.0,8.0,10.0,10.0,12.0,14.0,16.0,
     * 18.0,20.0,20.0,22.0,24.0,26.0,28.0,30.0/
c
c       FQN values for Zirc case
c
        data ((bla(m,n),n=1,6),m=7,9)/
     * 1.813,1.740,1.682,1.653,1.624,1.595,1.518,
     * 1.496,1.474,1.452,1.408,1.375,6*1.045/
c
c       F-radial (relative power) values for Zirc case
c
        data ((bla(m,n),n=1,6),m=10,12)/
     * 6*1.45,1.38,1.36,1.34,1.32,1.28,1.25,6*0.95/
c
c       Mole fraction data for Zirc case
c
        data ((fmz(m,n),n=1,3),m=1,7)/
     * 1.0,0.0,0.0,1.0,0.0,0.2,0.997,0.002,2.0,
     * 0.987,0.011,10.0,0.967,0.029,20.0,
     * 0.932,0.060,30.0,0.890,0.097,40.0/
c
        end
c
c*************************************************************
c
c
c       LHGR calculation
c
        subroutine accnd(mat,b,q)
        common/burnup/bu(6,6),bla(12,6),btot(2,24)
        if(mat.eq.2)goto 100
        ia=1
        iz=3
        jz=4
        m=0
        qavg=18.134
        goto 200
 100    ia=4
        iz=6
        jz=6
        m=3
        qavg=19.75
 200    do 300 i=ia,iz
        do 300 j=1,jz
 300    if(b.lt.bu(i,j))goto 400
 400    b1=bu(i,j)-bu(i,j-1)
        y0=bla(i+m,j-1)
        y1=bla(i+m,j)
        bq=b-bu(i,j-1)
        y=(y1-y0)*bq/b1+y0
        q=y*qavg
        return
        end
c
c
c       Local and average assembly burnup calculations
c
```

```
      subroutine burn(iskip,mat,b,bl,ba)
      common/burnup/bu(6,6),bla(12,6),btot(2,24)
      if(mat.ec.2)gcto 100
      ia=0
      ic=3
      kc=1
      ja=1
      jz=9
      goto 200
  100 ia=1
      ic=5
      kc=4
      ja=10
      jz=24
  200 if(iskip.eq.1)goto 350
      do 300 i=1,2
      bad=0.
      l=0
      do 300 j=ja,jz
      k=kc+(j-ja)/ic
      l=l+1
      if(l.gt.ic)l=1
      ig=i+ia
      bad=bad+gral(ig,k,l,bu(k,l+1))
      btot(i,j)=bad
  300 continue
  350 blo=0.
      bao=0.
      js=ia*3+1
      jf=js+2
      kf=ic+1
      do 400 j=js,jf
      do 400 k=2,kf
      if(b.lt.bu(j,k))goto 500
      blo=btot(1,ja)
      bao=btot(2,ja)
  400 ja=ja+1
  500 igl=ia+1
      iga=ia+2
      l=k-1
      bl=blo+gral(igl,j,l,b)
      ba=bao+gral(iga,j,l,b)
      return
      end
c
c
c     Integration routine for subroutine burn
c
      function gral(ib,k,l,b)
      common/burnup/bu(6,6),bla(12,6),btot(2,24)
      b1=bu(k,l+1)-bu(k,l)
      bg=b-bu(k,l)
      ii=k+(ib-1)*3
      y0=bla(ii,l)
      y1=bla(ii,l+1)
      gral=(y1-y0)*bg**2/b1/2.+y0*bg
      return
      end
c
c
```

```
c       Cold fuel radius calculation for local burnup
c
        subroutine rfuelc(r,dn0,b,rf,d)
        if(b.le.0.2)goto 100
        if(b.le.2.0)goto 200
        if(b.le.10.)goto 300
        if(b.le.20.)goto 400
        if(b.le.30.)goto 500
        d=-0.141*(b-30.)+93.57
        goto 600
 100    d=(96.5-dn0)*b/.4+dn0
        goto 600
 200    d=(96.5-dn0)*(b-0.2)/3.6+48.25+dn0/2.
        goto 600
 300    d=96.5
        goto 600
 400    d=-0.148*(b-10.)+96.5
        goto 600
 500    d=-0.145*(b-20.)+95.02
 600    rf=r*((dn0/d)**(1./3.))
        return
        end
c
c
c       Fill and fission gas mole fraction calculations
c
        subroutine gas(mat,bl,ba,gf)
        common/fisgas/wt(3),cd(3),fm(3),fr
        common/zgas/fmz(7,3)
        if(mat.eq.2)goto 700
        t=ba/(2.825e-2)
        if(t.le.190.)goto 100
        if(t.le.309.)goto 200
        if(t.le.450.)goto 300
        if(t.le.748.)goto 400
        if(t.le.1300.)goto 500
        fr=0.15
        goto 600
 100    fr=(1.e-4)*t
        goto 600
 200    fr=(7.899e-4)*t-0.13108
        goto 600
 300    fr=(2.6241e-4)*t+3.1915e-2
        goto 600
 400    fr=(8.3893e-5)*t+0.11225
        goto 600
 500    fr=-(4.529e-5)*t+0.2089
 600    fgas=(1.537e+20)*t
        gxe=fgas*fr*0.2183
        gkr=fgas*fr*0.0346
        ghe=(6.3298e+18)*gf
        xtot=ghe+gxe+gkr
        fm(1)=ghe/xtot
        fm(2)=gxe/xtot
        fm(3)=gkr/xtot
        return
 700    do 800 k=1,7
 800    if(bl.lt.fmz(k,3))goto 900
 900    b1=fmz(k,3)-fmz(k-1,3)
        bg=bl-fmz(k-1,3)
```

```
      fm(1)=fmz(k-1,1)+ba*(fmz(k,1)-fmz(k-1,1))/bi
      fm(2)=fmz(k-1,2)+ba*(fmz(k,2)-fmz(k-1,2))/bi
      fm(3)=1.0-fm(1)-fm(2)
      qhem=(9.4325e-6)*qf
      a=(1.0254e-2)*(0.2183+0.038o)*ba*fm(1)
      fr=qhem*(1.-fm(1))/a
      return
      end
c
c
c     Outside cladding temperature calculation
c
      function temp0(mat,q)
      if(mat.eq.2)goto 100
      if(q.le.18.0)temp0=279.+(29./18.)*q
      if(q.gt.18.0)temp0=308.+(30./11.)*(q-18.)
      if(q.gt.29.0)temp0=338.
      return
  100 if(q.lt.25.0)temp0=292.0+2.6*q
      if(q.ge.25.0)temp0=347.0
      return
      end
c
c
c     Cladding average thermal strain, temperature, and modulus
c
      subroutine cts(mat,q,rb,ra,tb,ta,tav,em,sst)
      ta=tin(mat,q,rb,ra,tb)
      del=(rb-ra)/30.
      suma=0.
      sumt=0.
      sume=0.
      do 100 i=2,30
      rad=rb-(i-1)*del
      tr=tin(mat,q,rb,rad,tb)
      coef=(-1.)**i+3.
      suma=suma+coef*rad*alpha(mat,tr)
      sumt=sumt+coef*rad*tr
      emod=emodul(mat,tr)
  100 sume=sume+coef*rad*emod
      rt0=rb*alpha(mat,tb)
      rt1=ra*alpha(mat,ta)
      sst=2.*del*(rt0+rt1+suma)/3./(rb**2-ra**2)
      rt=(ra*ta+rb*tb)
      tav=2.*del*(rt+sumt)/3./(rb**2-ra**2)
      e0=rb*emodul(mat,tb)
      e1=ra*emodul(mat,ta)
      em=2.*del*(e0+e1+sume)/3./(rb**2-ra**2)
      return
      end
c
c
c     Cladding temperature profile calculation
c
      function tin(mat,q,rb,rr,tb)
      if(mat.eq.2)goto 900
      t=tb+273.15
      qk=q*1000.
      ratio=rb/rr
      shl=(qk/2./3.14159)*alog(ratio)
```

```
      c0=9.01748
      c1=1.62997e-2
      c2=-4.80329e-6
      c3=2.18422e-9
      a1=c0+c1*t+c2*t**2+c3*t**3
      a2=c1/2.+c2*t+(3./2.)*c3*t**2
      a3=c2/3.+c3*t
      a4=c3/4.
      i=0
      j=0
      dtemp=shi/a1
100   rhs=a1*dtemp+a2*dtemp**2+a3*dtemp**3+a4*dtemp**4
      fun=rhs-shi
      if(fun)200,800,300
200   i=1
      if(j.eq.1)goto 400
      dtl=dtemp
      dtemp=dtemp+30.
      dtr=dtemp
      goto 100
300   j=1
      if(i.eq.1)goto 400
      dtr=dtemp
      dtemp=dtemp-30.
      dtl=dtemp
      goto 100
400   m=0
500   dtmid=(dtl+dtr)/2.
      dtemp=dtmid
      rhs=a1*dtemp+a2*dtemp**2+a3*dtemp**3+a4*dtemp**4
      m=m+1
      if(m.eq.15)goto 800
      fun=rhs-shi
      if(fun)600,800,700
600   dtl=dtmid
      goto 500
700   dtr=dtmid
      goto 500
800   tin=tb+dtemp
      return
900   ratio=rb/rr
      shi=(q/2./3.14159)*alog(ratio)
      c1=-1.015e+5
      c2=1.3959e-2
      c3=1.9485e-4
      c4=1.9704e-5
      c5=4.9261e-6
      tin=c1*(c2-(c3+c4*(c2*tb+c5*tb**2+shi))**.5)
      return
      end
c
c
c     Cladding thermal expansion calculation
c
      function alpha(mat,t)
      if(mat.eq.2)goto 100
      z=t+273.15
      tref=298.15
      alpha=(1.7887e-5+2.3977e-9*z+3.2692e-13*z**2)*(z-tref)
      return
```

```
 100    alpha=(6.721e-6)*t-(2.373e-4)
        return
        end
c
c
c       Cladding modulus of elasticity calculation
c
        function emodul(mat,t)
        if(mat.eq.2)goto 100
        emodul=(1.e+3)*(183.4+8.3*(260.-t)/111.1)
        return
 100    if(t.le.862.0)emodul=(1.148e+5)-59.9*(t+273.15)
        if(t.gt.862.0)emodul=(1.005e+5)-47.25*(t+273.15)
        return
        end
c
c
c       Cladding Meyer hardness calculation
c
        function hardn(mat,ta,hnum)
        if(mat.eq.2)goto 100
        yst=290.-0.245*(ta-25.)
        hardn=hnum*yst/290.
        return
 100    z=ta+273.15
        if(ta.lt.25.0)hardn=1.96e+3
        if(ta.ge.25.0.and.ta.lt.727.0)
     * hardn=(6.48e+3)-23.6*z+(3.29e-2)*z**2-(1.563e-5)*z**3
        if(ta.ge.727.0)hardn=100.0
        return
        end
c
c
c       Cladding stress and strain calculations
c
        subroutine ces(mat,rb,ra,pc,pa,pb,t,em,v,er,et,
     * sr,st,sz,econr,econt)
        sr=-(rb*pb+ra*(pc+pa))/(rb+ra)
        st=(ra*(pc+pa)-rb*pb)/(rb-ra)
        sz=(pa*ra**2-pb*rb**2)/(rb**2-ra**2)
        if(mat.eq.2)goto 100
        v=0.304+0.019*(t-260.)/111.1
        goto 200
 100    if(t.le.397.0)v=0.333-(1.26e-4)*(t+273.15)
        if(t.gt.397.0)v=0.248
 200    er=(-(rb*pb+ra*pa)/(rb+ra)-v*((ra*pa-rb*pb)/
     * (rb-ra)+sz))/em
        et=((ra*pa-rb*pb)/(rb-ra)-v*(sz-(rb*pb+ra*pa)/
     * (rb+ra)))/em
        econr=-(ra/(rb+ra)+v*ra/(rb-ra))/em
        econt=(ra/(rb-ra)+v*ra/(rb+ra))/em
        return
        end
c
c
c       Fuel surface temperature calculation
c
        subroutine temp2(mat,q,rf,ta,tf,cruf,fruf,pc,go,gn,hn)
        common/fisgas/w(3),c(3),f(3),frel
        hcon=0.
```

```
      dy=dn/100.
      if(pc.le.0.)goto 100
      tc=ta+273.15
      ck=(9.01748+(1.62997e-2)*tc-(4.80329e-6)*tc**2
     * +(2.18422e-9)*tc**3)*(1.e-3)
      if(mat.eq.2)ck=13.959e-3+ta*9.8522e-6
      pf=1.1316*dv/(2.-dv+10.*(1.-dv)**2)
      fk=pf*(3.824/(402.4+tf)+(6.12e-14)*(tf+273.)**3)
      cm=2.*ck*fk/(ck+fk)
      xl=exp(0.5825*alog(fruf)-3.598)
      hcon=(cm/(fruf*1.e-6))*xl*(pc/hr)**.5
  100 tq=(ta+tf)/2.+273.15
      c(1)=(3.366e-6)*tq**.668
      c(2)=(4.0288e-8)*tq**.872
      c(3)=(4.726e-8)*tq**.923
      if(f(2).ne.0.0)goto 150
      sumb=c(1)
      goto 400
  150 sumb=0.
      do 300 i=1,3
      suma=0.
      do 200 j=1,3
      if(j.eq.i)goto 200
      a1=(1.+((c(i)/c(j))**.5)*(w(i)/w(j))**.25)**2
      a2=(1.+(w(i)/w(j)))**.5*(2.**1.5)
      a3=a1/a2
      a4=(w(i)-w(j))*(w(i)-0.142*w(j))*2.41/((w(i)+w(j))**2)
      a5=a3*(1.+a4)*f(j)/f(i)
      suma=suma+a5
  200 continue
      a6=c(i)/(1.+suma)
  300 sumb=sumb+a6
  400 hfg=sumb*(1.e+6)/(fruf+cruf+gp)
      denom=(6.28319e-3)*rf*(hcon+hfg)
      tf=ta+q/denom
      return
      end
c
c
c     Fuel thermal and elastic strain calculations
c
      subroutine ftes(q,rf,tf,pc,pg,dr,emf,v,ft,fe,cf)
      p=(1.-dn/100.)
      e25=(2.23e+5)*(1.-1.92*p)
      g25=(8.42e+4)*(1.-1.66*p)
      sumt=0.
      sume=0.
      sumg=0.
      del=rf/40.
      do 100 k=1,39
      a=k
      r=rf-a*del
      tr=tint(q,rf,r,tf,p)
      epfr=fstr(tr)
      coef=3.-(-1.)**k
      sumt=sumt+coef*r*epfr
      if(tr.lt.2000.)rat=1.-(1.6e-4)*tr-(2.e-8)*tr**2
      if(tr.ge.2000.)rat=0.6-0.35*(tr/1000.-2.)
      ef=rat*e25
      g=rat*g25
```

```
      sume=sume+coef*r*ef
  100 sumg=sumg+coef*r*g
      epo=fstr(tf)
      ft=2.*del*(epo*rf+sumt)/3./rf**2
      if(tf.lt.2000.)rat=1.-(1.6e-4)*tf-(2.e-8)*tf**2
      if(tf.ge.2000.)rat=0.6-0.35*(tf/1000.-2.)
      emf=2.*del*(rat*e25+sume)/3./rf**2
      gf=2.*del*(rat*g25+sumg)/3./rf**2
      v=(emf/gf/2.-1.)
      fe=-pg*(1.-2.*v)/emf
      cf=-(1.-v)/emf
      return
      end
c
c
c     Fuel thermal strain relation
c
      function fstr(t)
      fstr=(1.14e-13)*t**3+(2.581e-9)*t**2+(7.107e-5)*t
     * -1.7929e-4
      return
      end
c
c
c     Fuel temperature calculation
c
      function tint(q,rf,r,tf,p)
      common/spline/spl(9,5)
      cf=1.136*(1.-p)/(1.+p+10.*p**2)
      fint2=3.824*alog(1.+tf/402.4)+
     * (1.53e-14)*(tf+273.)**4-(8.4985e-5)
      fintr=q*(1.-(r/rf)**2)/12.56637/cf+fint2
      m=fintr+1.
      a=spl(m,5)
      tempr=spl(m,1)*(fintr-a)**3+spl(m,2)*(fintr-a)**2+
     * spl(m,3)*(fintr-a)+spl(m,4)
      tint=tempr
      return
      end
c
c
c     Fast flux and fluence calculations
c
      subroutine flux(mat,jump,bu,flx,tnf)
      common/fluence/fx(6,4),tfx(7),ffcf
      if(jump.eq.1)goto 150
      sumf=0.
      tfx(1)=0.
      do 100 i=1,6
      a=(fx(i,2)+fx(i,1))/2.
      b=fx(i,4)-fx(i,3)
      c=a*b*ffcf*(8.64e+22)
      sumf=sumf+c
      tfx(i+1)=sumf
  100 continue
  150 denom=2.825e-2
      if(mat.eq.2)denom=2.994e-2
      t=bu/denom
      if(t.le.200.)goto 200
      if(t.le.300.)goto 300
```

```
      if(t.le.509.)goto 400
      if(t.le.748.)goto 500
      if(t.le.948.)goto 600
      m=6
      goto 700
200   m=1
      goto 700
300   m=2
      goto 700
400   m=3
      goto 700
500   m=4
      goto 700
600   m=5
700   x=(fx(m,2)-fx(m,1))*(3.6e+21)*ffcf
      y=(fx(m,4)-fx(m,3))*24.
      z=(t-fx(m,3))*24.
      flx=x*z/y+fx(m,1)*(3.6e+21)*ffcf
      tnf=tfx(m)+x*z**2/y/2.+z*fx(m,1)*(3.6e+21)*ffcf
      return
      end
c
c
c     Generalized and component creep strain rate calculation
c
      subroutine creep(mat,mod,sr,st,sz,sq,fxx,tavc,crx,ctx)
      if(mat.ec.2)goto 100
      if(mod.ec.1)accel=1.0
      if(mod.eq.2)accel=11.0
      if(mod.ec.3)accel=22.0
      if(mod.eq.4)accel=55.0
      if(mod.eq.5)accel=220.0
      const=(1.25-0.55*(tavc-177.)/250.)*(1.4504e-31)
      egen=const*fxx*sq*accel
      crx=egen*(2.*sr-st-sz)/sq/2.
      ctx=egen*(2.*st-sr-sz)/sq/2.
      return
100   if(mod.eq.1)accel=1.0
      if(mod.eq.2)accel=4.0/(3.**.5)
      if(mod.eq.3)accel=10./(3.**.5)
      u=6.8947*(4.77e+3-1.906*(1.8*tavc+32.))*(3.**.5)/2.
      arl=exp(-8851.5*(1.-sq*2./3.**.5/2697.9)/1.98/(tavc+273.15)
      egen=0.02*((fxx/(1.8e+19))**.613)*((sq/u)**1.130)*
     * arl*accel*(2./3.**.5)
      crx=egen*(2.*sr-st-sz)/sq/2.
      ctx=egen*(2.*st-sr-sz)/sq/2.
      return
      end
c
c
c     Printout of conditioned values
c
      subroutine out1(icheck)
      common/fisqas/wt(3),ca(3),fm(3),fre
      common/stress1/mat,mod,nit,pq,pc,pfl,pfill,pbulk,
     * bur,bul,bc,pcc,bcor,conv,tx,flx,tnf,fxx,tfxx,days
      common/stress2/emc,emf,vc,vf,cruff,fruff,
     * rn,hard,r0,r1,r2,rfo,ul,gap,der,dn,dnew
      common/stress3/sr,st,sz,sq,elr,elt,tsc,ecr,ect,esf,
     * tsf,evf,evold,etoff,ecrer,ecret,ecrtran,ecttran
```

```
      commcn/stress4/ac,ai,afp,pow,pcw,delpow,
     * celtim,crampl,t0,t1,t2,tavc,ecorr,econt,cf
      a1="  SS"
      a2=" 304"
      if(mat.ne.2)goto 100
      a1="   Z"
      a2="IRC "
100   cgn=-cg
      cgpc=-cg-pc
      cnx=cn
      if(icheck.eq.1)cnx=cnew
      elaf=esf+pc*cf
      totsf=tsf+elaf+evf
      rfcon=rfo*(1.+totsf)
      u1con=rfcon-r1
      cor=(1.-cn/100.)
      tc1=tint(ac,rfo,0.,t2,cor)
      d1=r0-r1
      d2=r0+r1
      elar=elr+econr*cc
      elat=elt+econt*pc
      if(icheck.gt.0)goto 150
      crek=(2.*sr-st-sz)/(2.*st-sr-sz)
      ect=(2.*u1con+elr*d1-elt*d2-2.*tsc*r1)/(d2-crek*d1)
      ecr=crek*ect
150   ett=tsc+elat+ect
      etr=tsc+elar+ecr
      u1mech=(ect*(r1+r0)-ecr*(r0-r1))/2.
      u0con=(etr*d1+ett*d2)/2.
      u2con=rfo*totsf
      r0con=r0+u0con
      r1con=r1+u1con
      cgap=(r1-r2)*(1.e+3)
      v0=1.e-3
      v1=emc*v0
      v2=emf*v0
      v0=100.
      v3=tsc*v0
      v4=elar*v0
      v5=elat*v0
      v6=ecr*v0
      v7=ect*v0
      v8=etr*v0
      v9=ett*v0
      v10=u0con*1000.
      v11=u1con*1000.
      v12=tsf*v0
      v13=elaf*v0
      v14=totsf*v0
      v15=u2con*1000.
      v16=evf*v0
      v17=u1mech*1000.
      if(icheck.eq.0)write(6,180)
      if(icheck.eq.1)write(6,190) days
      write(6,200) cbulk,dfl,cg,pc,pow
      write(6,300) ac,bc,bur,bul,frel
      write(6,400) fm(1),fm(2),fm(3),a1,a2,v1,v2,vc,vf
      write(6,500) hn,cruff,fruff,r0,r0con,r1,r1con
      write(6,600) r2,rfcon,cgap,gap,cen,dnx,sr,st,sz
      write(6,700) v3,v4,v5,v6,v7,v8,v9,v10,v11
```

```
      write(6,800) v17,t0,t1,tavc,pgpc,pdoc
      write(6,900) pgn,v12,v13
      if(icheck.eq.1)write(6,1000) v16
      write(6,1100) v14,v15,t2,tcl
180   format(////79("-")/79("!")/79("-")///18x,"* *  FUEL/CLADDING *JUST
     *CONTACT* DATA  * *")
190   format(/8x,"* *  CONDITIONED ROC DATA  -",f6.1," CORE EFPD AFTER C
     *ONTACT  * *")
200   format(/10x,58("-")/9x,"!",19x,"OPERATING CONDITIONS",19x,"!"/9x,"
     *!",53("-"),"-----!"/9x,"!  Bulk coolant pressure (MPa)",7x,"!",f13
     *.3,8x,"!"/9x,"!  Helium fill pressure  (MPa)",7x,"!",f6.3," (",f5.
     *3," HOT) !"/9x,"!  Clad-fuel contact pressure (MPa)  !",f13.3,8x,"
     *!"/9x,"!  % Full power operation",12x,"!",f13.1,8x,"!")
300   format(9x,"!  Local LHGR (kW/m)",17x,"!",f13.2,8x,"!"/9x,"!  Core
     *average burnup  (MWD/kgU)    !",f13.2,8x,"!"/9x,"!  Rel. assembly
     *burnup (MWD/kgU)    !",f13.2,8x,"!"/9x,"!  Local/max FQN burnup (M
     *WD/kgU)    !",f13.2,8x,"!"/9x,"!",7("--------"),"--!"/9x,"!",12x,"
     *FILL AND FISSION GAS RELEASE DATA",13x,"!"/9x,"!",7("--------"),"-
     *-!"/9x,"!  Fraction released",17x,"!",f13.4,8x,"!")
400   format(9x,"!  Helium mole fraction",14x,"!",f13.3,8x,"!"/9x,"!  Xe
     *non mole fraction",15x,"!",f13.3,8x,"!"/9x,"!  Krypton mole fracti
     *on",13x,"!",f13.3,8x,"!"/9x,"!",7("--------"),"--!"/9x,"!",13x,"AV
     *ERAGE HOT MATERIAL PROPERTIES",14x,"!"/9x,"!",7("--------"),"--!"/
     *9x,"!",36x,"!",2a4," !"," FUEL  !"/9x,"!",36x,"!",10("-"),"+",
     *10("-"),"!"/9x,"!  Young's modulus (GPa)",13x,"!",f8.3," !",f8.3,
     *"  !"/9x,"!  Poisson ratio",21x,"!",f8.3," !",f8.3," !")
500   format(9x,"!  Inside clad Meyer hardness (MPa)  !",f8.2," !",10x,
     *"!"/9x,"!  Surface roughness (um)",12x,"!",f8.2," !",f8.2," !"/9
     *x,"!",7("--------"),"--!"/9x,"!",20x,"DIMENSIONS/VALUES",21x,"!"/9
     *x,"!",7("--------"),"--!"/9x,"!",36x,"! BOL COLD ! HOT/COND !"/9x,
     *"!",36x,"!",10("-"),"+",10("-"),"!"/9x,"!  Outside clad radius (mm
     *)",10x,"!",f8.4," !",f8.4," !"/9x,"!  Inside clad radius  (mm)",
     *10x,"!",f8.4," !",f8.4," !")
600   format(9x,"!  Outside fuel radius (mm)",10x,"!",f8.4," !",f8.4,"
     * !"/9x,"!  Clad-fuel gap (um)",16x,"!",f8.3," !",f8.3," !"/9x,"!
     *  Fuel density (% TD)",15x,"!",f8.3," !",f8.3," !"/9x,"!",7("---
     *-----"),"--!"/9x,"!",9x,"ELEMENT STRESS/STRAIN/TEMPERATURE VALUES"
     *,9x,"!"/9x,"!",7("--------"),"--!"/9x,"!  Radial stress     (MPa)"
     *,11x,"!",f13.2,8x,"!"/9x,"!  Tangential stress (MPa)",11x,"!",f13.
     *2,8x,"!"/9x,"!  Axial stress      (MPa)",11x,"!",f13.2,8x,"!")
700   format(9x,"!  Thermal strain     (%)",12x,"!",f13.4,8x,"!"/9x,"!
     *Elastic strain - R (%)",12x,"!",f13.4,8x,"!"/9x,"!  Elastic strain
     *  - T (%)",12x,"!",f13.4,8x,"!"/9x,"!  Creep strain - R   (%)",12x,
     *"!",f13.4,8x,"!"/9x,"!  Creep strain - T   (%)",12x,"!",f13.4,8x,"
     *!"/9x,"!  Total strain - R   (%)",12x,"!",f13.4,8x,"!"/9x,"!  Tota
     *l strain - T   (%)",12x,"!",f13.4,8x,"!"/9x,"!  Outside radial def
     *lection (um)",4x,"!",f13.3,8x,"!"/9x,"!  Inside radial deflection
     *  (um)    !",f13.3,8x,"!")
800   format(9x,"!  Inside mech. deflection   (um)    !",f13.3,8x,"!"/9x
     *,"!  Outside clad temperature (C)",6x,"!",f13.2,8x,"!"/9x,"!  Insi
     *de clad temperature  (C)",6x,"!",f13.2,8x,"!"/9x,"!  Average clad
     *temperature (C)",6x,"!",f13.2,8x,"!"/9x,"!",7("--------"),"--!"/9x
     *,"!",10x,"FUEL STRESS/STRAIN/TEMPERATURE VALUES",11x,"!"/9x,"!",7(
     *"--------"),"--!"/9x,"!  Radial stress     (MPa)",11x,"!",f13.2,8x
     *,"!"/9x,"!  Tangential stress (MPa)",11x,"!",f13.2,8x,"!")
900   format(9x,"!  Axial stress      (MPa)",11x,"!",f13.2,8x,"!"/9x,"!
     *  Thermal strain (%)",16x,"!",f13.4,8x,"!"/9x,"!  Elastic strain (%
     *)",16x,"!",f13.4,8x,"!")
1000  format(9x,"!  Inc. volume strain (%)",12x,"!",f13.4,8x,"!")
1100  format(9x,"!  Total strain   (%)",16x,"!",f13.4,8x,"!"/9x,"!  Outs
```

```
     *ice radial deflection (um)     !",f13.3,8x,"!"/9x,"!  Outside fuel
     *temperature     (C)    !",f13.2,8x,"!"/9x,"!  Fuel centerline temper
     *ature (C)    !",f13.2,8x,"!"/10x,29("--")////)
       return
       end
c
c      Printout for transient values
c
       subroutine out2(icase,iramp,mramp,lstep)
       common/ramp/aramp(10,2),tramp(10)
       common/stress1/mat,mod,nit,pg,cc,ofl,cfill,pbulk,
     * bur,bul,bc,bco,bcon,conv,tx,flx,tnf,fxx,tfxx,days
       common/stress2/emc,emf,vc,vf,cruff,fruff,
     * hn,hard,r0,r1,r2,rfo,ul,pao,der,dn,dnew
       common/stress3/sr,st,sz,sa,elr,elt,tsc,ecr,ect,esf,
     * tsf,evf,evold,etoff,ecrer,ecret,ecrtran,ecttran
       common/stress4/ac,ai,afo,pow,pcwi,delpow,
     * deltim,cramp1,t0,t1,t2,tavc,eccr,econt,cf
       a1=" SS3"
       a2="04  "
       if(mat.eq.1)goto 100
       a1=" ZIR"
       a2="C   "
  100  if(delpow.eq.0.0.or.tramp(iramp).eq.0.0)goto 150
       rr=delpow/tramp(iramp)
  150  elar=(elr+econr*pc)
       elat=(elt+cont*pc)
       etr=(tsc+elar+ecrer)
       ett=(tsc+elat+ecret)
       elaf=esf+pc*cf
       u2=rfo*etoff
       u0=(ett*(r0+r1)+etr*(r0-r1))/2.
       por=(1.-dn/100.)
       tci=tint(ai,rfo,0.0,t2,por)
       uimech=(ecret*(r0+r1)-ecrer*(r0-r1))/2.
       v1=fxx/3.6e+21
       v2=tfxx*(1.0e-25)
       v0=100.
       v3=tsc*v0
       v4=elar*v0
       v5=elat*v0
       v6=ecrer*v0
       v7=ecret*v0
       v8=etr*v0
       v9=ett*v0
       v10=tsf*v0
       v11=elaf*v0
       v12=etoff*v0
       v13=u0*1000.
       v14=u1*1000.
       v15=u2*1000.
       v16=evf*v0
       v17=uimech*1000.
       txday=tx/24.
       efpd=pcc/conv
       if(lstep.ne.0)goto 300
       if(icase.ge.1.and.iramp.eq.1)write(6,400) icase
       if(delpow.eq.0.0)write(6,500) pcwi
       if(delpow.ne.0.0)write(6,600) rr
       write(6,700) mod,a1,a2
```

```
      write(6,800)
300   write(6,900) istep,v1,efpd,v3,v3,v10,v13,t0,sr
      write(6,1000) txday,v2,bco,v4,v5,v11,v14,t1,st
      write(6,1000) powi,v17,bur,v6,v7,v16,v15,t2,sz
      write(6,1000) al,pc,pul,v8,v9,v12,gap,tcl,sg
      if((istep+1).ne.mramp)return
      if(icase.eq.0)write(6,1100)
      if(icase.ge.1)write(6,1200)
400   format(5x,".",67("-"),"."/5x,"!",28x,"* CASE",i2," *",29x,"!"/5x,"
     *,",67("_"),",///)
500   format(1x,77("-")/"!",8x,"* *  TRANSIENT DATA FOR CONSTANT POWER A
     *T",f7.2," (% FP)  * *",9x,"!"/"!",77("-"),"!")
600   format(1x,77("-")/"!",13x,"* *  TRANSIENT DATA FOR",f8.3," (% FP/h
     *r) RAMP  * *",13x,"!"/"!",77("-"),"!")
700   format("! CREEP MODEL : ",i1,10x,"!",7x,"STRAIN (%)",7x,"!DEFLECT
     *! TEMP  ! STRESS !"/"! CLAD MATERIAL :",2a4,2x,"!",5x,"CLAD-R,T/FU
     *EL",6x,"!  (um)  !  (C)  !  (MPa) !"/"!",26("-"),"+",24("-"),"+",8
     *("-"),"+",7("-"),"+",8("-"),"!"/"!  STEP  !  FLUX  !  EFPD  !",8x,
     *"THERMAL",9x,"!   UC   !  TC   !   SR   !")
800   format("!  TIME  !FLUENCE !  BU-C  !",8x,"ELASTIC",9x,"!   U1   !
     * T1   !   ST   !"/"!% POWER ! U1mech !  BU-R  !",6x,"CREEP/SWELL",
     *7x,"!   U2   !  T2   !   SZ   !"/"! LHGR  !   Pc   !  BU-L  !",9x
     *,"TOTAL",10x,"!HOT GAP !  TCL  !   SG   !")
900   format("!",3(8("-"),"+"),24("-"),"+",4("-"),"+",7("-"),"+",8("-"),
     *"!"/"!",i7," !",f7.3," !",f7.2," !",3(f7.4,1x),"!",f7.2," !",f6.1,
     *" !",f7.2," !")
1000  format("!",3(f7.2," !"),3(f7.4,1x),"!",f7.2," !",f6.1," !",f7.2,"
     *!")
1100  format(1x,77("-")/1x,"All units as in previous table"/1x,"FLUX in
     *10E18 (n/m**2 s)"/1x,"FLUENCE in 10E25 (n/m**2)"///)
1200  format(1x,77("-")///)
      end
c
c
```

REFERENCES

1. Letter, R.H. Graves to B. Grier, Facility Operating License No. DPR-61, Docket No. 50-213, Reportable Occurrence LER 79-01/1T, February 1979, Preliminary Report LER 79-01/1P.

2. M.T. Pitek, Northeast Utility Service Company Staff Engineer, personal communication, March 1980.

3. Material transmitted by Northeast Utility Service Company Personnel (M.T. Pitek), December 1978.

4. Additional information suppled by Northeast Utility Service Company (M.T. Pitek), (see Ref. 3).

5. Maine Yankee information supplied by J.T. Maki, July 1979 (see also Refs. 9 and 26).

6. Material transmitted by Northeast Utility Service Company Personnel (M.T. Pitek), March 1979.

7. John E. Meyer, "Structural Mechanics in Nuclear Power Technology", MIT class notes, Course 22.314, Fall 1978.

8. Thomas A. Jaeger, "Structural Mechanics in Nuclear Power Technology", MIT class notes, Course 22.314, Fall 1976.

9. John T. Maki and John E. Meyer, "LWR Fuel Performance Analysis - Fuel Cracking and Relocation", MIT Energy Laboratory Report No. MIT-EL-78-038, October 1978.

10. Curtis F. Gerald, "Applied Numerical Analysis", Addison-Wesley Publishing Company, 1970, pp. 118-136.

11. E.R. Gilbert, "In-Reactor Creep of Reactor Materials", Reactor Technology, Vol. 14, No. 3, Fall 1971.

12. Donald R. Olander, "Fundamental Aspects of Nuclear Reactor Fuel Elements", ERDA, 1976, p. 133.

13. Othon L.P. daSilva, "Fuel Element Performance Maps for Nuclear Reactor Operational Decisions", MIT Nucl. Eng. thesis, December 1977, p. 109.

14. R. Christensen, Entropy Limited, "SPEAR Fuel Reliability Code System - General Description", EPRI, NP-1378, Interim Report, March 1980, pp. 6-8,9.

15. E.E. Bloom, "Irradiation Strengthening and Embrittlement", Seminar of the American Society for Metals - November 9 and 10, 1975, ASM, 1976.

16. Meek and Rider, NEDO Document No. 12154-2, 1977.

17. A.K. Agrawal et al., "An Advanced Thermo-hydraulic Simulation Code for Transients in LMFBR", Brookhaven Report No. BNL-NUREG-50733, 1978, pp. 242-243.

18. M.G. Andrews, H.R. Freeburn, and S.R. Pai, "Light Water Reactor Fuel Rod Modeling Code Evaluation, Phase II, Topical Report", CENPD-218, April 1976.

19. P.E. MacDonald and L.B. Thompson, "MATPRO: Version 09, A Handbook of Material Properties for Use in the Analysis of Light Water Reactor Fuel Rod Behavior", TREE-NUREG-1005, December 1976.

20. Wrought Stainless Steels, Materials Engineering, Material Selector Issue 6 No. 3, October 1967.

21. E. Paul DeGarmo, "Materials and Processes in Manufacturing", Fourth Edition, MacMillan Publishing Co., 1974, pp. 42-43.

22. V.K. Sikka and M.K. Booker, "Assessment of Tensile and Creep Data for Types 304 and 316 Stainless Steel", Journal of Pressure Vessel Technology, May 1977.

23. Y.Y. Liu and A.L. Bement, "A Regression Approach for Zircaloy-2 In-Reactor Creep Constitutive Equations", MIT Energy Laboratory Report No. MIT-EL-77-012, December 1977.

24. H.B. Meieran and E.L. Westermann, "Summary of Phase II of the EPRI LWR Fuel Rod Modeling Code Evaluations Project Using the CYGRO-3, LIFE-THERMAL-1 and FIGRO Computer Programs", ODAI-RP0397-2, RP-397-2, March 1976.

25. Donald R. Olander, "Fundamental Aspects of Nuclear Reactor Fuel Elements", ERDA, 1976, pp. 335-336.

26. John T. Maki, "Thermal Effects of Fuel Pellet Cracking and Relocation", MIT Master of Science thesis, July 1979.

27. Rapier, Jones, and McIntosh, Nuclear Science and Engineering, Vol. 50, 1973, pp. 283-306.

28. Gordon J. Van Wylen and Richard E. Sonntag, "Fundamentals of Classical Thermodynamics", 2nd edition, John Wiley and Sons, Inc., 1973.

29. M.M. El-Wakil, "Nuclear Engery Conversion", International Textbook Company, 1971.

30. M.M. El-Wakil, "Nuclear Heat Transport", International Textbook Company, 1971.